Papers Presented to the

CONFERENCE ON MULTI-RING BASINS

FORMATION AND EVOLUTION

Houston, Texas

10-12 November 1980

A Lunar and Planetary Institute
Topical Conference

UNIVERSITIES SPACE RESEARCH ASSOCIATION
LUNAR AND PLANETARY INSTITUTE
3303 NASA ROAD 1
HOUSTON, TEXAS 77058

PAPERS PRESENTED TO THE
CONFERENCE ON

MULTI-RING BASINS
FORMATION AND EVOLUTION

SPONSORED BY THE LUNAR AND PLANETARY INSTITUTE

10 — 12 NOVEMBER 1980

Compiled by the
Lunar and Planetary Institute
3303 NASA Road 1
Houston, Texas 77058

LPI CONTRIBUTION 414

PREFACE

The volume contains papers which have been accepted for publication by the Program Committee of the Conference on Multi-ring Basins: Formation and Evolution. Papers were solicited which address one of the following major topics:

1. Origin and nature of the impactors
2. Planetary record
3. Impact mechanics
4. Ejecta characteristics
5. Basin ring formation

The Program Committee consists of R. A. F. Grieve (*Department of Energy, Mines and Resources, Ottawa*), C. A. Hodges Co-convener (*U. S. Geological Survey, Flagstaff*), Odette James (*U. S. Geological Survey, Reston*), Jay Melosh (*State University of New York, Stony Brook*), Pamela Jones (*Lunar and Planetary Institute, Houston*), Dennis Orphal (*California Research and Technology, Livermore*), Carlé Pieters (*Brown University, Providence*), Peter H. Schultz, Co-convener (*Lunar and Planetary Institute, Houston*), Dieter Stöffler (*Lunar and Planetary Institute, Houston*), George Wetherill (*Carnegie Institution of Washington*).

Logistic and administrative support for this conference has been provided by P. H. Jones (*Conference Administrator, Lunar and Planetary Institute, Houston*). This abstract volume has been prepared under the supervision of P. R. Criswell (*Technical Editor, Lunar and Planetary Institute, Houston*).

Papers are arranged alphabetically by the name of the first author. Indices by lunar sample, subject, and author are provided.

The Lunar and Planetary Institute is operated by the Universities Space Research Association under contract No. NASW-3389 with the National Aeronautics and Space Administration.

TABLE OF CONTENTS

INDICES

ORBITAL CHEMISTRY OF LUNAR BASIN RINGS. Constance G. Andre, National Air and Space Museum, Smithsonian Institution, Washington, D.C. 20560.

Chemical ring patterns defined by variations of magnesium and aluminum in the surface soils of multiringed basins and large craters have been observed in orbital X-ray fluorescence (XRF) data. These patterns correspond to structural/chemical rim features that have been observed in natural terrestrial craters, laboratory simulations and explosion craters. These chemical rings represent material excavated from depth within the crater cavities (1,2,3). Such information about the subsurface from several large impacts can be combined to reconstruct the regional stratigraphy (4,5,6) in the same way terrestrial outcrops are used to trace a geologic formation. Data from the orbital X-ray experiment includes wide coverage of five lunar nearside basins and numerous large craters from both high- and low-altitude orbits of the Apollo 15 and 16 missions (7). A few low-altitude orbits provide high-resolution repetitive coverage of the Al-Khwarizmi-King and Mendeleev Basins on the eastern far side.

In this study there is an emphasis on the multiringed basin, Smythii, which is of special interest because it is located on the nearside/farside boundary. It has long been suspected that this boundary, separating regions of the terra with obvious differences in topography, chemistry (Fe, Ti, Th, Mg, Al), spectral reflectivity (FUV) and crustal thickness, marks the lateral boundary between two different geochemical provinces of the crust (8). The Smythii impact structure has 3 observable topographic rings as defined by Wilhelms and El-Baz (9). The innermost, 370 km in diameter, reaches elevations about 4 km above the present basin floor. This ring can be clearly identified in the orbital XRF data as an annulus of low Mg/Al chemical composition. The data used in this study are expressed as Mg/Al concentration ratios because this ratio discriminates most effectively among various terra rock types (10). The chemical ring is particularly well-defined on the flanks of the western rim of the basin because it contrasts with both the higher Mg/Al soils of the terra to the west of the basin (11) and the magnesium-rich soils inside the basin (12,13,14). See Table 1. The probable source of the Mg-rich surface inside the basin is "mantled" material draped over the basin floor (14). The chemical ring cannot be easily distinguished on the east side of the basin because soils there are distinctly more anorthositic, like the ring itself. The ring observed in the orbital XRF data can be equated to "overturned flaps" that encircle transient cavities formed by impacts into multi-layered targets. The overturned flaps display the inverted order of the strata excavated so that material from deep layers of the crater (basin) are exposed on the surface and extend radially from the crater rim (1,2,3). Although the flap thins with distance from the rim, the strata retain precisely their relative pre-impact positions as demonstrated by laboratory experiments, explosion tests and natural terrestrial craters (1,2,3). Thus, a stratified target may be identified by chemistry if the surface of an overturned flap has

CHEMISTRY OF LUNAR BASIN RINGS

Andre, C. G.

a different composition from surrounding surface soils. The composition of the Smythii ring, on the basis of Mg/Al values, resembles the soils of the Apollo 16 landing site and the eastern farside. These soils are more anorthositic than the average nearside terra. If the semi-circular segment of the ring bounding the west rim of the Smythii Basin represents the overturned flap, it implies that:

1) The transient cavity of the Smythii Basin is defined by the inner topographic ring rather than the outer ring (15, 16).
2) Strata of contrasting chemical composition were excavated on the western side of the Smythii Basin by the impact.
3) Although the geochemical province of the eastern far side does not extend west of the Basin on the surface, it may extend across the Smythii Basin to the near side as a subsurface unit. In fact, low-altitude, high-resolution XRF data for Langrenus Crater indicate that the anorthositic subsurface layer excavated from depth in the Smythii Basin may extend as far as 60E. Low Mg/Al values similar to those of the eastern far side are exposed both inside this Copernican crater and on the rim. This composition contrasts with surrounding terra soils that have higher Mg/Al ratios (See Table 1).

I propose that the eastern farside geochemical province dips toward the west at a low angle. It extends into the lunar near side as a subsurface layer on the west side of the Smythii Basin and extends at least as far as 60E. This highly anorthositic material was excavated from depth at the Smythii Basin and at the crater, Langrenus. Studies of other nearside terra craters and Crisium Basin ejecta are necessary to further evaluate this stratigraphic model. A topographic cross-section from 55E to 105E (Figure 1) shows the hypothetical subsurface contact between the nearside and farside geochemical provinces proposed here.

References: (1) Shoemaker E. (1961) Structure of the Earth's Crust and Deformation of rocks, p. 418-434. (2) Roddy D. et al. (1975) Proc. Lunar Sci. Conf. 6th, p. 2621-2644. (3) Gault D. (1974) NASA TM-X-62, p. 137-176. (4) Andre C. et al. (1978) Mare Crisium: The View from Luna 24, p. 1-12. (5) Andre C. et al. (1979) Proc. Lunar Planet. Sci. Conf. 10th, p. 1739-1751. (6) Andre C. et al. (1979) Lunar and Planetary Science 10, p. 38-40. (7) Adler I. et al. (1973) The Moon 7, p. 487-504. (8) El-Baz F. and Wilhelms D. (1975) Proc. Lunar Sci. Conf. 6th, p. 2721-2738. (9) Wilhelms D. and El-Baz F. (1977) Map I-948, USGS. (10) Andre C. and Adler I. (1980) Proc. Conf. Lunar Highlands Crust (in press). (11) Andre C. and Adler I. (1980) Lunar and Planet. Sci. XI, p. 23-25. (12) Andre C. et al. (1977) Proc. Lunar Sci. Conf. 8th, p. 925-931. (13) Conca J. and Hubbard N. (1979) Proc. Lunar Planet. Sci. Conf. 10th, p. 1727-1737. (14) Wolfe R. and El-Baz F. (1976) Proc. Lunar Sci. Conf. 7th, p. 2903-2912. (15) Strain P. and El-Baz F. (1979) Proc. Lunar Planet. Sci. Conf. 10th, p. 2609-2621. (16) Wilhelms D. et al. (1977) Impact and Explosion Cratering, p. 539-562.

- T A B L E 1 -

Longitude	Mg/Al concentration	Number of Data Points	Feature
60.5E - 61.5E	0.26	9	inside Langrenus
70E - 75E	0.37	33	terra west of Smythii
80E - 81E	0.23	3	west rim of Smythii
82E - 90E	0.43	56	southern floor of Smythii Basin
95E - 105E, 115E - 140E	0.24	140	terra east of Smythii

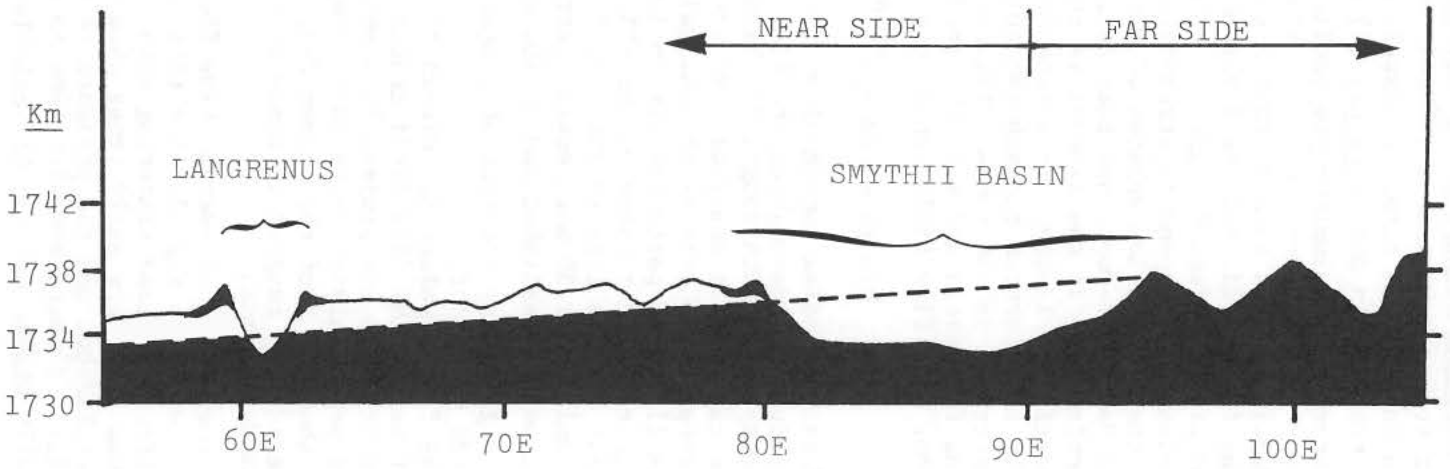

F I G U R E 1

Z-MODEL ANALYSIS OF CALCULATED IMPACT CRATERING FLOW FIELDS IN GABBROIC ANORTHOSITE, M.G. Austin, J.M. Thomsen, S.F. Ruhl, Physics International Co., San Leandro, CA 94577; D.L. Orphal, California Research and Technology, Inc., Livermore, CA 94550 and P.H. Schultz, The Lunar and Planetary Institute, Houston, TX 77058.

A continuum mechanics computer calculation of the impact of a 62 m diameter iron sphere into a gabbroic anorthosite half-space at 5 km/sec has been analyzed in terms of Maxwell's Z-Model. The method of analysis is that reported in Austin et al. (1) where it was applied to the laboratory-scale impact of an aluminum projectile into a plasticene clay half-space at 6 km/sec. The main conclusions of (1) hold here also. At specific times the Z-Model provides in many ways a good description and analysis of the cratering flow field, but the Z parameter which characterizes the shape of the flow field is time dependent. Time dependence of Z means that the flow occurs along time dependent streamlines so that much of the predictive simplicity of the steady flow version of the Z-Model is destroyed.

The Maxwell Z-Model has been described previously in detail (1,2,4,5). An essential part of the Z-Model is the regular power law decay of the flow field particle velocity. In a spherical polar coordinate system centered at a flow field center beneath the point of impact and on the axis of cylindrical symmetry, R is the radial distance from this center to a given point in the cratering flow field and θ is the angle measured from the vertically downward direction. The flow field can be described by:

$$\dot{R}(\theta,t) = \alpha(\theta,t) R^{-Z(\theta,t)}$$

where $\dot{R}$ is the radial component of the flow field velocity, α is a time-dependent coupling term describing the flow field strength; and Z defines the rate of velocity decay with range, R. Time from impact is t.

The calculation analyzed here was performed by D.L. Orphal et al.(3) and is referred to here as the GA1 calculation. Previous detailed Z-Model analysis (1,2) was performed for an impact into plasticene clay. This calculation is referred to here as the PL1 calculation. Z and α values determined from least squares fits to the flow fields in the GA1 calculation are shown in Figs. 1 and 2. At 50 msec energy partitioning is complete and the flow field is well established and at 400 msec the crater is almost bottomed out. In the significant fraction of crater formation time in between, Z and α are very time dependent.

The fitted values are within 10 % of the calculation's flow field velocities for the flow field center chosen for this analysis to be at a depth of 60 m or about one projectile diameter deep. Other possible flow field centers were analyzed every 10 m from 0 m deep to 200 m deep. Other centers within about 50 % of the chosen depth gave almost as good fits. Z and α calculated with respect to these other coordinate centers show similar degrees of time dependence.

A comparison of average flow field Z values for the PL1 and GA1 calculations is given in Fig. 3. The time scales are of course different for these very different sized cratering events. Both calculations exhibit Z values less than 2 at very early times when the cratering flow field is being established and the presence of the projectile has a significant effect on it (2). Z increases with time in both calculations. The Z values are eventually higher for the GA1 calculation.

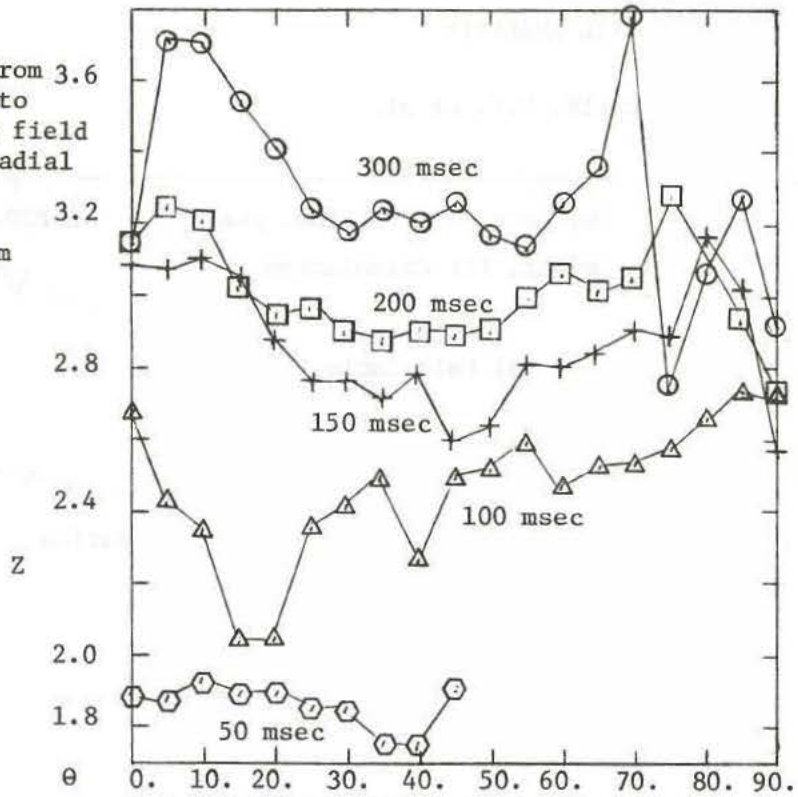

Figure 1. Z values from least squares fits to the calculated flow field velocity vectors' radial components with respect to a flow field center at 60 m below the original impact point for calculation GA1. θ is measured in degress from θ = 0 in the vertically downward direction.

LEGEND

- 300 msec
- 200 msec
- 150 msec
- 100 msec
- 50 msec

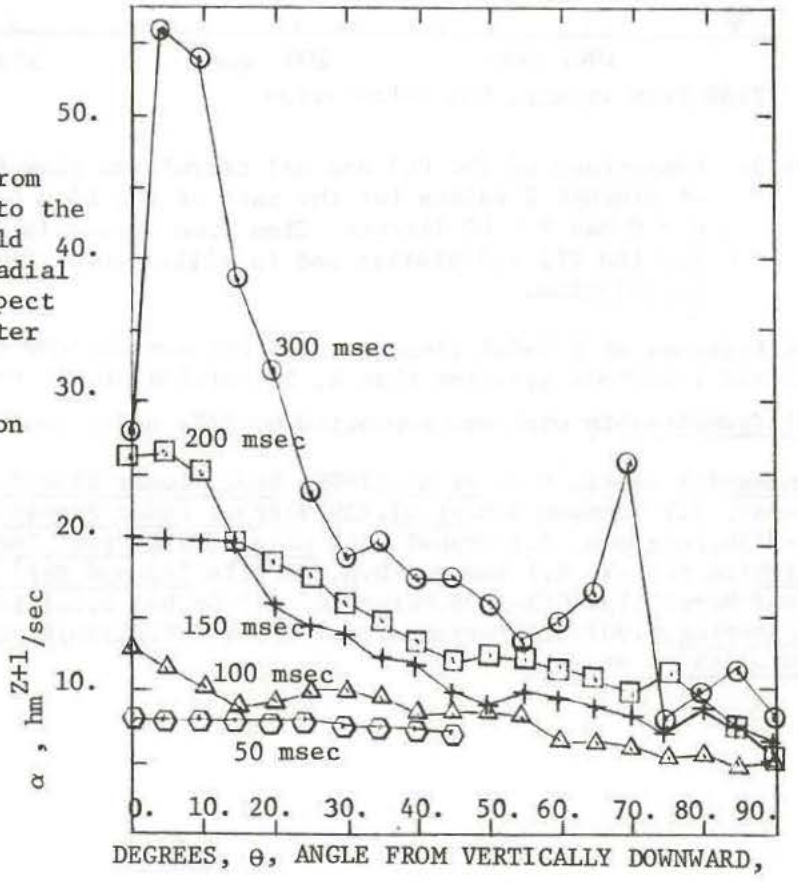

Figure 2. α values from least squares fits to the calculated flow field velocity vectors' radial components with respect to a flow field center at 60 m below the original impact point for calculation GA1. α is in units of hectometers to the Z + 1 power per second. (1 hectometer = 100 meters)

Z-MODEL ANALYSIS

AUSTIN, M.G. et al.

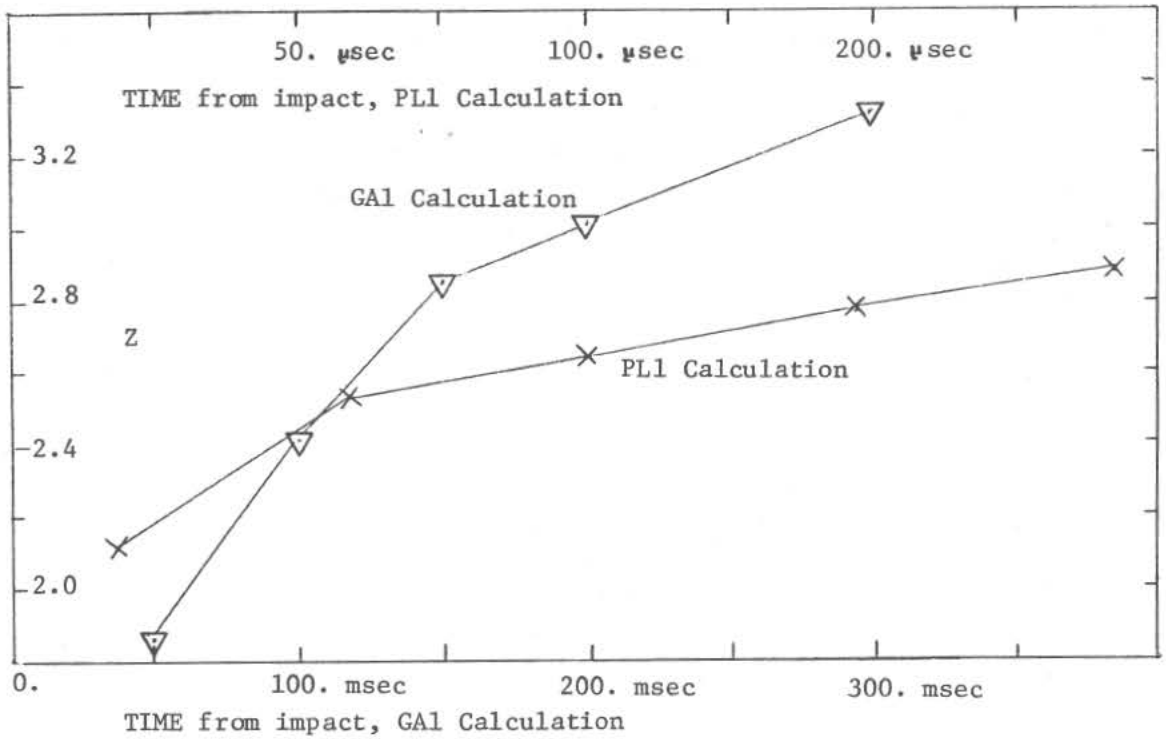

Figure 3. Comparison of the PL1 and GA1 calculated flow fields in terms of average Z values for the part of the flow field between $\theta = 0$ and $\theta = 60$ degrees. Time from impact is in microseconds for the PL1 calculation and in milliseconds for the GA1 calculation.

Applications of Z-Model ideas such as (6) can use the descriptive power of the Z-Model without assuming that Z, in particular, is time independent.

Acknowledgement-This work was supported by NASA under contract NASW 3168.

References-1.) Austin M.G. et al.(1980) Proc. Lunar Planet.Sci.Conf.11th (in press). 2.) Thomsen J.M.et al.(1979)Proc. Lunar Planet.Sci.Conf.10th, p.2741-2756,Pergamon. 3.) Orphal D.L. et al.(1980)Proc. Lunar Planet.Sci. Conf.11th(in press). 4.) Maxwell D.E.(1977)In Imp.and Expl.Cratering(Roddy, Pepin and Merrill)p.1003-1008,Pergamon. 5.) Orphal D.L.(1977) In Imp.and Expl.Cratering,p.907-917,Pergamon. 6.) Croft S.K.(1980)Proc.Lunar Planet. Sci.Conf.11th(in press).

ON THE ORIGIN OF THE PLANETESIMALS THAT PRODUCED THE MULTI-RING BASINS; Ralph B. Baldwin, Oliver Machinery Co., Grand Rapids, MI 49504.

From analyses of crater counts and crater morphology, it is concluded that the primary pre-mare lunar craters form a continuous series of related structures all formed by impact within a rather limited period of less than 600 million years. Consequently it follows that the bodies that formed these craters and basins came from a single population, now extinct, of solar system planetesimals whose numbers declined rather smoothly from the smallest to the largest in exponential fashion.

The multiple ringed basins were formed by the largest bodies of a single family of such bodies. The problem then becomes, where in the solar system were these bodies stored and when did they strike?

From crater counts within large craters, from the appearance and heights of crater rims, ten classes of craters can be distinguished. The youngest, Class 1, are post-mare craters. The oldest, Class 10, extends back to the time that crater saturation of the moon's surface ceased. It appears clear that the crater forming infalls declined in number exponentially from the time the moon accreted to its present size to about the time the maria were formed. From these data, a relative time scale of pre-mare events can be established and converted into an approximate absolute scale by assuming a date for the end of saturation. It now appears that that date should be about 4.3×10^9 years, with the age of the moon at 4.65×10^9 years. The moon seems to have had a crust at least by 4.5×10^9 years. The half life of these planetesimals would have been 225×10^6 years if the date of saturation were 4.5×10^9 years ago, and 143×10^6 years if it were 4.3×10^9 years.

From the observed distribution of craters with time, and the masses of crater forming objects, we may determine the amount of material that fell on the moon from the date of the end of saturation to about 3×10^9 years ago when this source of planetesimals became depleted. It was about 2.4×10^{23} g and if it all stayed on the moon would have formed a layer 1.88 km thick at a minimum. The rate of infalls was greatest at the earliest observable time.

The total amount of material that fell on the moon, based on extrapolation of the observed rate changes after the end of saturation is a function of the date of the end of saturation. Any date from 4.2 to 4.5×10^9 years is reasonably consistent with the amount of meteoritic material now present there, but for more recent dates we have two alternatives, either the mass of infalls was hugely excessive or the planetesimals must have been stored somewhere in the solar system and then started to impact the moon after several hundred million years.

These observations and conclusions are diametrically opposed to the "Terminal Lunar Cataclysm" hypothesis. They are supported by the tentative radiometric ages of various lunar basins derived by Nunes et al (1) and Schaeffer and Husain (2). It is concluded that the multi-ring basins of the moon came from impacts of the largest bodies in a family of bodies of all sizes in eccentric solar orbits. Such bodies abounded in the early solar system out to at least Saturn.

1. Nunes, P.D., Tatsumoto, M., and Unruh, D.M. (1974). Proc. Lunar Sci. Conf. 5th, 1487-1514.

2. Schaeffer, O.A. and Husain, L.,(1974). Proc. Lunar Sci. Conf. 5th, 1541-1555.

ON THE TSUNAMI THEORY OF THE ORIGIN OF MULTI-RING BASINS;
Ralph B. Baldwin, Oliver Machinery Co., Grand Rapids, MI 49504.

The only theory that seems to fit all the observations of the multi-ring basins on the moon is that these structures were formed by impacts of giant planetesimals and that the energies released fluidized the area in some fashion so that tsunami-like waves could radiate from ground zero and after the energy density from the impact had decayed sufficiently with distance from the impact point so that the slow moving tsunami could no longer distort the surface, the wave froze into position as a ripple in the moon's crust. The ripple extended above the surface as seen from the outside, and was followed on its inner side by a pronounced depression.

The central peaks and central peak rings at these basins were formed by the rebound following the impact. Such a rebound would be a substantial fraction of the crater diameter in height. Multiple inner rings would have been formed by oscillating rebounds and collapses.

There are five sets of observations that lead to this model.

1. Counts of primary impact craters intersecting the crests of the main rings (Altai and Cordillera) surrounding Mare Nectaris and Mare Orientale, compared with counts of post-impact craters within the great basins show the essential equivalence of the ages of each basin and its ring.

2. There is a great difference in the appearance of the lunar surface inside and outside of the Cordillera ring at Mare Orientale. Pre-mare craters are distinctly visible under the ejecta outside, while inside the ring there are no pre-mare craters. This is considered to be evidence that the inner surface was fluidized and the pre-mare surface destroyed, not just covered by ejecta.

3. Rothmann G is a large and ancient crater whose rim intersects the Altai ring for at least 90^{o} of the circumference of Rothmann G. Within the Altai ring the crater rim is completely gone. It did not simply sink down as it should be still visible. It was fluidized and merged into the new surface inside the Altai ring.

4. Both the Altai ring and the Cordillera rings are ripple shaped. They project well above both the interior and exterior surfaces.

5. At basin associated circumferential faults there are no evidences of vertical motions. These ring faults simply generated rilles without differences in height of the two sides of the rille. Other theories of the origin of the multi-ring basins call for slippage along such faults.

It is concluded that the tsunami model of the origin of ring structures at the largest pre-mare basins on the moon is very probably correct.

THE EXCAVATION STAGE OF BASIN FORMATION, S. K. Croft, Lunar and Planetary Institute, 3303 NASA Road 1, Houston, TX 77058.

The complex morphological structures of multiringed basins are the result of a cratering process that may be divided into three stages: 1) a short, high-pressure stage of initial contact between projectile and the planetary crust, 2) a longer excavation stage culminating in the formation of the transient crater, and 3) a still longer (?) modification stage during which the transient crater is transformed into the observed final geologic form. This paper considers the natures of the excavation stage and the resultant transient crater. The high-pressure and excavation stage have been analyzed both empirically (1) and by computer simulation (e.g., 2,3). These analyses indicate that during the excavation stage, material previously processed by the primary shock moves in an orderly cratering flow field. The formation of the transient crater is primarily governed by the nature of the cratering flow field and by the planet's gravitational field.

THE CRATERING FLOW FIELD: A modification of Maxwell's (4) simple Z-model appears to provide a reasonable first-order quantitative description of cratering flows generated by impacts of individual, low-porosity projectiles (5). The simplified model provides insight into both the physics and spatial properties of the excavating flow. Physically, the flow approximates that of an incompressible fluid. Streamline shapes are geometrically proportional throughout the flow and appear to pass without discontinuities through ruptured, plastic, and elastic portions of the target (2,6). The flow forms in response to the primary shock and subsequent rarefactions generated at free surfaces, thereby implying that radical changes in the flow field can only result at interfaces between zones of sharply differing shock impedences (e.g., at a solid-liquid interface). This suggests that a large scale cratering flow field in a lithosphere-aesthenosphere planetary crust, such as the early lunar crust (7), would not be greatly different from a flow field completely within the lithosphere. Significantly different flow fields may occur on planets with thin, solid crusts overlying liquid mantles. Spatially, the cratering flow is divided by the streamline passing through the hinge of the ejecta flap into two portions: an excavated portion that defines an excavation cavity, and a downdriven portion that forms the walls and floor of the transient crater (5). The excavation cavity and transient crater resulting from the division of the flow field are not identical: they have the same apparent diameter ($=D_a$) but the excavation cavity is not bowl-shaped, and has a depth of only $\sim 0.1\ D_a$, significantly shallower than the inferred depth of $\sim 0.3\ D_a$ for the transient crater. The volume difference between the excavation cavity and the transient crater is driven along streamlines downward and outward, displacing an equivalent volume of surface material around the transient crater into a structurally uplifted rim. The heights of rim uplift attained during the excavation stage are transient and subsequently collapse — even during the formation of simple craters (8). Apparently, the rims have dynamically "overshot" any gravitationally stable configuration.

THE ROLE OF GRAVITY: Streamline shapes, derived from the assumption of incompressibility and the role of decay of particle velocities behind the primary shock, are independent of gravity (4). Gravity, however, determines which streamline will pass through the hinge of the ejecta flap, and thereby determine the size of the transient crater relative to the flow field (5). This is the physical basis for gravitational scaling of large craters (9,10). For every given combination of impact velocity, projectile and target properties, a strength crater, or zone of destruction, can be defined whose diameter ($\equiv D_s$) scales directly with the projectile diameter and consequently, as the cube root of the impact energy. Similarly for each impact, a gravity-controlled

diameter may be defined (D_g) that scales according to gravity and to the $1/\alpha$ power of the impact energy, where α is defined or the gravitational scaling coefficient (11). Where D_g is smaller than D_s, D_g is equivalent to the transient crater diameter. It can be shown that the ratio of D_s/D_g may be given by:

$$D_s/D_g = K\, D_g^{\alpha/3-1}$$

where K is a function of α and the transition diameter between strength-scaled and gravity-scaled craters. Suggested values of α vary between ~3.4 and 3.6. This implies, as might be expected, that the diameter of the gavity crater becomes progressively smaller relative to the strength crater with increasing diameter (11,12,16). Therefore, with increasing gravity and/or increasing diameter, the streamline passing through the hinge is located relatively closer to the point of impact. This implies that with increasing diameter, material comprising the floor and walls of the transient crater experience increasingly higher levels of shock, and are consequently more highly heated and comminuted, and possess higher particle velocities than wall materials in smaller craters (11,12). For strength-gravity transition diameters of a few tens to a few hundreds of meters appropriate to the Earth and Moon, respectively (13), values of D_s/D_g range from ~2 to ~6 for basin transient craters 100 to 1,000 km in diameter. Thus, at basin dimensions, the transient crater is relatively small cavity at the center of a much larger zone of destruction whose material the properties change drastically with increasing range from the point of impact, and for which the fluid approximation inherent in the Z-model is suggested to become more appropriate. The geometric similarity of streamlines throughout the entire flow field (except very near the point of impact), and the independence of their shape on gravity imply that no matter which streamline is determined by gravity to bound the excavation cavity, its geometric cross-section remains proportionally the same. Consequently, the excavation cavaties of basins are inferred to exhibit proportional growth.

A depth of excavation of ~0.1 the transient crater diameter inferred from model cratering flow fields and limited field observations (5) suggest a possible constraint on the relation of the transient crater to the observed multiringed structures: the paucity of recognized samples of the lunar mantle on the surface around the Imbrium basin sets an upper limit on the diameter of the transient crater of the basin to ~10 x the thickness of the local lunar crust, or about 600 to 700 Km. If, however, the ultramafic spinel cataclasite clast in 15445,177 is indeed a sample of the lunar mantle (ref. 14 suggests it is a logical candidate) excavated by the Imbrium impact, then its existence, plus the lack of similar samples suggest that excavation extended a very short distance into the mantle, setting the transient crater diameter near 700 Km. This diameter is approximately equivalent to the diameter of the innermost Imbrium basin ring remnants (the peak ring, 11). The peak ring itself is not considered to be a remnant of the transient crater rim because the highly fractured rim would probably be lost as a distinct structure during modification, but has been proposed as a rebound structure just inside the transient crater rim (11,15).

In summary, the nature of excavation flow fields and the consequences of gravity vs strength scaling imply that basin transient craters 1) exhibit proportional growth; 2) have depths of excavation equal to ~0.1 D_a; 3) are about 3 to 6 times smaller than their respective strength craters; hence, they are relatively small cavities inside a much larger zone of destruction and are lined with highly comminuted, high velocity particles; and 4) are surrounded by a large volume of fractured material whose strength properties increase significantly with increasing range. In addition, this volume of highly

fractured material is dynamically thrust a significant height above its original equilibrium position and represents a significant potential source of energy for driving the modification phase. The nature of the transient crater and its surroundings at basin scales should not be neglected in construction of models of ring formation and basin modification because they represent the boundary conditions from which the final basin structures are derived.

References

1. Gault D. E., Quaide W. L. and Oberbeck V. R. (1968) Shock Metamorphism of Natural Materials, p. 87-99.
2. Kreyenhagen K. N. and Schuster S. H. (1977) IEC*, p. 983-1002.
3. O'Keefe J. D. (1977) Impact Phenomena on the Terrestrial Planets, Ph.D. Thesis, UCLA, 166 pp.
4. Maxwell D. E. (1977) IEC*, p. 1003-1008.
5. Croft S. K. (1980) Proc. Lunar Planet. Sci. Conf. 11th, in press.
6. Ullrich G. W. (1976) The Mechanics of Central Peak Formation in Shock Wave Cratering Events. AFWL-TR-75-88.
7. Head J. W. and Solomon S. C. (1980) Lunar and Planetary Science XI, p. 421-423.
8. Cooper H. F. and Sauer F. M. (1977) IEC*, p. 1133-1163.
9. Ivanov B. A. (1976) Proc. Lunar Sci. Conf. 7th, p. 2947-2965.
10. Killian B. G. and Germain L. S. (1977) IEC*, p. 1165-1190.
11. Croft S. K. (1979) Impact Craters from Centimeters to Megameters. Ph.D. Thesis, UCLA, 264 pp.
12. Schultz P. H. and Mendell W. (1978) Proc. Lunar Planet. Sci. Conf. 9th, p. 2857-2883.
13. Gault D. E., Guest J. E., Murray J. B., Dzurisin D. and Malin M. C. (1975) JGR 80, 2444-2460.
14. Herzberg C. T. and Baker M. B. (1980) Proc. Conf. Lunar Highlands Crust, p. 113-132.
15. Croft S. K. (1979) Lunar and Planetary Science X, p. 245-247.
16. Dence M. R., Grieve R. A. F. and Robertson P. B. (1977) IEC*, p. 247-275.

*IEC = Impact and Explosion Cratering, D. J. Roddy, R. O. Pepin and R. B. Merrill, eds., Pergamon, New York.

THE MODIFICATION STAGE OF BASIN FORMATION: CONDITIONS OF RING FORMATION, S. K. Croft, Lunar and Planetary Institute, 3303 NASA Road 1, Houston, TX 77058.

Multiring basin structures are the result of a complex cratering process that may be divided into (a) a high-pressure stage of initial contact between the projectile and planetary surface, (b) a low-pressure excavation stage culminating in the formation of the transient crater, and (c) a modification stage during which the transient crater is transformed into the final observed form (1). Although later volcano-tectonic modification may be important (2), the basic structures and morphologies of basin rings are thought to be established during the modification stage. Physical models of particle flow and ring formation during the modification stage are critically dependent on the nature of the transient crater, which represents the initial conditions of the modification stage. Several different states of the transient craters of basins have been suggested (e.g., 3, 4, 5). However, the following new model of the transient crater is proposed on the basis of recent analyses of the cratering flow field (6, 7) and the consequence of gravity scaling and strength scaling for crater formation (8). At basin dimensions the transient crater is a deep, proportionally grown cavity at the center of a zone of fractured material (the strength crater) about three to six times larger than the transient crater in all dimensions. Strength properties of material in the fractured zone increase strongly with increasing range from the point of impact because of the decreasing levels of shock experienced by material at increasing range. Material in the entire fracture zone is in motion and, at the end of the excavation stage, it is dynamically uplifted.

Forces operating to modify the dynamic material in the fracture zone around the transient crater include gravity and possibly elastic forces. Elastic forces may have operated early in the cratering event during pressure release and generation of volumetric bulking by shock induced fracturing to produce a "spring action" during dynamic rebound of the crater floor (9). Elastic forces also may have operated late in the cratering event producing recoil of material strained along streamlines in the elastic zone surrounding the fracture zone. Elastic strains are small (on the order of a few percent), but the volume throughout which such strains apparently occur is an order of magnitude or two larger than the volume of the transient crater, implying a potentially significant effect upon release. Gravity pulls fragmented material downward and subsequently inward toward the transient crater. Because the fragmented material is significantly uplifted above its initial configuration, individual particles will collapse in free-fall through a large vertical drop, gaining considerable kinetic energy before interacting again as a continuous medium. Such large gains in kinetic energy due to extensive free-fall in a gravitational field appear to generate the conditions necessary to fluidize dry, long run-out landslides on the Earth (10). Consequently, it is postulated that at least the inner portions of the fracture zone fluidize (8). Gravitationally driven collapse of craters in a fluid medium also produces a dynamic floor rebound that begins before the end of the excavation stage at small scales (11). The postulated fluidized state of the inner fracture zones of basins suggests that a similar mechanism can produce rebounds at large diameters.

The evidence for rebound and uplift supplied by terrestrial explosive and impact craters (which may be the mechanistic result of either elastic or gravitational force) implies a division of the modification flow field into two zones: an inner zone associated with the gravity-scaled transient crater where motion is down-up-down, and an outer zone associated with the strength-scaled fracture zone where motion is simply uplift, then collapse. Both particle velocities and the extent of fracturing diminish with increasing range, thereby

implying dominance of fluid or plastic deformation in the center that grades to dynamic brittle failure farther out.

Another initial condition that has been suggested to be important in basin ring formation is the thermal structure of the planet at the time of impact: i.e., an elastic lithosphere overlying a plastic aesthenosphere (12). This suggestion was motivated in part by an analytic model of ring formation employing an elastic slab over a liquid or plastic layer (5). Material in the plastic layer is allowed to flow into the transient crater, and failure is assumed to occur in the elastic slab where stresses are greatest. If the transient crater model proposed here is correct, the fractured and dynamic state of material within the fracture zone may raise difficulties with the elastic-plate model for all rings in this zone, including (see below) the Orientale Cordillera equivalent rings (though the elastic model may apply in the elastic zone outside the fracture zone). Conceivably, the location of failure scarp rings (of which the Cordillera is an example, 8) would be more influenced by the change of strength properties with increasing range from the point of impact than by fluid stresses accumulating at depth. Further, the brittle/ductile transition marking the lithosphere/aesthenosphere boundary is not only temperature dependent, but also rate dependent (13), hence fragmentation mechanics may dominate over plastic deformation on the short time scale of shock passage and material failure.

An empirical model of basin formation described previously (8, 14), based on 1) ring morphology, 2) ring morphometry, 3) volumetric modification models, 4) gravity anomaly signatures, 5) mass deficiency analyses, and 6) geology of terrestrial impact craters, interprets origins of specific ring structures that correlate with the proposed transient crater. Specifically, the peak rings of basins appear to scale gravitationally and correlate with the dynamic rebound inside the transient crater, and the Cordillera equivalent rings appear to be inward facing failure scarps that exhibit strength scaling. The occurrence and appearance of other rings also fit into the framework supplied by the proposed transient crater. Although this model of basin ring formation is still very primitive, it illustrates how initial conditions may influence the interpretation of ring structures. Clearly, much work remains to be done in evaluating mechanisms of ring formation, not the least of which is the determination of the material conditions under which ring structures originate.

References

1. Croft S. K (1980) The excavation stage of basin formation. This volume.

2. Schultz P. H. (1979) Conference on the Lunar Highlands Crust, 141-142.

3. Dence M. R., Grieve R. A. F. and Robertson P. B. (1977) IEC*, p. 247-275.

4. Hodges C. A. and Wilhelms D. E. (1978) Icarus 34, 294-323.

5. Melosh H. J. and McKinnon W. B. (1978) Geophys. Res. Lett. 5, 985-988.

6. Maxwell D. E. (1977) IEC*, p. 1003-1008.

7. Croft S. K. (1980) Proc. Lunar Planet. Sci. Conf. 11th, in press.

8. Croft S. K. (1979) Impact craters from centimeters to megameters, Ph.D. Thesis, UCLA, 264 pp.

9. Ullrich G. W. (1976) The mechanics of central peak formation in shock wave cratering events, AFWL-TR-75-88.

10. Hsü K. J. (1975) Bull. Geol. Soc. Am. 86, 129-140.

11. Gault D. E. and Greeley R. (1978) Icarus 34, 486-495.

12. Head J. W. and Solomon S. C. (1980) Lunar and Planetary Science XI, p. 421-423.

13. Lawn B. R. and Wilshaw T. R. (1975) Fracture of brittle solids, Cambridge, 204 pp.

14. Croft S. K. (1980) Lunar and Planetary Science XI, p. 183-185.

*IEC = Impact and Explosion Cratering, D. J. Roddy, R. O. Pepin and R. B. Merrill, eds., Pergamon.

THE IMBRIUM BASIN: A STRUCTURAL MODEL, R. A. De Hon, Department of Geosciences, Northeast Louisiana University, Monroe, LA 71209.

A long history of geologic observation and speculation has not produced a fully comprehensive and acceptable model for the origin of the Imbrium Basin (1-4). While an impact origin for the basin is universally accepted, controversy still exists concerning the detailed structure and the origin of some of the most prominent features. The Imbrium Basin is flooded by mare basalts and its configuration and structure are known only in part, yet it served as the type example of a multi-ringed basin prior to acquisition of Orbiter images of the Orientale Basin. Orientale, which is less flooded, now serves as a type for multi-ringed basins studies. Unfortunately, baseline data for the Orientale Basin is incomplete; hence, Imbrium remains an important example in the formulation of basin theory.

An isopach map of the mare basalt within the Imbrium Basin provides improved understanding of the location and configuration of the salient buried topography. However, a map based entirely on estimates of basalt thickness at partially buried craters (5) is not fully satisfactory due to the small number of clustered data points. As with any major circular basin, the depth of the basin precludes preservation of a significant population of buried craters due to the low crater density and inherent depth of burial. Thus, the isopach map constructed for Mare Imbrium involves interpretation of sparse crater data and correlation of other observations to establish trends and overall thickness distributions. Data and observations which restrict the model consist of the following: 1) basalt thickness derived from partially buried craters; 2) location of the mare contact with terra materials; 3) location of crest line of the outer mountain ring; and 4) location of massifs and mare ridges marking the inner basin rim.

The isopach map (Fig. 1) is characterized by a thick central lens of basalt surrounded by a ring of moderately thick basalt. A model of the subsurface topography (Fig. 2) is constructed by subtracting the basalt thickness from a 12th degree harmonic model of the surface topography (6). The resulting paleomorphologic map exhibits a deep central basin surrounded by a wide shelf. An inner raised ring, approximately 650 km in diameter, separates the central basin from the shelf. The outer raised rim of the basin is approximately 1350 km in diameter. The southeast rim of the basin (Montes Apenninus) averages 9700 m in elevation. The surface outside the basin averages 6000 m in elevation. The total thickness of the mare basalt is not measured directly, but it is estimated to be 1500-2500 m thick (7). Hence, the inner basin floor may be estimated at 2700-3200 m in elevation. The total relief of the basin before flooding is on the order of 6500-7000 m.

THE IMBRIUM BASIN

De Hon, R. A.

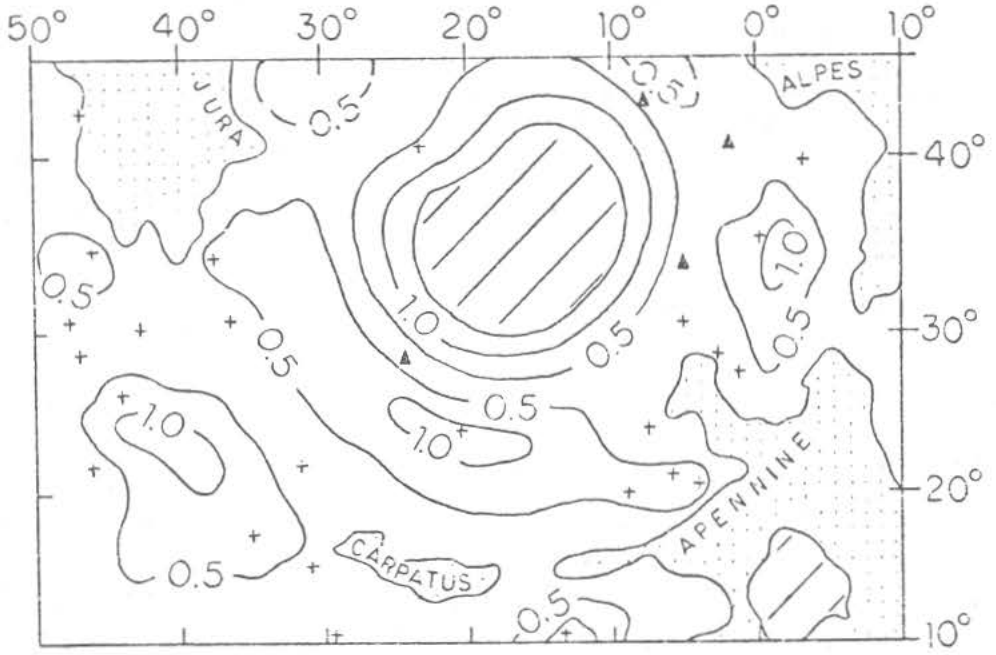

Figure 1. Isopach map of Mare Imbrium basalt. Isopach interval is 0.5 km. Crosses mark the location of measured basalt thickness. Diagonal lines indicate region of unknown values.

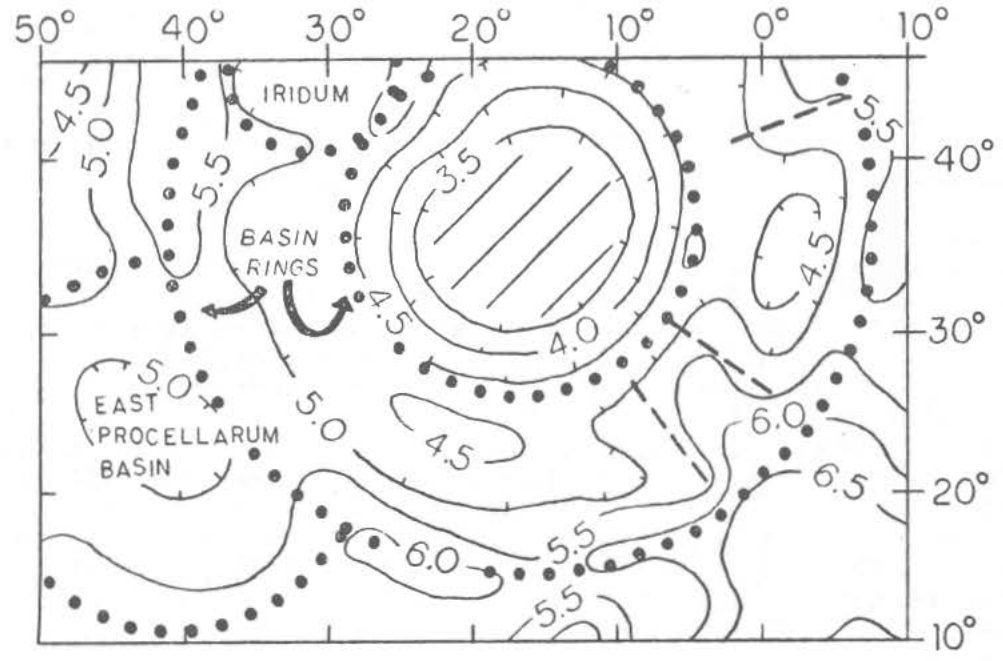

Figure 2. Paleotopography of the Imbrium Basin. Contour interval is 0.5 km. Datum is 1730 km radius vector. Dots mark crests of inferred rings. Dashed lines are "tear faults" in rim flap.

THE IMBRIUM BASIN

De Hon, R. A.

The resulting topographic model of the original Imbrium Basin is that of a two-ringed basin. The inner ring is marked by the position of the mare ridges and isolated massifs such as Montes Spitzbergensis, Mons Pico, and Mons La Hire. The position of the outer ring is controversal, but it is assumed to be eccentric to the inner ring and composed of high standing terra of Montes Carpatus, Montes Apenninus, Montes Caucasus, Montes Alpes, and terrain north of the mare. The outer ring is radially offset between the Montes Alpes and Montes Caucasus by a tear fault (8) caused by an uneven roll-back of the rim flap during excavation of the outer portion of the crater. Similarly, incomplete excavation results in remnant material of the Apennine Bench which rises above the basalt fill on the basin shelf. The subdued topography of the northern outer rim may represent lateral or vertical inhomogenies of the target material.

The outer raised rim of the basin is broken and discontinuous. The 260 km diameter Iridum Basin is superposed on the northwest Imbrium shelf. The Iridum rim overlaps both the inner and outer rings of the Imbrium Basin. Large discontinuities in the Imbrium outer ring mark the locations of interaction between Imbrium excavation and pre-existing basins. In the east, a small gap between Montes Apenninus and Montes Caucasus is formed where the Imbrium Basin impinges on the Serenitatis Basin. In the south, a break between Montes Apennius and Montes Carpatus marks the infringement of the Imbrium Basin on the older Stadius-Aestuum (South Imbrium) Basin. The largest break in the Imbrium rim occurs in the southwest between Montes Carpatus and Montes Jura where a full one-fifth of the rim is submerged beneath mare basalts or is missing. Isopach mapping reveals a heretofore unrecognized 600 km diameter basin centered just beyond the nominal Imbrium Basin rim in this locality. The East Procellarum Basin (9) represents the remnant of a pre-Imbrium impact basin partially destroyed by the Imbrium impact.

In a strict sense the model presented here is independent of the mechanisms of basin formation. However, this model does not require faulting along the Apennine Front to form the outer ring (10-11). The basin configuration is controlled in part by pre-existing topography and in part by impact and isostatic adjustments prior to the emplacement of mare basalts. Hence, total relief within the basin may have been greater at the time of basin excavation.

References: (1) Gilbert, G.K. (1893) Philos. Soc. Washington Bull., 12, 241-292. (2) Baldwin, R.B. (1949) in The Face of the Moon, Univ. of Chicago Press. (3) Hartmann, W.K. and Kuiper, G.P. (1962) Ariz. Univ. Lunar and Planetary Lab. Commun., 1, 13, 51-66. (4) Spurr, J.E. (1945) in Geology Applied to Selenology, Science Press. (5) De Hon, R.A. (1974) Proc. Lunar Sci. Conf. V, 244-259. (6) Bills, B.G. and Ferrari, A.J. (1977) Icarus, 82, 244-259. (7) McCauley et al. (1980) Icarus, in press. (8) Thurber, C.H. and Solomon, S.C. (1978) Proc. Lunar and Planetary Sci. Conf. IX, p 3481-3498. (9) De Hon, R.A. (1980) Proc. Lunar Sci. Conf. XI, in press. (10) Wilhelms, D.E. et al. (1977) in Impact and Explosion Cratering, Pergamon Press, 539-562. (11) Hodges, C.A. and Wilhelms, D.E. (1978) Icarus, 34, 294-323.

IMPACT BASINS: IMPLICATIONS FOR FORMATION FROM EXPERIMENTS

R. Greeley, J. Fink, Center for Meteorite Studies, Arizona State University, Tempe, AZ 85281 and D. E. Gault, Murphys Center of Planetology, Murphys, CA 95247

Impact basins appear to occur on all the terrestrial planets and on some of the Galilean satellites. In some planets, such as the Moon, basins constitute the major structural elements of the surface. Yet, despite their widespread occurrence, obvious importance, and study for more than two decades, a great many questions about basins remain unanswered, particularly in regard to the details of their formation and various structural relationships. Of particular interest are basin-forming impacts into relatively thin lithospheres overlying viscous mantle or core materials, comparable to interiors proposed for icy satellites and the early Moon. To simulate qualitatively such conditions in the laboratory, a series of impact experiments was carried out at the NASA-Ames Vertical Gun Facility involving a thin layer of either bonded or unbonded particles (simulated elastic lithosphere) overlying a substrate of viscous material (simulated mantle/core). Variables in the experiments were: 1) *thickness* of the "lithosphere" (0.6, 1.2, and 1.9 cm); 2) *strength* of the "lithosphere" (6.2×10^5 to 3.6×10^6 N m^{-2}); 3) subsurface material plastic *viscosity* (125 to 275 N – s m^{-2}) and *yield strength* (5 to 10 N m^{-2}); and 4) impact *energy* (90 to 560 joules).

Impacts into models involving weakly bonded particles (simulated lithosphere) underlain by viscous material yielded the following sequence and relationships: 1) upon initial impact, the surface material was severely fragmented, forming an ejecta plume of disaggregated material; 2) as the transient cavity enlarged, the ejecta consisted of larger pieces of the upper layer plus clots derived from the viscous substrate; the angle of the ejecta plume became steeper as more of the viscous material was excavated. Because the ejecta trajectory was relatively steep, most of

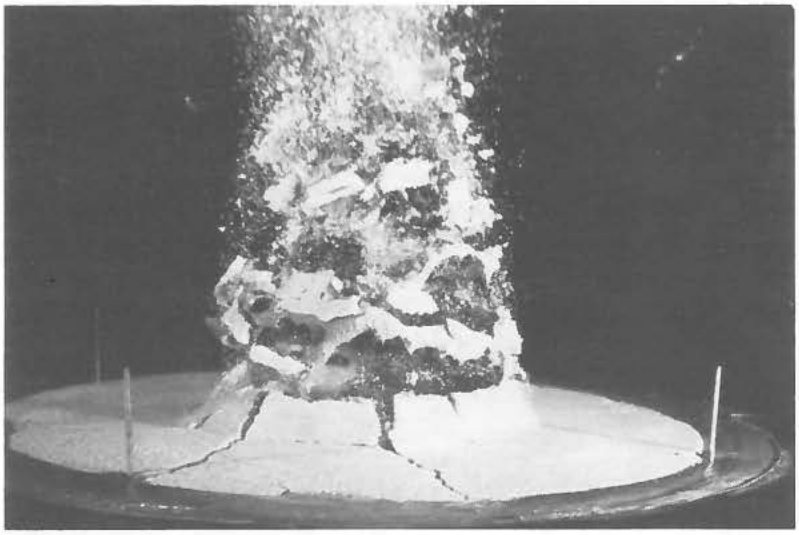

FIGURE 1. Shot 800643 showing impact (energy = 490 joules) into 1.2 cm thick layer of weakly bonded quartz particles underlain by a viscous clay slurry; note the directed ejecta plume, uptilted crustal plates, and fracture pattern (width of target is approximately 1 m).

the material landed within two crater radii (maximum transient cavity) of the point of impact; 3) as the transient cavity grew, a wave passed through the viscous substrate, accompanied by radial and concentric fracturing of the "lithosphere"; 4) as the growth of the transient cavity ceased, the upper elastic layer was too massive to be ejected; 5) in some cases it was simply overturned as the transient cavity collapsed, further fracturing the elastic material and a rising central mound of viscous material was generated; in some experiments, as the central mound collapsed, it sent a surge of viscous ejecta over the fractured plates; 6) the outlines of the fractured plates remained visible; commonly one complete and one partial ring fracture formed; the ratio of the inner rim diameter to the crater diameter increased roughly in proportion to the thickness of the "lithosphere" layer. Although only 13 experiments were conducted involving the bonded particles overlying a viscous substrate, the results suggest that there is a critical balance between the thickness (and/or strength) of the upper layer and the viscosity of the underlying material to produce multiple ring fractures; if the upper layer was too thin (or weak), a palimpsest-like feature formed with very little topographic expression; if the upper layer were too thick (or strong), the impact simply punched into it, leaving a bowl-shaped crater.

In the 16 experiments involving an upper layer of unbonded (hence, very weak) particles, the apparent diameter of the crater increased as the upper layer decreased in thickness. Although it is unlikely that physical modelling of impact basin formation can be applied quantitatively because of the orders of magnitude differences in size between laboratory and full-scale events, such modelling may provide qualitative insight into some of the mechanisms of basin formation.

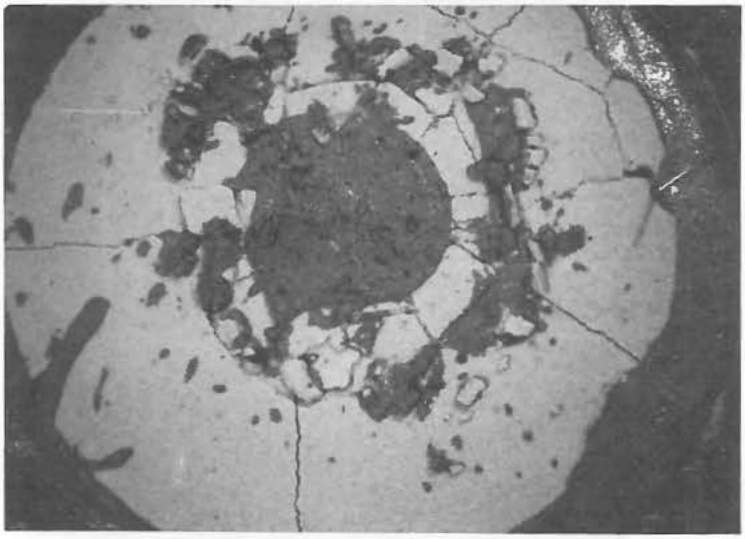

FIGURE 2. Vertical view, post-impact, of shot 800643, showing radial and concentric fracture pattern.

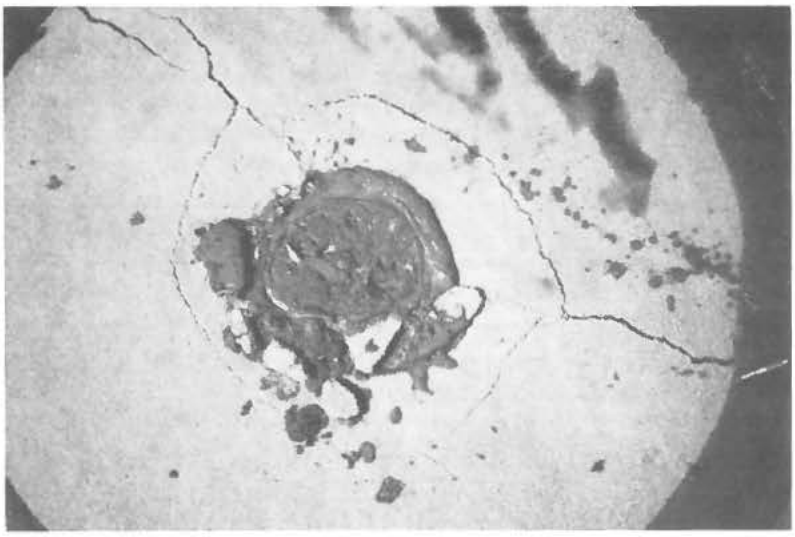

FIGURE 3. Shoot 800646 showing impact (energy 190 joules) into 1.2 cm thick layer of weakly bonded quartz particles underlain by viscous clay slurry; note the more simple fracture pattern than in the more energetic impact of shot 800643.

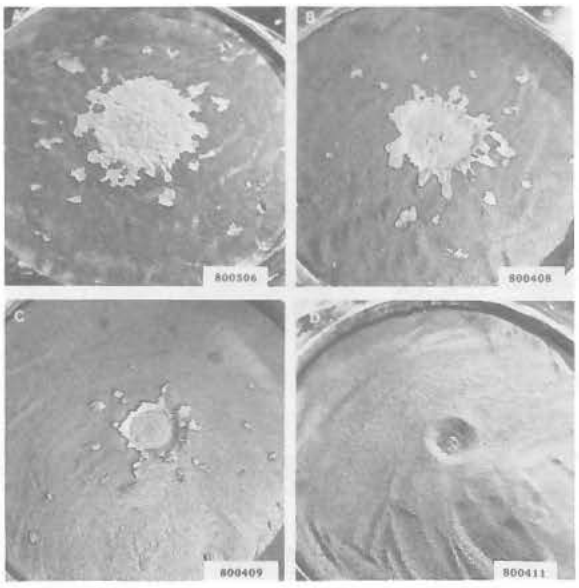

FIGURE 4. Sequence (A to D) of shots showing the smaller apparent crater diameter of impact into progressively thicker upper layer of particles underlain by viscous medium.

BASIN FORMATION: A MODEL FROM TERRESTRIAL ANALOGUES, R.A.F. Grieve and M.R. Dence, Earth Physics Branch, Dept. Energy, Mines & Resources, Ottawa, Canada K1A 0Y3

BACKGROUND: Impact structures show a morphological progression with increasing diameter from simple bowl craters to complex central peak craters, central peak basins (CPB), peak ring basins (PRB) and multi-ring basins (MRB) (1). Final crater form is a function of impact energy, modified by the effects of gravity, target and possibly the relative contributions of projectile mass and velocity to the impact energy. There are no known terrestrial structures equivalent in size to the multi-ring basins on the other planets. However, the smaller, but morphologically similar, terrestrial structures are relevant to the origin of larger basins on other planets in that they are a source of ground data and structural information. Relatively well-preserved terrestrial structures indicate different depth/D relationships for sedimentary and crystalline targets (2 - 4). This illustrates the effect of target, either strength or structure (2, 5), on form for a fixed g and projectile population. Projectile identifications at terrestrial structures are still too few to adequately determine an effect due to relative projectile mass and velocity. Theoretical considerations and computer models indicate that a shallow crater form can be produced by a low density projectile (6, 7) and it has been suggested that specific complex terrestrial craters are due to shallow excavation by cometary bodies (7). This, however, is not a requirement for complex crater forms, as the present data indicate that simple and complex structures can be produced by both irons and stones (9, 10). In addition, structural uplift data from large terrestrial craters indicates that a shallow excavation is also not a requirement for a complex form (3, 4).

Interplanetary comparisons have been restricted to the earth and moon. This minimizes projectile and target effects, as (relatively) dry crystalline targets are known on both planets and similar projectile types with equivalent cosmic velocities are likely. Comparison of the depth to the top of the breccia lens with apparent depths of lunar craters indicates terrestrial craters are shallower and the simple-complex transition occurs at a smaller D. The relative differences are described by an inverse function of g, given the dispersion in the data. (When other planets are considered, the inverse g relationship is less well defined (5), possibly reflecting target and projectile differences). If the major simple-complex transition is a function of gravity, it suggests that the other less severe changes in form, e.g. CPB to PRB to MRB, are also related to gravity. Gravity scaling of lunar transition diameters (1) gives D-25 km for terrestrial CPB's in crystalline targets, D-30 km for PRB's and D-60 km for MRB's. Although the population of large terrestrial structures is small, a case can be made for gravity scaling, e.g. Mistastin, D-28 km, has vestiges of a ring and a central peak (CPB), W. Clearwater, D-32 km, has a well-developed ring (PRB) and Popigai, inner crystalline crater D-70 km, and Manicouagan, D-75 km, have multiple rings (MRB). Unlike their lunar counterparts (14), terrestrial PRB's and MRB's have either a small topographic central peak or its structural equivalent. In general, terrestrial structures in the size range of expected PRB's and MRB's are eroded to the extent that they have little or no topography (original topography was relatively minor, probably ~500 m) and their main element is a structural uplift in the center (2 - 4). These observations agree with the suggestion that ring formation is linked to and is an extension of the factors causing central peaks (11). This inter-relationship between peaks and rings has been criticized, as the progression from CPB to PRB does not appear to hold on Mars (12). Mars, like the earth, is a geologically complex planet. It may have various target materials

BASIN FORMATION: A MODEL

R. A. F. Grieve and M. R. Dence

(crystalline, sedimentary, volatile-rich?) and there is evidence for erosion and deposition. If the classification of terrestrial structures was also based solely on remote imagery of surface characteristics, a similar uncertainty between the presence of a peak and/or ring at given diameters would occur.

THE MODEL: Uncertainties exists in virtually all aspects of basin formation and it is apparent from terrestrial, experimental and model studies that more than one process can produce ring forms. It is important therefore to discriminate between general processes and those requiring specific conditions, e.g. layered targets or cometary impacts (12, 8). The following model has as its principal constraint terrestrial data and its major thesis is that basin (ring) formation is an extension of central peak formation.

The least controversial feature of a basin is the outer rim or main outer ring (11). Morphological data on lunar MRB's suggest it is a fault scarp (11, 14). A similar conclusion is reached at terrestrial structures with the occurrence of a peripheral fault system or graben (8, 15). Remnants of post-cratonic sedimentary cover occur within this peripheral graben at some complex structures in shield areas and can be found as close to the center as 0.5 final radius (15). This suggests either the rim of the excavated cavity (EC) was $\lesssim$ 0.5 final radius or EC was shallow in this outer region. The latter is favoured in some interpretations of structures in sedimentary targets (8). The excavated cavity depth (d_e) is a source of controversy, with arguments centering on whether or not depth increases proportionally with diameter. It is our contention that the rocks stratigraphically above the uplifted and now exposed material at the center of large terrestrial structures were removed by excavation and thus the amount of uplift is a measure of d_e (3, 4). Structural uplift (SU) can be described by $SU = 0.06\ D_a^{1.1}$, which is approximately equivalent to the d_e relationship for simple craters, $d_e = 0.15\ D_a^{0.92}$, after account is taken of ~ 100% enlargement in D_a in going from simple to complex forms. This suggests proportional growth for d_e, to at least D = 140 km on earth (4).

The question remains whether it is valid to extrapolate to structures the size of Imbrium, where changes in the physical properties of the crust with depth might play a role in cratering mechanics (23). At face value, the terrestrial d_e relationship, corrected for the effects of gravity (16), suggests an event energetic enough to form Imbrium may have excavated to a depth of ~ 120 km. This depth is not equivalent to transient cavity depth or depth of sampling (17). Transient cavity depth has both excavation and displacement components (4, 15). Sampling depth is based on material that travels beyond the final rim. However, much of the excavated material will not be ejected beyond ~ 2r (~ final diameter) and is simply redistributed within the final crater (18).

Given erosional uncertainties, it appears that the physical height of terrestrial central peaks and/or rings does not exceed final crater depth (3). A similar relation occurs on the moon, where it is also apparent that peak height (and diameter) increases with final diameter (19, 20) and reaches a maximum at the transition from CPB to PRB (3). These various observations suggest a casual link between peaks and rings. A central peak is the topographic expression of structurally uplifted material and the amount of uplift and the height of the peak increases with increasing diameter (impact energy). Maximum peak height is restricted to some physical equilibrium value determined by rock properties and planetary gravity. There is, however, no similar restriction on the amount of structural uplift (3). With increasing crater size the amount of uplift increases until the central peak becomes overheightened with respect to its final equilibrium height. As a result it collapses back on itself, with the excess uplifted volume being manifested in the

BASIN FORMATION: A MODEL

R. A. F. Grieve and M. R. Dence

topographic form of a ring. Terrestrial examples suggest the position of this initial ring corresponds approximately to the rim of the original deep EC (ring spacing ~ 2). With continued uplift, the additional excess volume, which can not be accomodated in the inner ring, goes to form a second ring approximately half-way between the inner ring and D_a (ring spacing $\sqrt{2}$). This second ring may form by interaction with the inwards collapse of the outer main ring (rim). If the inner rings are produced by peak collapse, the model requires that the uplifted materials have low strengths. It is not clear how this is achieved, although it has been suggested that these conditions may exist during the early stages of impact (21). Hypotheses as to how EC modifies can be separated into "push" and "pull". The push mechanism calls for collapse following excavation, with deep centripetal sliding forcing up of the cavity floor (15). The pull mechanism considers volumetric rebound of the cavity floor following compression, possibly while excavation is still proceeding at the outer edges of the cavity (4, 22). These two mechanisms are not mutually exclusive and terrestrial data can be cited in favour of both. Shock studies indicate some volumetric reduction and minor rebound below simple craters (15). Volumetric reduction is accomplished principally by displacement and the rocks are no longer in a compressed state. However, as the cavity deepens with increasing energy, lithostatic load may increase to the point where it retards outward displacements, thus reducing compactibility and increasing the probability of significant volumetric rebound (22). Other data favour gravitational collapse, where rock strength is an important parameter (23). The smaller onset D for complex structures in sedimentary targets is more consistent with collapse, particularly as sediments may be more compactible and less liable to undergo rebound. The observation that, with the exception of the uplifted central area, the strata below the floor of complex structures are remarkably undeformed, has also been cited in favour in rebound (8, 24). However, gravity and seismic data suggest considerable fracturing within the final crater and some seismic data are interpreted as indicating inward-dipping planes of slip (25). It appears that there is evidence for both modification processes and the general case may be a competition between collapse and rebound, with each promoting the other. The problem then becomes one of relative timing.

REFERENCES: (1) Wood, C.A. and Head, J.W. (1976) PLSC 7th, 3629-3651; (2) Grieve, R.A.F. and Robertson, P.B. (1979) Icarus 38, 212-229; (3) Dence, M.R. and Grieve, R.A.F. (1979) LPS X, 292-294; (4) Grieve et al. (1980) this vol.; (5) Pike, R.J. (1980) PLSC 11th (in press); (6) Kieffer, S.W. and Simonds, C.H. (1980) Rev. Geoph. Space Phys. 18, 143-182; (7) O'Keefe, J.D. and Ahrens, T.J. (1980) LPS XI, 830-832; (8) Roddy, D.J. (1979) PLSC 10th, 2519-2534; (9) Wolf et al. (1980) GCA 44, 1015-1022; (10) Masaitis, V.L. and Sysoev, A. (1975) Lett. Astrn. Jour. 1, 43-47; (11) Croft, S.K. (1980) LPS XI, 183-185; (12) Wood, C.A. (1980) LPS XI, 1271-1273; (13) Hodges, C.A. and Wilhelms, D.E. (1978) Icarus 34, 294-323; (14) Head, J.W. (1977) IEC*, 563-573; (15) Dence, M.R. et al. (1977) IEC, 247-275; (16) Grieve, R.A.F. and Dence, M.R. (1979) Icarus 38, 230-242; (17) Head, J.W. et al. (1975) PLSC 6th, 2805-2829; (18) Stöffler D. et al. (1975) JGR 80, 4062-4077; (19) Pike, R.J. (1977) IEC, 489-511; (20) Hale, W. and Head, J.W. (1979) PLSC 10th, 2623-2633; (21) McKinnon W.B. and Melosh, H. J. (1980) LPS XI, 708-710; (22) Ullrich, G.W. et al. (1977) IEC, 959-982; (23) Melosh, H.J. (1977) IEC, 1245-1260; (24) Pike, R.J. (1980) Icarus (in press); (25) Brenan, R.L. et al. (1975) Wyoming Geol. Assoc. Earth Sci. Bull 8, No. 3. *Impact and Explosion Cratering, Pergamon.

CAVITY FORM AT LARGE IMPACT STRUCTURES: CONSTRAINTS FROM TERRESTRIAL DATA, R.A.F. Grieve, P.B. Robertson and J.F. Sweeney, Earth Physics Branch, Dept. Energy, Mines and Resources, Ottawa, Canada K1A 0Y3.

There are two opposing views as to the original cavity form in large impact structures: (i) proportional growth, in which a "deep" bowl-shaped excavated cavity, known from simple craters, grows in size with increasing impact energy and above some threshold value collapses or rebounds to form a shallow complex form (1, 2); (ii) non-proportional growth, in which the geometry of the original cavity varies with energy, becoming shallower with increasing size through some change in excavation mechanics (3), possibly associated with a shallow scaled depth of burst and low density projectiles (4). If large multi-ring basins on the planets are the high energy variants of smaller terrestrial complex central peak and ring structures, then some constraints on the form of the original cavity in multi-ring basins are forthcoming.

As terrestrial and planetological workers deal with slightly different data sets, we define the following terms: The final or apparent crater (AC) has a diameter D_a and an apparent depth (d_a) and true depth (d_t), which are measured from the rim to the top and base, respectively, of the allochthonous breccia/melt lens. Peak height (ph) is the elevation of the central peak/rings above the base of AC. Structural uplift (SU) is the amount of uplift undergone by the deepest marker horizon now exposed at the center of a complex structure. The excavated cavity (EC) is the cavity formed solely by excavation of material and the transient cavity (TC) is that formed by excavation plus the outward and downward radial displacement of the cavity base and wall. EC and TC represent hypothetical geometries in that maximum radial excavation and displacement do not occur simultaneously in all areas of the cavity.

MORPHOLOGIC AND GEOLOGIC OBSERVATIONS: The most important observations from terrestrial structures with D > 1 km are: (i) d_t/D_a and d_a/D_a relations show the well-established break in slope at the transition from simple to complex forms, occurring at 1 - 2 km for sedimentary and 3 - 4 km for crystalline targets (5); (ii) irrespective of target, ph does not exceed d_t (2); (iii) SU in complex structures is not limited by d_t and can be described by $SU = 0.06\ D_a^{1.1}$ (2); (iv) if d_t is restricted to direct estimates from drilling, simple craters have $d_t = 0.298\ D_a^{0.92}$ (n=6), an earlier estimate, $d_t = 0.326\ D_a^{0.79}$, included 3 indirect estimates of d_t based on gravity (5). This better constrained relationship now has approximately the same exponent as d_a/D_a for simple craters on earth, $d_a = 0.138\ D_a^{1.02}$, and other planets (6).

These observations are not based on results from a particular structure but apply to the total population of well-preserved and investigated terrestrial structures. Comparison with similar results from the other planets suggests the following conclusions: (i) the D_a of the simple-complex transition is a function of impact energy (2), target material and planetary g (5, 7); (ii) ph is an equilibrium height determined by target strength (5) and planetary g (2); (iii) SU is also a function of impact energy and has approximately the same exponent as the d_t/D_a relation of simple craters. Material exposed in the central uplift represents the EC base (in the absence of direct observation of SU an estimate of d_e can be obtained from the deepest unit included in allochthonous breccias). Thus this relationship for SU, by itself, argues for some form of proportional growth in EC's, which result in final D_a's ranging over 2-140 km.

It is instructive to compare further the SU relation with d_t/D_a for simple craters. The measured d_t in natural and experimental simple craters is partly due to excavation and partly to displacement (8, 9), i.e. it has more relevance

to TC than EC (10). The Brent structure (D_a = 3.8 km) is the largest known simple crater and it is estimated that 50% of d_t is due to displacement (8). On this basis, we suggest that d_e, the depth of EC in a simple crater, can be described by $d_e = 0.298/2\ D_a^{0.92}$, i.e. $d_e \sim 0.15\ D_a^{0.92}$ compared with SU = $0.06\ D_a^{1.1}$, for complex structures. Furthermore, it is apparent that $D_e \neq D_a$ in complex structures, where D_e is EC diameter. For complex structures formed in shield areas with a thin cover of platform sediments at the time of impact, it is a common observation that remnants of post-cratonic cover are preserved in the outer 50% of D_a (8). This suggests that the excavated cavity either lay within ~ 0.5 D_a or only minor near surface excavation occurred in the outer ~ 0.5 D_a (2, 8). A similar conclusion can be reached in structures totally in sediments, where reconstruction of the excavated strata indicates a "deep" central EC with none or only very minor excavation in the outer portions of D_a (4, 11). The outer rim at a complex structure, i.e. D_a, is determined by a fault scarp equivalent to an enlargement of the "deep" portion of EC by approximately 100%. Thus SU becomes ~ $0.13\ D_e^{1.1}$ in complex structures, which is very similar to the previously derived relationship from simple craters of $d_e \sim 0.15\ D_a^{0.92}$. Given the uncertainties in the data, we believe that this near identity in the two relationships argues strongly in favour of proportional growth for the depth of EC over at least nine orders of magnitude in energy, in the case of terrestrial impact structures. We note that the largest multiring basins on the terrestrial planets are only 2 - 4 orders of magnitude greater in energy than the largest impact structures on earth.

SHOCK STUDIES: These are most relevant in crystalline targets, where there is no stratigraphic control on SU but where quartz and feldspar are present. Peak pressures recorded at the base of the cavity at simple craters (Brent, > 23 GPa (12)) and at the surface in the center of complex structures (Manicouagan, W. Clearwater, L. St-Martin, ~ 25 GPa (13)) are essentially equivalent. If shock attenuation does not vary with energy, then this simple observation supports the previous conclusion that SU (complex) is equivalent to extrapolated values of d_e (simple). It has been suggested that attenuation rate does vary, specifically $P \alpha R^{-2}$-R^{-3} at simple (Brent) whereas $P \alpha R^{-4.5}$-$R^{-5.5}$ at complex structures (Charlevoix), where R is radial distance normalized to TC radius (12). There is, however, an error in this suggestion. The rate for Brent was corrected for an estimated 600 m of displacement between the EC depth and the present depth, d_t (8). The Charlevoix rate was calculated by restoring the rocks of the central uplift along trajectories derived from Gosses Bluff and fitting them to a TC extrapolated from Brent (Fig. 6 in (12)), i.e. no account was made for displacements in going from EC to TC. As displacement trajectories under the center are near vertical, no anomaly was apparent in the restoration procedure. If the Charlevoix data are recalculated accounting for Brent-like displacements, then the attenuation rates for simple and complex craters converge. The recalculated attenuation rates, normalized to estimated projectile radius, and corrected for displacements are $P \alpha r^{-1.8}$ and $P \alpha r^{-1.5}$ for Brent and Charlevoix, respectively. (Charlevoix is also assumed to have been produced by a stone). These similar natural rates are close to calculated values (14) and those measured in experimental craters of $P \alpha r^{-2}$ (15) and offer additional support for proportional growth of d_e.

Characteristic shock features are not present in the rim rocks of simple craters. Rim pressures were thus below the Hugoniot elastic limit, with estimates for natural and experimental craters generally < 2 GPa (8, 15). At complex structures, shock features are confined to the central uplifted area and generally lie closer to the center than the remnants of cratonic cover. Their position is thus consistent with the suggestion that there was little or no

CAVITY FORM: CONSTRAINTS FROM TERRESTRIAL DATA

R. A. F. Grieve et al.

deep excavation beyond 0.5 D_a.

GEOPHYSICAL STUDIES: These contribute only indirectly to our knowledge of the EC but in general are consistent with models based on geologic data. Reflection seismic data have contributed to determining SU, in particular the pre-impact position of marker horizons, and indicate that the major structural disturbance is confined to within 0.5 D_a of the center in complex structures. This central area is often surrounded by a peripheral ring depression and D_a is defined by a fault scarp (8, 11). Unless there are major density contrasts within the target rocks, terrestrial craters are gravity lows. Simple craters have negative anomalies which mirror their bowl-shaped form and result from reduced density due to fracturing around the cavity and filling by breccias. Complex craters are also lows but generally have a relative central positive axisymmetric with the overall anomaly. This positive does not rise above the regional level. A gravity signature of this type can be modelled as a central block of target material of relatively reduced fracture porosity compared to a surrounding annulus of more extensively fractured material. This is consistent with the rocks of the central uplift being relatively compressed (seen as bed shortening, reverse faulting (11)). The compression arises from the geometries of a deep EC and final crater form. There is a relative volume reduction in uplifting the base of the EC to its position at the surface, with the amount of volume reduction being greatest at the center. Although generally less constrained, gravity models of specific impact structures give d_e values in the same range as those derived from geologic and shock studies (16). The terrestrial gravity data also suggest that the massive positives over large lunar basins, such as Orientale, are not a function of the cratering process itself but are due to a density contrast within the basin, possibly produced by the uplift of relatively dense sub-crustal or mantle material.

CONCLUSION: We believe that the above data are inconsistent with a shallow depth of burst and shallow EC as the general process leading to the formation of complex crater forms. We do not disagree that low density projectiles will have shallow penetration depths and may produce shallow EC's. However, there is now sufficient evidence to demonstrate that complex crater forms also result from the impact of various types of stony and iron projectiles (5, 17). We consider that the terrestrial data are more consistent with models that call for some form of proportional growth to the excavated cavity, up to and including impact energies sufficient to form multi-ring basins, and its subsequent modification to the final crater form (2, 7).

REFERENCES: (1) Dence, M.R. (1973) Meteoritics, 8, 343-344, (2) Dence, M.R. and Grieve, R.A.F. (1979) LPS X, 292-294, (3) Settle, M. and Head, J.W. (1979) J.G.R., 84, 3081-3096, (4) Roddy, D.J. (1979) PLSC 10th, 2519-2534, (5) Grieve, R.A.F. and Robertson, P.B. (1979) Icarus, 38, 212-229, (6) Pike, R.J. (1980) Icarus (in press), (7) Grieve, R.A.F. and Dence, M.R. (1980) this vol., (8) Dence et al. (1977) IEC*, 247-276, (9) Borg, I.Y. (1972) Amer. Geophys. Union Mono. 16, 293-311, (10) Croft, S.K. (1980) LPS XI, 180-182, (11) Brenan, R.L. et al. (1975) Wyoming Geol. Assoc. Earth Sci. Bull. 8, No. 3, (12) Robertson, P.B. and Grieve, R.A.F. (1977) IEC, 687-702, (13) Simonds et al. (1978) LPS IX, 1065-1067, (14) Ahrens, T.J. and O'Keefe, J.D. (1977) IEC, 639-656, (15) Cooper, H.F. (1977) IEC, 11-44, (16) Sweeney, J.F. (1978) J.G.R. 83, 2809-2816, (17) Wolf et al. (1980) G.C.A., 44, 1015 - 1022.
*Impact and Explosion Cratering, D.J. Roddy, R.O. Pepin and R.B. Merrill, eds., Pergamon Press.

THE ORIGIN OF PEAK RINGS AND THE CRATER TO BASIN TRANSITION. Hale, W., and Head, J. W., Dept. of Geological Sciences, Brown Univ., Providence, RI 02912

Impact basins are distinguished from craters by the presence of prominent concentrically developed structures.[1] Peak ring basins display an inner concentric ring of massifs termed a peak ring while multi-ringed basins are characterized by the presence of a peak ring surrounded by two or more inward-facing scarps.[2,3] In contrast, complex craters (diameter >10km) are characterized by a prominent central peak surrounded by flat floors and terraced walls.[4,5,6] Central peak basins, which display both central peaks and basin rings, have been suggested to be transitional between craters and basins.[3] These primary morphologic characteristics are believed to reflect the partitioning of impact energy into the target and the target's subsequent mechanical response.[7,10] The transition from crater to basin morphology, characterized by the appearance of a peak ring, may thus reflect significant changes in the mechanical response of the target to impact. As such, it is the subject of much interest and ongoing debate.[11,14] A transition from central peak craters to peak ring basins has been proposed to occur on the Moon at rim diameters from 150-200km where central peak basisn occur.[3,12]

Studies to date have demonstrated a linear relationship between peak ring diameter (Dpr) and basin rim diameter (Drc)[13] and between central peak diameter (Dcp) and crater rim diameter (Drc) on the Moon.[15] The basin Dpr/Drc relation remains constant on Mercury and Mars[14], and the crater Dcp/Drc relation also applies in Mercurian craters.[17] These two curves have markedly different slopes indicating that central peak and peak ring diameters increase at different rates relative to rim crest diameters. Further, these two relationships do not intersect at the diameter range where the central peak basins Antoniadi and Compton are observed (Figure 1). The purposes of this work are: 1) to summerize the morphologic and morphometric data for central peak craters and peak ring basins; 2) detail the morphology and morphometry of the recognized 'transitional' central peak basins; 3) review the presently proposed models for peak ring formation; 4) look for evidence of peak ring precursers in large craters. Since high resolution images and topographic data are available only for the Moon, this study concentrates on lunar craters and basins. Data is derived from Lunar Orbiter and Apollo imagry and NASA/DMA Topographic Orthophotomaps.

Central Peak Craters - a linear relationship has been defined between central peak diameter (Drp) and rim crest diameter (Drc), Dcp=0.20 Drc +0.42 for lunar craters from 17-175km in diameter.[15] Morphologically, central peaks may be classified by complexity (simple or complex) and geometry (linear, symmetric or arcuate). Neither complexity nor geometry shows a strong dependence on rim diameter and central peaks show no strong trend towards increasing complexity at large crater diameters.[15]

Peak Ring Basins - peak rings consist of concentrically oriented arcs of massifs surrounding a central basin. Individual massifs resemble central peaks developed in craters.[3] A linear relationship has been defined between peak ring diameter (Dpr) and basin rim diameter (Drc), Dpr=0.56 Drc-17.55 for 12 lunar peak ring basins.[13]

Central Peak Basins - the recognized central peak basins Antoniaid (Drc=140km) and Compton (Drc=175km) have peak ring diameters consistant with the Dpr/Drc curve for large basins (Figure 1). Both have simple, symmetric central peaks which morphologically resemble those developed in large craters, but are smaller than would be predicted from the Dcp/Drc relation (Figure 1). Surrounding the peak within the peak ring the basin floor appears relatively

PEAK RINGS AND CRATER TO BASIN TRANSITION

Hale, W.

smooth (inner floor). Outside the peak ring the floor is notably rougher, with a knobby texture (outer floor). In both Antoniadi and Compton inner floor material appears to flow around or between the peaks of the ring. In Compton, lobate flow edges are discernable just outside the ring, where outer floor is overlain by inner floor.[16]

Peak Ring Models - the origin of basin peak rings has been examined by many workers and two models currently exist. The first suggests that the peak ring represents a second or nested rim crest created by the interaction of the propagating shock wave with density discontinuities at depth. This interaction is predicted to result in differential excavation in the deeper layer, resulting in a pair of nested craters. Cintala et.al.(1977)[6] have related the occurrance of central peaks in small craters to terrain type and found that more coherent targets favor peak development. From this, the abrupt increase in density at depth required for the formation of a nested crater[11,12] would be expected to encourage the development of a central peak within the nested crater (peak ring). However central peaks cease to appear at diameters much above those where peak rings are observed.[2,3]

Alternatively peak rings have been suggested to form through disruption of the central peak at increasingly large crater diameters.[2,12,13] In this model peak fragments would form a concentric ring in the rim diameter range of (140-180km) where central peak basins occur. However, studies of central peak morphology demonstrate no strong trend towards increasing peak complexity (disruption) at large crater diameters.[15,17] Thus, neither of these models seems sufficient to explain the morphology of central peak craters and peak ring basins. In addition, both of these models would predict the beginning of peak ring formation at the diameter(Drc=140-180 km) where central peak basins are first observed. However, as discussed earlier, the intersection of morphometric relationships would more naturally predict the beginning of peak ring formation at rim diameters as small as 50km (Figure 1). Thus the floors of large (Drc >50km) craters should be investigated for evidence of structural precursers to the peak ring.

Peak Ring Precursers - workers have long noted the presence of large hummocks and knobby patches on the floors of craters larger than 50km in diameter. Detailed images and/or topographic data is available for the floors of four such craters: Tycho, Copernicus, Theophilus and Langrenus. Floor hummocks in these craters are distinguished from central peak material by an order of magnitude of relief. Small floor hummocks (10-100m of relief) extend in general from crater walls to the central peaks. But, the largest hummocks (100's m relief 10-100's m across) in all four craters form a discontinuous ring around the central peak. Measurements of wall widths at points of maximum and minimum floor roughness indicate no correspondance between the degree of wall slumping and the degree of floor roughening. Thus floor hummocks are not considered to be toes of slump blocks from the walls. Finally, the diameter of the discontinous ring of large floor hummocks is consistent with the peak ring diameter predicted by the Dpr/Drc relationship for each of these four large craters.

Discussion - current models for the formation of basin peak rings appear insufficient to explain: 1) the low intersection diameter of primary crater and basin morphometric relationships; 2) the morphology of central peak basins and the lack of central peaks in peak ring basins; 3) the lack of a strong trend towards central peak expansion at large crater diameters. Thus the mode of origin for peak rings remains uncertain. The presence of discontinuous rings of large floor hummocks in craters may provide important clues for the formation of basin peak rings. We are presently examining

PEAK RINGS AND CRATER TO BASIN TRANSITION

Hale, W.

evidence for peak ring precursers in additonal lunar craters, and terrestrial central uplift craters in an effort to better characterize the crater to basin transition. References: [1]Hartmann,W.K. and Kuiper, G.P. (1962) Comm. LPL v. 1 p. 51-66. [2]Hartmann, W. K., and Wood, C.A. (1971) The Moon 3, p. 2-78. [3]Wood, C. A. and Head, J. W. (1976) PLSC 7 p. 3629-3651. [4] Dence, M. R. (1965) Ann. N.Y. Acad. Sci. 123, p. 941-969. [5]Wood, C. A. and Anderson, L. (1978) PLPSC 9, p. 3669-3689. [6]Cintala, M. J., et al (1977) PLSC 8, p. 3409-3425. [7]Baldwin, R. B. (1963) The Measure of the Moon, p. 128. [8]Gault, D. W. and Heitowit, E. D. (1963) Proc. 6th Hypervel. Imp. Symp. 2 p. 419-459. [9]Gault, D. E. et al (1975) JGR v. 80, p. 2444-2459. [10]Pike, R.J. (1977) in Impact and Explosion Cratering p. 481-487. [11]Wilhelms, D. E., et. al. (1977) in Impact and Explosion Cratering p. 539-562. [12]Hodges, C. A. and Wilhelms, D. E. (1978) Icarus 34, p. 294-323. [13]Head, J. W. (1978) in Impact and Explosion Cratering, p. 563-573. [14]Head, J. W. (1978) LPS X, p. 485-487. [15]Hale, W. S., and Head, J. W. (1979a) PLPSC 10, p. 2623-2633. [16]Hale, W. S. and Head, J. W., (1979b) NASA TM-80339, p. 160-162. [17]Hale, W. S. and Head, J. W. (1980) LPS XI, p. 382-384.

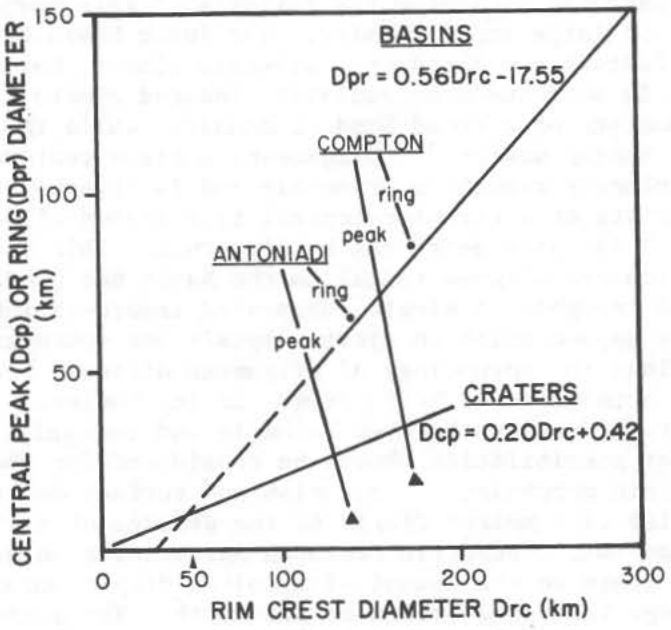

Figure 1 - Plot of Dpr/Drc relation for basins and the Dcp/Drc relation for craters. Intersection occurs at Drc = 50 km. Central peak basins Antoniadi and Compton are also plotted. Triangles and central peak diameters, circles are peak ring diamerts.

ORIGIN OF THE VALHALLA RING STRUCTURE: ALTERNATIVE MODELS. Hale, W., Head, J.W. and Parmentier, E.M., Dept. of Geological Sciences, Brown Univ., Providence, RI 02912.

Images acquired by the Voyager spacecraft have shown the existence of prominent multi-ringed features on the surface of Callisto.[1] Valhalla, the largest and best imaged, is centered at 10^0, 55^0.[1] Although unquestionably comprised of ring-like concentric structures, Valhalla differs in several important respects from multi-ringed impact basins on the silicate planets, including the large multiplicity of rings, lack of a topographic basin and lack of radially lineated ejecta.[1,2] These differences suggest the possibility of formational mechanisms other than those associated with impacts. This study utilizes multiple working hypotheses to analyze the present morphology of Valhalla in an effort to relate these to its formational mechanisms.

Valhalla consists of a bright, roughly circular central region surrounded by an extensive ring system. Rings appear as relatively narrow, high albedo sinuous features separated by wide, dark regions. Scarps, where observed, face outward[2], and impact crater density increases outward from the bright central region.[1] No mountain or massif rings are observed.[1] Although an impact origin has been suggested for Valhalla[1,9], this morphology differs greatly from that of large impact basins. The lunar basin Orientale, a relatively fresh feature developed on a silicate planet, has only three concentric rings and is surrounded by radially lineated ejecta deposits. The innermost ring consists of a broad band of massifs, while the outer two rings consist of inward facing scarps.[3-6] Gilgamesh, a basin centered at -60, 125^0 on Ganymede more closely resembles Orientale and is probably of impact origin.[7,8] It consists of a circular central flat region ~175 km in diameter[7] within which 4 or 5 isolated peaks can be discerned. This is surrounded by blocky massifs which are aligned radial to the basin and grade outward into radial grooves and troughs. A single, segmented inward-facing scarp forms the outermost ring beyond which an ejecta deposit and secondary crater chains are developed.[7] Thus the morphology of Gilgamesh differs from that of Valhalla, despite both features being formed on icy bodies.

The important differences between Valhalla and recognized impact basins suggests that other possibilities should be considered for the origin of Valhalla's concentric morphology. Volcanism and surface deformation associated with the rise of a molten diapir or the descent of a lithospheric diapir may also generate concentric features surrounding an area at high albedo. We concentrate on the ascent of a molten diapir analogous to the emplacement of large intrusive bodies on the Earth. The purpose of this work is: 1) to examine the morphology of Valhalla structures; 2) to determine the expected morphological expression of a large impact and the near-surface emplacement of a molten diapir; and 3) to relate these expected morphologies to the origin of Valhalla. Data is derived from Voyager I and II images.

Morphology of Valhalla - Valhalla may be divided into 4 discrete zones based on the degree of ring development (Figure 1). Zone I consists of the bright central core of the ring system which has an average radius of 350 km in its eastern portion. No high resolution coverage of this zone is available at present, but medium resolution images suggest a granular texture and the presence of small dark areas. No rings are detectable within this zone. Zone II begins at the first occurrence of rings, and varies in width from ~200 km in the southeast to 330 km in the northeast. Rings in this region consist of fairly continuous bright, narrow bands separated by wider, intermediate albedo terrain. These narrow, bright rings appear sinuous to

VALHALLA RING STRUCTURE

Hale, W.

scalloped in map view. Zone III is characterized by weak to discontinuous ring development and varies in width from ~400 km in the southeast to ~200km in the northeast. Occaisioral rings in this zone form short segments morphologically similar to the more continuous rings developed in Zone II. Zone IV, the outermost region of ring development, displays wide variations in width and ring morphology. In the south and east, Zone IV is ~550km wide. Rings here consist of narrow, bright-floored, sinuous troughs or furrows separated by wider, low albedo, heavily cratered terrain. To the northwest, the width of Zone IV increases greatly to 1400km. In this wider region, rings are developed to a radial range of 2330km from the center of the system. In the region where Zone IV widens, the furrow rings of the south merge into rings of a different type, consisting of outward-facing scarps with dark, heavily cratered backslopes. Bands of lighter material occur below the scarp faces, grading onto the backslope of the next scarp ring outward and flooding crater rims. Where scarps cut completely preserved craters no displacements or shortening of the crater can be detected. Scarp rings merge outward and northward with very narrow furrow rings which have higher outward-facing sides. In addition to these various ring types, a single bright ray-like feature is developed across Zones II and III in the northeast and 3 possible crater chains are discernable in the east and southeast. Thus Valhalla's concentric rings show azimuthal asymmetric in both morphology and radial range.

Formation by Impact - By analogy with Orientale (silicate target) and the Gilgamesh (icy target), a large impact would be expected to produce extensive radially lineated ejecta deposits, crater chains, and concentric rings. The innermost ring should consist of concentric peaks or massifs (peak rings). The next ring outward should be an inward-facing scarp which approximates the rim of the crater cavity.[3,4,6] Succeeding rings should consist of inward-facing scarps.[4,6] Melosh and McKinnon have suggested that impact basin rings could form by faulting in a thin brittle layer. Stresses in this layer result from the inward flow of underlying viscous material and shallowing of the transient cavity. This model predicts the number and spacing of rings to be a function of lithospheric (brittle layer) thickness at the time of impact.[11] According to the model, outer scarp rings are the result of downward and inward motion of material along concentric normal faults. However, strike-slip rather than normal faults would be expected to form in response to the compressional radial and hoop stresses predicted by this model. Viscous relaxation of a transient crater cavity on a thick viscous layer results in isostatic doming of the surface that is neglected by this model. The stresses in the near surface brittle layer due to the combined affects of flow in an underlying viscous layer and surface uplift would be more favorable for the formation of normal faults.

Formation by Diapiric Emplacement - By anology with well-studied terrestrial igneous intrusions[12,13], the ascent of partially molten material can cause surface doming and stresses in a near surface brittle layer which lead to the formation of cone sheets. These nested conical sheets which extrapolate to a common vertex at depth are made up of material intruded from the magma body. In map view, cone sheets would have the form of narrow multiple concentric rings of intruded material.[13,14] Surface doming above the ascending magma body can be accomodated by the emplacement of intruded material and shear displacements along the cone sheets. Continued ascent into the brittle layer may allow a region of the surface above the intruding body to collapse downward, forming a caldera.[14] The caldera may be subsequently flooded by volcanic materials derived from the intruding magma body.[14]

VALHALLA RING STRUCTURE

Hale, W.

Discussion - An impact model for the formation of Valhalla would predict inward-facing scarps, a central topographic basin, radially lineated ejecta deposits and crater chains. Viscous flow in the target leading to reduction in topographic relief has been suggested to account for the lack of a basin associated with Valhalla.[1] Ring assymetry could result from regional variations in lithospheric thickness or from oblique impact. Decreasing crater counts inward[1] could result from the emplacement of a non-lineated ejecta deposit. Current impact models do not, however, appear to explain the observed morphology of Valhalla's rings.

Alternatively, the near surface emplacement of a partially molten diapir could produce concentric intrusive cone sheets. On Callisto, such intrusive material would be expected to be silicate poor and therefore have a high albedo. The bright floors of furrow rings as well as the bright flooded backslopes of scarp rings could be explained by the emplacement of such material. Surface doming above the magma body, accomodated by shear displacement and progressive thickening of cone sheets, could generate the outward-facing scarps in northeast Valhalla. Caldera collapse and flooding by silicate poor material could produce the bright central core. The regional asymmetry of the rings and the possible existence of crater chains is less easily explained by this model.

At present, insufficient evidence exists to firmly establish either impact or diapiric mechanisms for the formation of Valhalla's complex structure. More detailed modelling currently underway of: 1) viscous degradation of impact structures; 2) emplacement of an ascending molten diapir; 3)descent of a sub-lithospheric diapir, will help to develop criteria to compare with Voyager observations of Valhalla's structure.

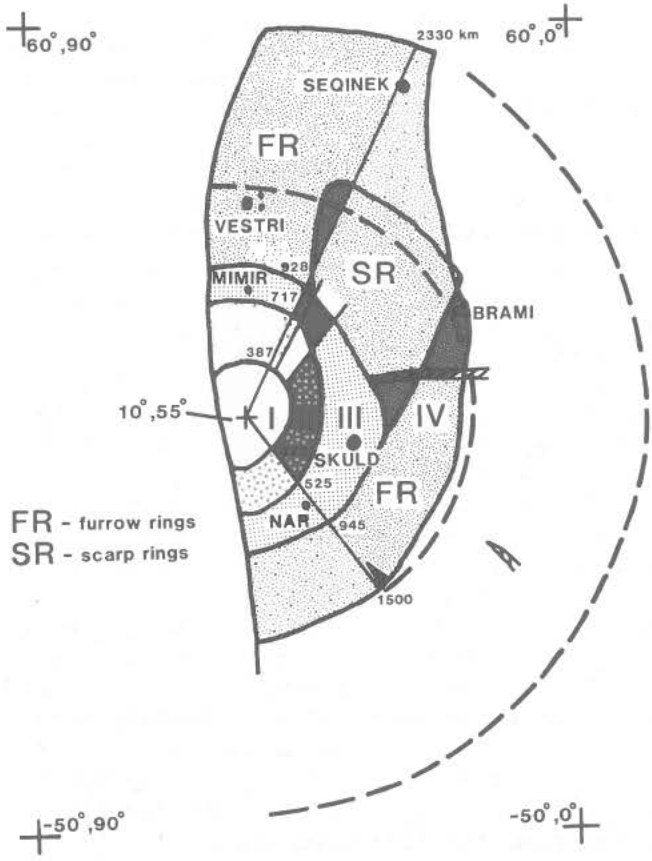

References: [1]Smith,B.A.,et al., (1979) Science 204 p.951-971. [2]Hale,W.S. (1980) IAU Coll.No.57, 6-17. [3] McCauley,J.F., (1968) U.S. G.S. Inter Ag. Rep. p.32-33. [4]Head,J.W. (1974) The Moon 11, p. 327-356. [5]Howard,K.A. et al., (1974) Rev. Geophys. Space Phys. 12, p.309-327. [6]Head,J.W. (1977) in Impact and Explosion Cratering, p.563-573. [7]Smith,B.A., et al., (1979)Science 206 p.927-951. [8]Passey,Q.R., et al.,(1980) IAU Coll. No.57, 6-8. [9]Melosh,H.J. & McKinnon,W.B.(1980) IAU Coll.No. 57,7-7. [10]Parmentier,E.M. & Head, J.W.(1979)PLPSC 10,p.2403-2419. [11]Melosh,H.J. & McKinnon,W.B. (1978)GRL v.5 p.985-988.[12]Richey, J.E.,(1961)in Scotland: the Tertiary Volcanics District p.55-62. [13] Anderson,E.M.(1963)Proc.Roy. Soc.Edin. Vol.56 p.128-157.[14]Smith R.L. & Bailey,R.A.(1968)GSA Mem. 116 p.613-662.

Figure 1-Sketch map of Valhalla. Dotted lines are min. and max. radius of Zone IV. See text for details.

A MODEL FOR IMPACT BASIN EVOLUTION. Jack B. Hartung, Planetary and Earth Sciences Division, NASA Johnson Space Center, Houston, TX 77058.

The largest impacts on terrestrial planets form multiring impact basins. Essential characteristics of this process are (1) excavation of material at the impact site, (2) deposition of that material over an area surrounding the impact site, (3) filling of the short-lived, or transient, crater mainly by material which originally was located below the transient crater and radially outward from its axis, and (4) downward motion or collapse of surrounding areas which received ejecta deposits. Part of the crater may be expected to be filled by material moving downward and inward from the crater walls. Thus, a material transport cycle is initiated by a large impact, outward above the surface, upward along the crater axis, inward below the surface, and downward in surrounding areas. Considerable experimental, field, and theoretical work supports this general picture of basin formation. The details of how transient craters are filled are subject to controversy, as is the mechanism for concentric ring formation. However, how these controversies are resolved does not affect the following discussion of the subsequent evolution of impact basins.

After the formation of an impact basin is complete, probably hours to days after the impact, topographically it may be described as low in the middle surrounded by a concentric high. Another important characteristic, which is less easily established, is the distribution of mass below the surface or the extent to which isostatic equilibrium or disequilibrium prevails. First, the process of filling the transient crater during the formation of the basin is a process which seeks to restore equilibrium. Secondly, to establish and maintain a disequilibrium configuration requires either material strong enough to withstand the attendant stresses or a continuous driving mechanism and a corresponding source of energy. Rocks are strong enough to withstand stresses due to several kilometers of topographic relief, but they are not strong enough to withstand stresses associated with several tens of kilometers of topographic relief, which would be typical of transient craters leading to basins. Finally, no driving mechanism is known which would maintain a disequilibrium configuration following a large impact. Therefore, we are led to the view that during the formation of large impact basins the affected region achieves or approaches a state of isostatic equilibrium. This is equivalent to saying that a column of material of a given cross-sectional area to a given depth taken at the center of the basin contains very nearly the same amount of mass as a similar column taken outside the basin rim.

Basin evolution on a planet begins with a topographic low at the center, a surrounding topographic high, and both areas approximately in isostatic equilibrium with respect to each other. This configuration requires only that the mass defficiency corresponding to the central topographic low be compensated for by more dense material uplifted beneath the basin floor. In the absence of any subsequent mass transport processes this configuration, being in equilibrium, is a stable one. No further motions would be expected; the basin would remain unchanged indefinitely. An example of this type of basin is Mare Orientale on the Moon, if the minor amounts of basalt within the basin are ignored.

If significant lateral transport of material occurs, such as basalt flows, wind-blown deposits, or water-borne sediments, there will be a strong tendency for material to accumulate in topographically low areas, that is, in impact basins. Such an accumulation represents a mass addition at the center of the basin. If the deposited material is derived from surrounding topographically higher areas, a mass loss occurs from these areas. These processes act so as to disturb the initial state of isostatic equilibrium. If the materials

IMPACT BASIN EVOLUTION

Jack B. Hartung

involved are not strong enough to withstand the newly introduced stresses, the system will react in a way to move the system back toward equilibrium. The central part of the basin will sink while the surrounding area undergoes uplift. The mass addition at the basin center due to deposition is compensated for by the sinking of once-uplifted more dense material, so that the total mass in a column at the center remains essentially the same. During basin evolution a reverse material transport cycle develops; inward at or above the surface, downward at the basin center, outward below the basin, and upward in surrounding areas.

If we assume that the time scale on which the system is capable of sinking, that is, the time scale for isostatic response, is short compared to the time scale for material accumulation on the basin floor, then the rate of sinking will be controlled by the rate deposition. If deposition is very slow or even stops, then sinking will be slow or will stop. Examples illustrating this characteristic are the Argyre and Hellas basins on Mars, which may be described as partially submerged as a result of apparently very slow accumulation of dust and possibly basalt flows or other sediments. Basalt-filled basins on the Earth-facing side of the Moon, such as Nectaris and Crisium,are also only partially submerged.

A natural limit to basin subsidence will be reached when both isostatic and topographic equilibrium are established in the region of the impact. The center of the basin will continue to receive material and the basin floor will continue to subside until the uplifted more dense material below the basin is "pushed" back down to the approximate level it maintained before the impact occurred. Correspondingly, the surrounding area will rise until the down-dropped more dense material reaches approximately the position it occupied before the impact. If the density of the material filling the basin is different from that of the surrounding rocks, then the pre-impact configuration of the underlying rocks may not be recovered exactly.

Although no example of an impact basin representing this final state has been positively identified, we may use this model in the search for evolved impact basins on the Earth, where sedimentation rates are much higher than on the Moon or Mars. What we should expect to find to mark the site of a basin-forming impact on the Earth is a circular sedimentary basin. The rim and ejecta material would be expected to have been lost to erosion; and the impact basin floor may have sunk, essentially, "out of sight."

A candidate structure which displays these characteristics and deserves further investigation is the Michigan Basin. Interestingly, relatively shallow-water sediments up to a thickness of about 4000 meters were being deposited in the Michigan Basin throughout most of the Paleozoic era and as recently as the upper Jurassic period, a time interval of about 400 million years from about 550 to 150 million years ago. Such a long period of sedimentation and associated subsidence is not readily explained in terms of plate tectonic processes but is consistent with subsidence controlled by the sedimentation rate.

Shown in Figure 1 are schematic drawings which represent cross-sections through the region of an impact basin at different times during its evolutionary history. At each stage and from one stage to the next the drawings are consistent with a state of continued isostatic equilibrium. Uncertainty in the behavior of material in the vicinity of the basin rim is indicated by dashed lines.

The author is a National Research Council Senior Postdoctoral Research Associate at the NASA Johnson Space Center.

IMPACT BASIN EVOLUTION

Jack B. Hartung

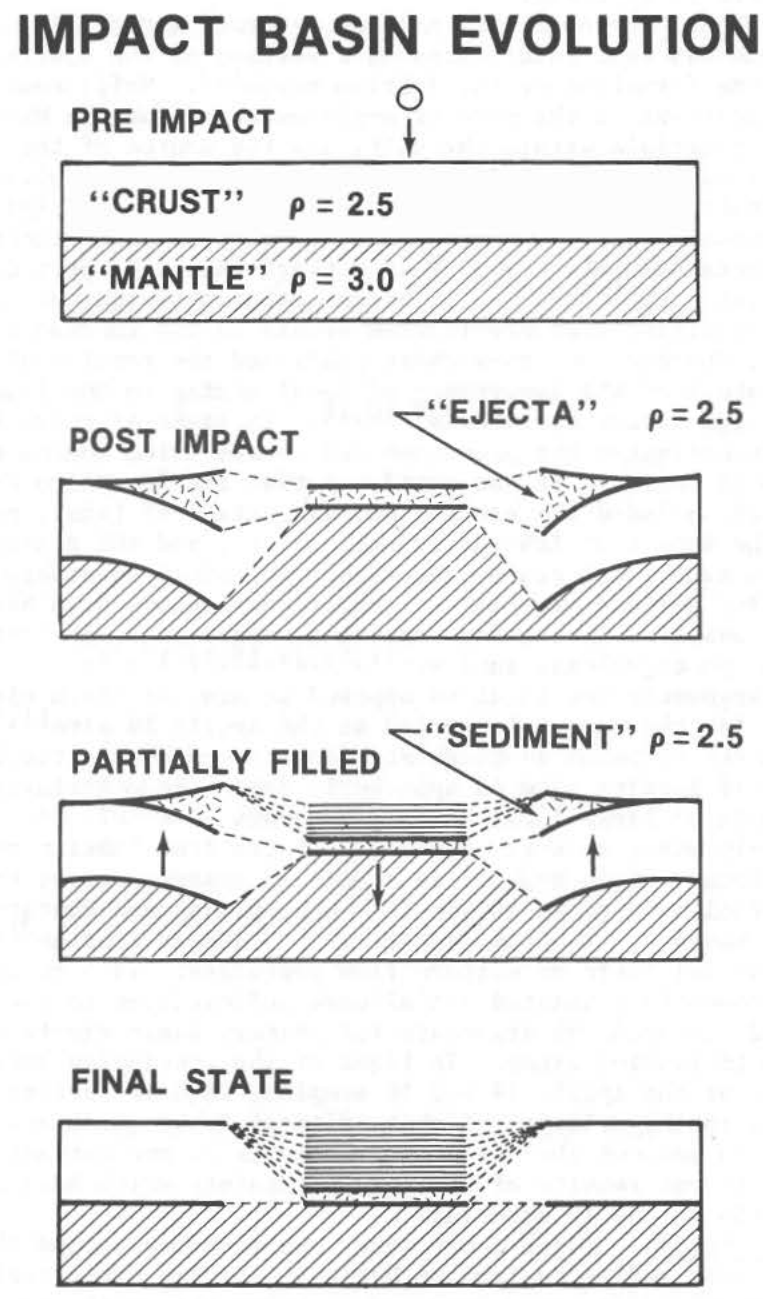

THE DISTAL DEPOSITS OF LUNAR BASINS AS EXEMPLIFIED BY MATERIAL COLLECTED AT THE APOLLO 14 AND 16 LANDING SITES. B.R. Hawke, Hawaii Inst. of Geophys., Univ. of Hawaii, Hon., HI 96822; J.W. Head, Dept. of Geological Sci., Brown Univ., Prov., RI 02912.

Introduction: The Apollo 14 mission returned material from the Fra Mauro Formation which has been interpreted as a portion of the ejecta blanket deposited during the formation of the Imbrium basin[1,2]. Major controversy has centered on questions of the mode of emplacement of the Fra Mauro Fm., the provenance of materials within the unit, and the source of the range of thermal effects exhibited by the returned samples. Preliminary results of sample studies were thought to be consistent with an Imbrium ejecta origin and the variety of thermal effects was attributed by some to the autometamorphism of a thick, hot ejecta blanket[3,4,5]. Other workers have interpreted the Fra Mauro Fm. as a deposit derived from the Imbrium crater but with the range of metamorphic effects resulting from pre-Imbrian events in the Imbrium target site[6,7,8]. More recently, Oberbeck and co-workers published the results of numerous studies which emphasized the importance of local mixing in the formation of distal deposits of large impact structures[9,10,11]. In light of these findings, Head and Hawke[12] investigated the processes and events which dominated the history of the Apollo 14 region. It was concluded that the Fra Mauro Fm. was formed by a process which included the erosion and excavation of local, pre-Imbrian material by the impact of Imbrium primary ejecta, and the mixing of this Imbrium ejecta with local crater deposits, to produce an ejecta blanket dominated by locally derived material. Similar conclusions have been reached in other studies based on laboratory cratering experiments, theoretical cratering mechanics, and photogeologic analysis[11,13,14,15,16,17,28].

Similar arguments for local as opposed to distant basin ejecta origin have been advanced for the material sampled at the Apollo 16 site[11,13,18]. According to the hypotheses proposed in these studies, the general stratigraphic sequence at the Apollo 16 landing site is apparently dominated by Nectaris basin deposits and the products of large local cratering events (see Ref. 18, p. 91) and contains relatively minor amounts of primary ejecta from Imbrium and Orientale basins. The local origin hypothesis stands in sharp contrast to suggestions that the material sampled at Apollo 16 (Cayley plains and Descartes Mts.) represents primary basin ejecta from Orientale[19,20] and/or Imbrium[21,22] basin that was emplaced by ballistic or surface flow processes. In a recent publication, Wilhelms and co-workers pointed out alleged deficiencies in the local mixing hypothesis and restated the arguments for primary basin ejecta deposits at the Apollo 14 and 16 landing sites. In light of the continuing uncertainty as to the provenance of the Apollo 14 and 16 samples, we have initiated a variety of studies to aid in the solution of this critical lunar question. The purpose of this paper is to present the preliminary results of our current research and to summarize the recent results of other investigators which have relevance to the origin of Apollo 14 and 16 material.

Fra Mauro region: Major controversy has centered around the nature and origin of features radial to Imbrium basin in the Fra Mauro region. We have re-analyzed these radial structures and compared them with analogous features around Orientale basin. Numerous large (4-13 km in width) radial grooves were identified. These grooves appear to be akin to Imbrium sculpture and are clearly erosional as opposed to depositional in origin. These grooves slash topographic features with little regard for pre-existing terrain. The grooves exhibit roughly parallel walls having a scalloped or crater-form aspect. These large radial features are interpreted as Imbrium sceondary chains. Where best preserved, individual, clearly defined secondary craters can be identified. The large ridges between the large secondary chains appear to be erosional

DISTAL BASIN DEPOSITS

B.R. Hawke and J.W. Head

remnants modified by the later debris surge. Little evidence was found to support the argument that these large ridges are flows or features resulting from surface flow.

Many smaller radial features have been identified at a variety of scales. One class of such radial features ranging from 0.5 to 5 km in width was mapped by Eggleton[27] and Head and Hawke[12] and interpreted to be secondary crater chains formed by Imbrium ejecta. New mapping has established the existence of these features in the immediate vicinity of the Apollo 14 landing site. A series of very small ridges have been mapped in the Fra Mauro region and appear to be analogous to the braided texture seen in the Hevelius Formation.

An attempt has been made to calculate the percentage of Imbrium primary ejecta actually present in the Fra Mauro Fm. at the Apollo 14 site. Eggleton[27] first noted that some local, pre-Imbrium material was probably incorporated into the Fra Mauro by the impact of Imbrium secondary projectiles but no quantitative estimates were made. Morrison and Oberbeck[13] presented the results of calculations which suggested that the Fra Mauro contained between 15% and 20% Imbrium material. We have made similar calculations based on the equations and assumptions presented by Oberbeck and co-workers[11,13] and using the measured diameters of Imbrium secondaries. As noted above, these secondaries range from about 0.5 km to 13 km in diameter with the larger structures being concentrated in chains 25 to 50 km east of the landing site. The identifiable secondary craters and crater chains in the immediate vicinity of the Apollo 14 site are about 1-2 km in diameter. If impact angles of 15° and 30° from the horizontal are assumed, the calculations yield values of 9.5% to 19% for the amount of Imbrium primary ejecta in the deposits of these secondary impact structures. Values for the surrounding region range from 7% to 32%.

Objections to the local mixing hypothesis have been raised on the basis of the inferred size of basin ejecta fragments and the supposed scarcity of secondary craters[20,29,30,31]. Morgan et al.[29] assumed that the bulk of distant basin ejecta was of millimeter to decimeter size. They describe a process in which the first material to arrive mixes thoroughly with the local regolith to a depth on the order of the diameter of the larger fragments (~10 cm) and successive 10 cm layers mix with material containing progressively larger amounts of basin ejecta thus diluting the concentration of local material in the deposit to the degree where it is no longer important. However, recent work has demonstrated that secondary craters from Imbrium basin are much more common than had been previously recognized[32,12,13]. Apparently these craters were formed by either large individual blocks of Imbrium ejecta or by clumps of smaller fragments that are launched on similar trajectories and thus act as a single body in ballistic flight and upon impact with the surface[14,15]. Morrison and Oberbeck[15] reviewed evidence to support the idea that large masses of jointed rocks can remain intact after ejection from the crater.

Additional support for a local as opposed to Imbrium ejecta origin for the Fra Mauro samples has been obtained by analyses of petrologic and geochemical data for the Apollo 14 samples and remote sensing data for the Fra Mauro region. This evidence was discussed in detail by Hawke and Head[16,17].

Descartes Region: Many of the arguments advanced in support of the local origin of the bulk of the Fra Mauro Fm. also apply to the Apollo 16 site. While it is not our purpose to present a detailed view of Apollo 16 site geology at this time, certain points should be discussed and emphasized.

First, the effect of material ejected by Orientale basin on the Apollo 16 region seems minimal[18]. McGetchin et al.[24] predict less than 2 m average thickness at the Apollo 16 site. No Orientale secondaries have been identified in the Apollo 16 region and studies of Orientale basin secondaries and secondaries show a distinct lack of these structures in the quadrant toward the Apollo 16

DISTAL BASIN DEPOSITS

B.R. Hawke and J.W. Head

region. A thin blanket of Orientale ejecta in the central highlands appears to be ruled out by systematic east to west changes in the composition of the central highlands as revealed by the Apollo orbital geochemistry data[17,25].

The Descartes region was affected by the formation of Imbrium basin. The region is surrounded by a variety of features radial to Imbrium. Imbrium sculpture interpreted to be the product of the impact of Imbrium secondary-forming projectiles, is particularly well-developed NW of the landing site where these radial structures cut the rims of Dollond B and C. More clearly defined Imbrium secondary chains are superposed on Descartes Mts. material north and south of the site. Major quantities of local, non-Imbrium ejecta must have been incorporated into the deposits of these Imbrium secondaries. Morrison and Oberbeck[13] presented the results of calculations based on the measured diameters of Imbrium secondaries in the Descartes region which indicated that deposits emplaced by Imbrium secondary craters at the Apollo 16 site could contain only 13-18% primary Imbrium ejecta. These estimates may overestimate the actual percentages because of effects of surface scour by the subsequent debris surge and the dilution of surface material by material from post-Imbrium impact events. Debris surges resulting from the formation of Imbrium secondaries in the region may have played an important role in the emplacement of Cayley plains material.

The origin the Descartes Mts. material has been the source of considerable controversy. The bulk of the evidence favors an origin as hummocky Nectaris basin deposits which were later furrowed by Imbrium secondaries[e.g.18,26]. It has been suggested that the Descartes Mt. material represents Imbrium primary ejecta emplaced by surface flow down a long Imbrium-radial trough[23]. As noted above, Imbrium secondaries are superposed on the unit. For reasonable ejection angles (e.g. 15°-30°), the secondary-forming projectiles would have impacted in the Apollo 16 region about 7-13 minutes after ejection. It seems unreasonable that the Descartes Mt. material was emplaced in its final form prior to the arrival of the Imbrium secondary projectiles. An extremely rapid mode of surface transport would be required.

In conclusion, the bulk of the currently available evidence supports the origin of most Apollo 16 material as Nectaris basin ejecta and the products of large craters in the Descartes region.

References: 1) R. Eggleton (1964) Astrogeol. Studies, Ann. Prog., Aug. 1962-Jul.1963, 46. 2) D. Wilhelms (1970) USGS Prof. Paper 599-F. 3) H. Wilshire and E. Jackson (1972) USGS Prof. Paper 785. 4) J. Warner (1972) PLSC 3, 623. 5) R. Williams (1972) EPSL 16, 250. 6) E. Chao et al. (1972) PLSC 3, 645. 7) M. Dence and A. Plant (1972) PLSC 3, 379. 8) E. Chao (1973) USGS Jour. Res. 1, 1. 9) V. Oberbeck et al. (1973) NASA TM X62-302, 1. 10) V. Oberbeck et al. (1974) PLSC 5, 111. 11) V. Oberbeck et al. (1975) The Moon 12, 19. 12) J. Head and R. Hawke (1975) PLSC 6, 2483. 13) R. Morrison and V. Oberbeck (1975) PLSC 6, 2503. 14) V. Oberbeck (1975) Rev. Geophys. Space Phys. 13, 337. 15) R. Morrison and V. Oberbeck (1978) PLSC 8, 3763. 16) R. Hawke and J. Head (1977) PLSC 8, 2741. 17) R. Hawke and J. Head (1978) PLPSC 9, 3285. 18) J. Head (1974) The Moon 11, 77. 19) E. Chao et al. (1973) LS IV, 127. 20) E. Chao et al. (1975) USGS Jour. Res. 3, 379. 21) C. Hodges (1972) NASA SP-315, sec. 29-D. 22) H. Moore et al. (1974) PLSC 4, 71. 23) D. Wilhelms et al. (1980) LPS XI, 1251. 24) T. McGetchin et al. (1973) EPSL 20, 226. 25) R. Hawke and P. Spudis (1979) Lunar Highland Crust Conf., 53. 26) D. Wilhelms (1972) NASA SP-315, sec. 29-F. 27) R. Eggleton (1970) USGS Map I-708, sheet 2. 28) V. Oberbeck and R. Morrison (1976) PLSC 7, 2983. 29) J. Morgan et al. (1977) Proc. Soviet-Amer. Conf. Cosmochem. of the Moon and Planets, 659. 30) E. Chao (1974) PLSC 5, 35. 31) P. Schultz and M. Mendenhall (1979) Lunar Highland Crust Conf., 143. 32) D. Wilhelms (1976) PLSC 7, 2883.

A COMPARISON OF MARTIAN CRATER AND BASIN DEPOSITS: PRELIMINARY RESULTS. B. Ray Hawke, Hawaii Inst. of Geophysics, Univ. of Hawaii, Hon., HI 96822; P.J. Mouginis-Mark, Dept. of Geological Sciences, Brown Univ., Prov., RI 02912.

Introduction: In recent years, considerable attention has been focused on martian crater deposits both because of the unique and enigmatic nature of the deposits themselves and because of the possible information these deposits may provide concerning the existence, thickness, and extent of a proposed subsurface volatile layer. With few exceptions[1], studies have concentrated on craters less than 55 km in diameter. An effort is underway to investigate the distribution, nature, origin, and mode of emplacement of the exterior and interior deposits associated with large martian craters and small martian basins in the diameter range of 50 to 250 km. This paper presents the initial results of this project. Emphasis is placed on studies of Lyot and Lowell basins and a comparison of the deposits of these basins with those associated with Curie[1] (D=119 km) and Bamburg[1,2] (D=55 km) craters.

Lyot basin - Lyot is a relatively unmodified 200 km central peak basin located at 50°N, 330.5°W[7]. From Mariner 9 images, the feature was interpreted to be excavated in cratered plains material[3]. The structure exhibits a central peak and a well-developed peak ring approximately 100 km in diameter. The inner basin floor is relatively flat in contrast to the more rugged outer basin floor. Major portions of the basin interior appear subdued, perhaps by relatively thin eolian debris deposits.

Extremely rugged hummocky rim material completely surrounds the outer ring and is particularly well-developed NE of the basin where it extends almost 40 km from the ring crest. A major expanse of smooth material appears to have ponded to a level surface adjacent to a ring crest low north of the basin. Two dominant continuous ejecta facies were identified. An inner deposit of rough radial material occurs generally within 70 km of the outer ring. This unit exhibits a rough irregular surface texture and is, in part, arranged in large ridges crudely radial to the basin. The distal portion of the continuous deposit is characterized by a smooth though often undulatory surface. In places, distinct flow lobes and distal ridges can be identified. This smooth continuous ejecta unit has overridden and subdued secondary craters and crater chains associated with Lyot. The maximum extent of the smooth continuous ejecta is 187 km (0.94D) but the mean radial extent is approximately 125 km (0.63D). Lyot exhibits a well-developed field of secondary craters. While unmantled secondary craters can be identified within 103 km (0.52D) of the outer ring crest, features interpreted as partly buried secondaries can be identified as close to the basin as 48 km (0.24D).

Evidence was found that both ballistic flight and surface flow were significant processes in the emplacement of Lyot ejecta. Evidence for ballistic transport includes the following: (1) the presence of secondary craters and crater chains demonstrates ballistic transport at large radial distances, (2) the identification of subdued basin secondaries in areas now covered by continuous ejecta and in areas relatively protected from surface flow by obstructions suggests the importance of ballistic flight nearer the basin, (3) textured ejecta deposits have been located on pre-existing topographic highs where it could have only been emplaced in ballistic trajectories, and (4) the more restricted extent of the continuous ejecta deposits ($\sim$0.63D) compared to those of Bamburg (2.1D)[2] and the much smaller rampart craters ($\sim$2D)[2] suggests a relatively more important role for ballistic as opposed to surface flow processes.

Still, abundant evidence exists for radial flow of material after initial deposition: (1) surface flows appear to have been obstructed in places by large pre-impact topographic highs, (2) what appears to be shadow zones exist

MARTIAN CRATER AND BASIN DEPOSITS

Hawke, B.R. and Mouginis-Mark, P.J.

in the lee of some obstacles, (3) in places, secondary craters have been overridden by material which originated nearer the basin rim, and (4) morphologic features (flow lobes, distal ridges) indicative of surface flow have been tentatively identified. As noted above, the continuous deposits of Lyot are relatively less extensive than those at smaller structures with well-developed ejecta flows. Still, the Lyot ejecta deposit extent is far greater than would be expected if ballistic processes alone were responsible. Carr et al.[4] pointed out that since the gravity fields of Mercury and Mars are similar, the radial extent of continuous ejecta on both planets should be approximately the same ($\leq$0.4D) if the ejecta configuration is controlled primarily by ballistic processes. Based on the work of Gault et al.[5], the average radial extent of continuous ejecta around a fresh 200 km mercurian crater would be about 48 km or 0.24D. The average value for Lyot (0.63D) determined in the present study is far in excess of that (0.24D) predicted for final deposit emplacement by purely ballistic processes. In certain areas, the maximum continuous deposit extent exceeds the values predicted for ballistic processes by a factor of 3.5 to 4!

Lowell basin - Lowell is a relatively undergraded 190 km double-ring or peak ring basin centered at 52.3°S, 81.3°W[7,8]. The pre-impact target site was dominated by ancient hilly and cratered terrain and cratered plateau material[3,6]. The structure is almost exactly the same diameter (190 km) as Lyot (200 km) but differs in that it does not exhibit a central peak. Lowell does have a well-developed central peak ring (D=95 km) similar to the inner ring of Lyot. The relatively flat inner basin is partly covered by a thick, smooth-textured deposit lobe which is probably sedimentary material of eolian origin. In contrast, the narrow outer basin floor exhibits a somewhat rougher texture but some portions appear to have been subdued by sedimentary material.

A hummocky rim unit, similar to that mapped at Lyot, completely surrounds the outer ring. This unit is extremely rugged near the ring crest and is characterized by numerous outward facing scarps and ridges which are concentric to the basin ring. The rim unit is surrounded by a rough radial unit which is relatively thick and characterized by a rough surface texture and abundant radial features. Since these radial features occur at a variety of scales and exhibit a range of morphologies, multiple origins are likely. Many are clearly secondary crater chains since they are continuous with better defined crater chains at greater distances from the basin. Similar features were identified in the rough radial unit around Lyot but they are more numerous and better-developed at Lowell. As at Lyot, the rough radial material extends at most 70-80 km (0.40-0.42D) from the outer ring crest. A distal radially textured unit has also been mapped. This unit is thin, relatively flat (though not necessarily smooth), and exhibits abundant radial lineations at a variety of scales. Several subunits have been defined. A well-developed smooth radial subunit exists SW of the basin. This unit displays a relatively smooth surface with faint radial lineations and is interpreted to have originated by surface flow from a point nearer the basin. Similar but smaller subunits have been identified in other areas. Another major subunit is composed of closely spaced secondary crater chains which have been buried to varying degrees by later material. Outside the limits of the distal radial unit, numerous secondary craters and crater chains can be identified. These features are not so abundant as around Lyot.

Discussion and Conclusions: A recent study of martian craters from 15 to 119 km in diameter concluded that increasing crater diameter accentuates variations in interior morphology. Inclusion of Lyot and Lowell in this population suggests that this trend also extends to impact structures 200 km in diameter.

Extensive mapping of Bamburg crater allowed the identification of six

MARTIAN CRATER AND BASIN DEPOSITS

Hawke, B.R. and Mouginis-Mark, P.J.

exterior deposit units as well as a secondary crater field[1,2]. A hummocky rim unit similar to the equivalent unit around lunar craters and to the rim unit mapped around larger structures in this study extends completely around the crater rim. At greater radial distances, rough radial and mass flow material are the dominant ejecta deposits. Both rough radial material and mass flow material extend up to 1-1.5D from the crater rim crest and both have appear to have been emplaced as surface flows which have overridden more distal deposits. The distal continuous deposits of Bamburg are dominated by smooth radial material which has commonly overridden secondary craters and crater chains. Less extensive deposits of pitted terrain material and smooth terrain material were mapped. Pitted terrain was not identified at the other impact structures studied in this project.

A comparison of the exterior deposits around Curie with those associated with Bamburg revealed certain similarities but also basic differences. The exterior deposits of both craters were dominated mass flows, lobate flows, and secondary crater fields. Curie deposits differ in both the more restricted radial extent of the ejecta facies from the crater rim, the absence of pitted terrain, and the relative importance of the various ejecta units. Both the lobate flows and mass flows at Curie have been interpreted to be the result of a surface-flow mechanism operative after original deposition at a late stage in the cratering event[1]. Small smooth terrain deposits were identified just outside the northern rim crest of Curie. Similar deposits were located just north of the outer ring of Lyot. The different positions of the smooth terrain deposits at Curie and Lyot relative to similar material at Bamburg make different origins and modes of emplacement possible. On the southern rim of Curie, a slump deposit, morphologically similar to lobate flows, was observed at the foot of a scarp slope on the adjacent mass flow[1]. This deposit extends over 70 km from its apparent source and is quite similar to certain martian landslides. It appears to have formed by the failure of one side of the mass flow after its emplacement. This relationship coupled with the large horizontal distance the material was transported from its source argue for extreme fluidity and the presence of a lubricating agent such as liquid water.

The exterior deposits around the small martian basins described above exhibit many similarities as well as some interesting differences when compared to the deposits of Curie and Bamburg. Deposits with grossly similar features occur in the same relative positions around both large craters and small basins. Differences center around detailed surface morphology and relative radial extent. All of the impact structures exhibit secondary crater fields although they are developed to different degrees. In all cases, some secondary crater clusters and chains can be seen to have been buried by surface flows originating closer to the parent structure. Evidence from the basin deposit study suggests that ballistic ejecta emplacement has been more important at these large structures. Still, a comparison of martian basin deposit extent with what would be expected if ejecta configuration was controlled primarily by ballistics and the morphology of the deposits themselves strongly suggest that radial surface flow has played an important role in the final emplacement of martian basin continuous ejecta depostis.

References: 1) P. Mouginis-Mark and J. Head (1979) LPS X, 870. 2) P. Mouginis-Mark (1979) PLPSC 10th, 2681. 3) D. Scott and M. Carr (1978) USGS Map I-1083. 4) M. Carr et al. (1977) J. Geophys. Res. 82, 4055. 5) D. Gault et al. (1975) J. Geophys. Res. 80, 2444. 6) G. McGill (1978) USGS Map I-1077. 7) C. Wood and J. Head (1976) PLSC 7th, 3629. 8) D. Wilhelms (1973) J. Geophys. Res. 78, 4084.

LUNAR BASIN EJECTA DEPOSITS COMPOSITIONS: A SUMMARY OF CHEMICAL MIXING MODEL STUDIES. B.R. Hawke, Hawaii Inst. of Geophy., Univ. of Hawaii, Hon., HI 96822, P.D. Spudis, Dept. of Geology, Arizona State Univ., Tempe, AZ 85281, A.E. Metzger, Jet Propulsion Lab., Calif. Inst. of Technology, Pasadena, CA 91103

Introduction: Valuable insight concerning lateral and vertical changes in the chemical composition of the lunar crust can be provided by studies of material ejected by the lunar basins. These impact structures have excavated material from a variety of depths and deposited this ejecta in a systematic manner. Studies of lunar samples thought to have been derived by basins, notably Imbrium and Serenitatis, have yielded important information but there is a need to extrapolate the detailed chamical information for the individual landing sites to much larger regions of the lunar surface. This has been made possible largely through the use of the Apollo orbital geochemistry data[1-4] plus some geochemical information provided by other remote sensing techniques (i.e. reflectance spectroscopy[5,6]). Geochemical data are currently available for portions of the highlands surrounding several large multi-ring basins, interpreted as ejecta deposits of the impact structures. Chemical mixing model calculations have been performed on the remotely sensed chemical compositions of the deposits related to Crisium, Nectaris, Orientale, and Imbrium basins in order to establish which chemically-defined rock types are likely to be present and to make quantitative estimates of their relative abundances[7,8]. The purpose of this paper is to summarize the results of these calculations and discuss their significance for the solution of problems concerning the lunar basins.

A least-squares mixing model program was used to translate the chemical composition of each region into the best mixture of given endmembers[9]. Up to six elements (Mg, Th, Fe, K, Al, Ti) were used. The chemical data for the regions under study are those presented by Adler and Trombka[10], Bielefeld et al.[2,3,11], and Metzger et al.[4]. Endmember selection was guided by lunar sample chemistry, regional geological considerations, and previous analyses of the orbital geochemistry data[4,12]. Endmember compositions were selected from Taylor[13] and Ridley[14]. The best solutions obtained for the various regions are presented in Table 1.

Crisium Basin Ejecta: Crisium predates Imbrium and Orientale and is younger than Fecunditatis, Nectaris, and possibly Serenitatis[15]. The circum-Crisium highlands might be expected to contain significant amounts of Crisium ejecta and variations in the composition of this highland region may reflect the pre-impact chemical variations in the crust of the Crisium target site. A recent study by Bielefeld et al.[11] correlated chemistry and albedo in the Crisium area and several data clusters were identified in the highlands S and SW of Crisium. Al and Mg data for these clusters were used along with regional chemical data to perform mixing model calculations (Table 1). Units C and D are the most extensive and generally ring Mare Crisium separating it from neighboring maria. The mixing model results show that both regions are dominated by anorthositic gabbro and contain lesser amounts of LKFMB. These components comprise the same relative proportions of the highland material present in both units. The units differ mainly in the amounts of mare basalt calculated to be present (∿19% in D vs. ∿3% in C). This difference can be understood in terms of the distribution of units in relation to the nearby mare surfaces. Unit D commonly separates C from nearby basalt deposits and probably represents a zone of small scale lateral mixing from the nearby mare deposits. The much smaller mare component in unit C is consistent with its occurrence at generally greater distances from the maria. Mixing model solutions for unit B, which is generally even more distant from mare surfaces, suggest that

essentially no mare basalt is present. The unit can be modeled as a mixture of anorthositic gabbro and LKFMB present in approximately the same relative proportions as in the highland components of units C and D.

In summary, the highlands around Crisium basin can be modeled as mixtures of anorthositic gabbro, LKFMB, and mare basalt. Little evidence is found for major changes in the composition of the highland components as a function of distance from the basin rim. If this highland component is taken to be largely Crisium ejecta, the lack of major changes in the relative proportions of the dominant rock types suggests that these materials may have been thoroughly mixed in the upper portion of the Crisium target site prior to basin formation. An earlier orbital mixing model study of Imbrium basin ejecta (Apennine Region)[7] suggested higher fractions of LKFMB as an ejecta component. Its lower abundance in the Crisium deposits adds support to arguments tha LKFMB is derived from deep crustal levels[16] since Crisium, being smaller than Imbrium, would excavate shallower crustal materials.

Nectaris Basin Ejecta: Although Nectaris is relatively older than several other major nearside basins (Imbrium, Crisium, and Serenitatis), its great distance from these structures and recent studies emphasizing the importance of local mixing[17] suggest that the composition of the surrounding highlands might be expected to reflect the nature of the Nectaris target site. Support is provided by the fact that numerous workers have related individual Apollo 16 samples to the Nectaris basin[18,19]. In particular, it has recently been proposed that the KREEP-rich Apollo 16 samples were excavated from a deep crustal layer by the Nectaris impact event[18]. If so, the distribution of LKFMB might be expected to vary in a systematic manner with respect to the basin. The results of preliminary mixing model calculations along the Apollo 16 groundtrack show that regions N and NE of the basin (1-4; 20.5°-42°E) contain a large highland component dominated by anorthositic gabbro. LKFMB comprises between 20% and 30% of the total highland material. No clear trend relative to basin structure can be recognized. Theophilus ejecta contains a large highland component which dominates the mare regions north of the crater. Major changes in composition occur in the Descartes region (14°-20.5°E). Anorthositic material becomes more abundant, and mare basalt is present in only trace amounts.

Central Highlands and Fra Mauro Region: The mixing model results suggest that there is a systematic east to west change in the composition of the Central Highlands. West of the Descartes region (6, 5°-14°E), a medium-K Fra Mauro basalt (MKFMB) component yields better solutions in mixing calculations that LKFMB. East of Ptolemaeus crater, MKFMB comprises only 37% of the total highland component. West of Ptolemaeus, MKFMB dominates (∿86%) the non-mare component present in this highland terrain. Similar percentages of MKFMB are found in the highlands area further west and south of Fra Mauro crater.

Two points should be stressed. First, the systematic east-west change in the composition of the Central Highlands appears to rule out the possibility that the Central Highlands are blanketed with a thin layer of Orientale ejecta. Second, the correlation of the change in geochemistry and KREEP abundance with the decline in elevation at the western edge of the Central Highlands near Ptolemaeus suggests that KREEP emplacement was controlled by a process sensitive to topographic variations such as volcanism[7].

Orientale Basin Ejecta: Mixing model calculations were performed on the composition of a portion of the ejecta blanket north of the Orientale basin. The area is near the inferred rim of the transient crater cavity and thus should contain material excavated from the lower levels of the cavity. This area can best be modeled as a mixture of about 60% anorthositic gabbro and 40% gabbroic anorthosite. Models which employ LKFMB as an endmember result in fits which are less good. It is too early to draw firm conclusions regarding the

apparent absence of LKFMB in Orientale basin ejecta, and this region is currently undergoing continued analysis.

References: 1) Andre, C. et al. (1977) Science 197, 986. 2) Bielefeld, M. et al. (1976) PLSC 7, 2661. 3) Bielefeld, M. (1977) PLSC 8, 1131. 4) Metzger, A. et al. (1977) PLSC 8, 949. 5) Pieters, C. and McCord, T. (1976) PLSC 7, 2677. 6) Charette, M. et al. (1977) PLSC 8, 1049. 7) Hawke, B. and Head, J. (1978) PLPSC 9, 3285. 8) Hawke, B. and Spudis P. (1979) Lunar Highland Crust Conf., 53. 9) Hawke, B. and Ehmann, W. (1976) Lun Sci VII, 351. 10) Adler, I. and Trombka, J. (1977) Phys Chem Earth 10, 17. 11) Bielefeld, M. et al. (1978) Mare Crisium: View from Luna 24, 33. 12) Schonfeld, E. (1977) PLSC 8, 1149. 13) Taylor, S.R. (1975) Lunar Science, Pergammon Press. 14) Ridley, I. (1976) Ann Rev Earth Planet Sci 4, 15. 15) Wilhelms, D. (1976) PLSC 7, 2883. 16) Ryder, G. and Wood, J. (1977) PLSC 8, 655. 17) Oberbeck, V. (1975) Rev Geophys Space Phys 13, 337. 18) Maurer, P. et al. (1978) GCA 42, 1687. 19) Head, J. (1974) Moon 11, 77.

Table 1. Results of mixing model calculations for selected regions around lunar basins. Crisium A, B, C, and D refer to units defined by Bielefeld et al.[11].

Region	Longitude	Anorthosite	Gabbroic Anorthosite	Anorthositic Gabbro	LKFMB	MKFMB	Mare Basalt
Nectaris Basin, Central Highlands, and Fra Mauro Region							
1. HL West of M. Fecunditatis	37.5°-42°E	---	---	62	23	---	15
2. Isidorus & Capella	30°-37.5°E	---	---	75	25	---	---
3. Mare Nectaris S. of Torricelli	26°-30°E	---	---	51	22	---	27
4. Portion of Theophilus ejecta	20.5°-26°E	---	---	66	16	---	18
5. Descartes	14°-20.5°	21	---	47	28	---	4
6. HL West of Descartes	5°-14°E	9	---	64	---	15	12
7. Portion of Central HL	3°-5°E	18	---	37	---	45	---
8. HL East of Ptolemaeus	0.5 -3°E	10	---	53	---	37	---
9. Ptolemaeus Crater	4°W-0.5°E	9	---	41	---	50	---
10. HL West of Ptolemaeus	9°W-5°W	---	---	13	---	79	8
11. South of Fra Mauro	19°-13°W	---	---	5	---	82	13
12. West of Bonpland	20°-19°W	---	---	5	---	73	24
Crisium Basin							
A	---	---	---	75	23	---	2
B	---	---	---	79	21	---	---
C	---	---	---	75	22	---	3
D	---	---	---	61	20	---	19
Orientale Basin							
Orientale rings and ejecta	110°-76°W	---	40	60	---	---	---

BULK MAGNETIZATION PROPERTIES OF THE FRA MAURO FORMATION. L.L. Hood, Lunar and Planetary Laboratory, The University of Arizona, Tucson, AZ 85721.

A resolution of the problem of lunar crustal magnetization is an obvious prerequisite for reliably interpreting the permanent magnetic properties of bodies in the solar system with cratered or partially cratered surfaces. Studies of the magnetic properties of returned samples, surface magnetic field investigations, and analyses of orbital magnetometer and electron-reflectance data strongly suggest that ejecta materials produced during large meteoroid impacts are among the more strongly magnetized materials on the lunar surface (1-4). One approach toward discriminating between a local, small-scale magnetizing field such as may have been produced by the impact (5) and a field of global or larger scale (6) is by studying the bulk magnetization properties (direction and intensity per unit area) of these surface geologic units. Primary ejecta such as the Fra Mauro Formation peripheral to the Imbrium basin are well-suited for this purpose because each unit has a relatively wide distribution and was formed at essentially the same time. Here we report a modeling analysis of Apollo 16 subsatellite magnetometer data in which the bulk magnetization properties of two separate exposures of Fra Mauro terrain are inferred.

Low-altitude, direct measurements of the crustal magnetic field across a narrow equatorial section of the lunar near side were obtained during orbits 180 to 270 of the Apollo 16 subsatellite mission. General associations of medium-amplitude anomalies with areas dominated by the Fra Mauro and Cayley Formations were reported (3) and contour maps of the vector components of the crustal magnetic field in these areas have been constructed (7,8). In one region, extending from 31° to 41° W. longitude and from 3° to 8° N. latitude, minimal fields were detected over the craters Encke and Kepler (mare-aged and Copernican, respectively) while two separate anomalies with radial-component amplitudes of +2 and -5 gammas were detected over remnants of the Fra Mauro that have escaped mare flooding. Elsewhere, areas dominated by mare basalt were characterized by minimal magnetic fields.

Assuming that surficial layers of Fra Mauro material are the sources of the observed magnetic anomalies, an iterative procedure was used to find a distribution of uniformly magnetized circular plates separated by unmagnetized material which yielded a minimum variance between the calculated field values and the data (9). The method of Talwani (10) was used to calculate the model magnetic field at individual points along available orbit tracks. Final model parameters are listed in Table 1. Fig. 1 contains contour maps of the model field magnitude, the three vector components, and a pictorial representation of the plate locations and radii listed in Table 1. Plates 1-3 represent the source of the largest observed anomaly maximum (radial component -5 gammas) and plates 4-7 represent the source of the smaller 2-gamma radial-component maximum. The locations of these surface plates closely correspond to separate exposures of the Fra Mauro Formation shown on standard geologic maps (11).

As seen in Table 1, each of the Fra Mauro sources are magnetized nearly uniformly on scales up to 100 km. However, the two separate exposures, separated by a mean distance greater than 100 km, are magnetized in very different directions. Since the maximum thickness of the Fra Mauro layer in the Kepler region is about 1 km, the dipole moments per unit area given in the last column imply a lower bound on the mean intensity of magnetization within this unit in the range 18 to 82 gammas. Assuming a mass density of 3 g/cm^3, these values correspond to a range of 6 to 27 x 10^{-5} e.m.u./g and are not

Magnetization of the Fra Mauro Formation

L.L. Hood

TABLE 1

#	W. Long	N. Lat.	Rad. (km)	θ	ø	G-cm
1.	35.1°	5.2°	20	160°	298°	38
2.	35.9°	6.0°	20	160°	298°	22
3.	35.7°	4.4°	10	160°	298°	82
4.	38.4°	5.9°	13	27°	123°	18
5.	38.8°	5.2°	13	27°	123°	34
6.	39.1°	4.8°	13	27°	123°	20
7.	38.0°	6.3°	8	27°	123°	25

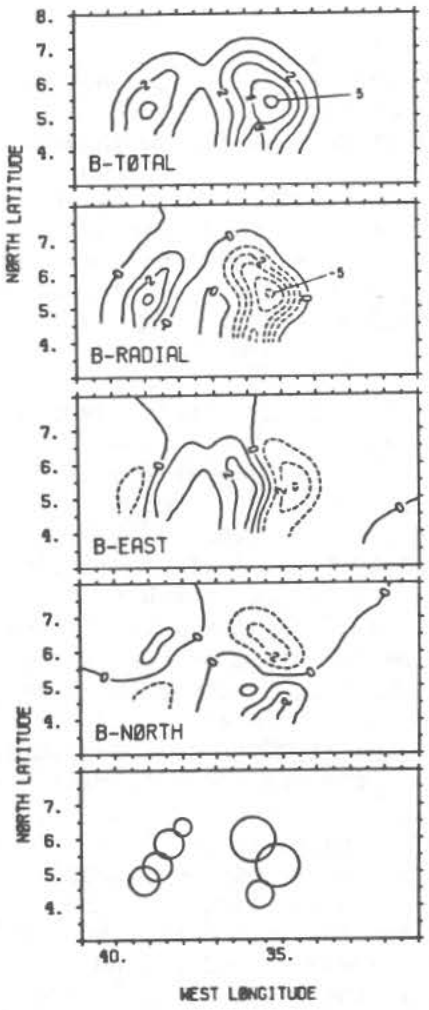

Fig. 1. Contour maps of the model field magnitude and field components produced at sub-satellite altitudes by the distribution of surface plates shown on the bottom panel. The magnetization parameters for each plate are listed in Table 1.

inconsistent with laboratory data for the returned breccias and soils.

It is likely that the several exposures of the Fra Mauro Formation formed within a very brief interval following the Imbrium impact. Bulk magnetization characteristics were probably acquired during roughly the same interval although exact simultaneity in the acquisition of these properties may have been prevented by different cooling rates, etc. The inferred properties of the present magnetization of this unit suggest the absence of directional coherence and also possibly of intensity coherence on horizontal scales greater than 100 km. This result is most easily understood if relatively local processes, such as those associated with the impact, either greatly distorted any existing large-scale magnetizing field or themselves generated short-lived magnetic fields of the required intensities. Further work to confirm the inferred large-scale inhomogeneity of magnetization for the Fra Mauro Formation is needed.

Acknowledgments. Computational assistance by T. Trebisky is appreciated. Supported by NASA under grant 7020.

References. (1) Strangway D.W., W. Gose, G. Pearce, R.K. McConnell (1973) Nature 246, p. 112-114. (2) Dyal, P., C.W. Parkin, W.D. Daily (1974) Rev. Geophys. Space Phys. 12, p. 568-591. (3) Hood, L.L., P.J. Coleman, Jr., D.E. Wilhelms (1979) Science 204, p. 53-57. (4) Anderson, K.A. and D.E. Wilhelms (1979) Earth Planet. Sci. Lett. 46, p. 107-112. (5) Srnka, L.J. (1977) Proc. Lunar Sci. Conf. 8th, p. 785-792. (6) Runcorn, S.K. (1979) Proc. Lunar Planet. Sci. Conf. 10th, p. 2325-2333. (7) Hood, L.L., P.J. Coleman, Jr., D.E. Wilhelms, Proc. Lunar Planet. Sci. Conf. 10th, p. 2235-2257. (8) Hood, L.L., C.T. Russell, P.J. Coleman, Jr. (1980) J. Geophys. Res., in press. (9) Hood, L.L. (1980) Proc. Lunar Planet. Sci. Conf. 11th, in press. (10) Talwani, M. (1965) Geophys. 30, p. 797-817. (11) Hackman, R.J. (1962) U.S. Geol. Surv. Map I-355.

THE "BUNTE BRECCIA" OF THE RIES: TERRESTRIAL ANALOGUE OF BASIN EJECTA. Friedrich Hörz, SN6/NASA Johnson Space Center, Houston, TX 77058

INTRODUCTION: The 26 km diameter Ries Crater is the largest terrestrial impact structure with substantial parts of the continuous ejecta deposits still preserved. The "Bunte Breccia" (BB) formation comprises >>90% of all materials displaced beyond the crater rim. The original target stratigraphy is well documented and consists of a crystalline basement overlain by a variety of Triassic, Jurassic and Tertiary sediments of such distinct lithologies and/or colors that they are easily identified in the field. We obtained drill cores for 9 different BB locations at radial ranges of ≈16 to 37 km from the crater center. Following are some of the major findings.

GRAIN SIZE DISTRIBUTION: All clasts >1 cm were measured individually; the "matrix" (<1 cm) was wet sieved; the results are illustrated in Fig. 1A. Accordingly, overall grain size distribution is highlyheterogeneous and ranges from μm to >10 m diameter components. The >1 cm clasts comprise 30-90% of the total core. The <1 cm fraction ("matrix") consists predominantly of Tertiary sands, silts and clays, thus the proponderance of relatively small grain sizes. The most distal cores appear also to be the most fine grained ones. The relative coarse grain sizes observed in cores D, E and F are largely due to Tertiary clasts from the local substrate. Although not illustrated, deep-seated target materials are more comminuted than shallow target horizons. Furthermore, there is no systematic trend regarding grain size in vertical profile. "Primary" crater and locally derived clasts have similar grain size distributions. No evidence for aerodynamic sorting was observed.

TARGET STRATIGRAPHY AND CRATER EJECTA: All clasts >1 cm were categorized into their respective target horizons: crystalline (<600 m deep), Triassic (600-400 m), Lower and Middle Jurassic (400-250 m) and Upper Jurassic (250-0 m). Figure 1B illustrates the results: the primary ejecta are completely dominated by Upper Jurassic limestones which occupy approximately the uppermost 10-15% of the overall stratigraphic section for a crater ≈2 km deep. The total of all cores averages at .16% crystalline, 2.15% Triassic, 6.67% Lower and Middle Jurassic and 91.02% Upper Jurassic. We thus conclude that large scale continuous deposits at any radial range are dominated by relatively shallow target stratigraphies. Note also that all target lithologies are represented in each individual core, even in grossly similar proportions. Importantly the distribution of primary ejecta in vertical profile is chaotic; no systematic trends were recognized. Therefore the concept of inverted target stratigraphy appears to have limited utility for large scale continuous deposits.

LOCAL COMPONENTS: Tertiary sands, silts and clays dominate the BB cores, either in the form of discrete clasts or as intimately mixed matrix. Most of these Tertiary components are demonstrably of "local" origin, dislodged from the crater environs, rather than from the crater cavity. As illustrated in Figure 1C, Tertiary clasts alone mostly outweigh the total crater ejecta; if clasts and matrix are combined, the locally derived components make up typically some 70-90% of the total deposits. A weak trend towards increased incorporation of local materials with increasing range exists.

SHOCK METAMORPHISM: The entire resolvable shock history of BB resides in the rare crystalline clasts; none of the sediments display shock effects resolvable by standard optical microscopy. As illustrated in Figure 1D, the maximum shock level in the crystalline materials is ≈40 GPa; specifically no impact melts occur; many crystalline clasts appear unshocked. These observations - coupled with the paucity of crystalline clasts - lead to the important

"BUNTE BRECCIA" OF THE RIES

Hörz, Fred

conclusion that large scale continuous deposits are emplaced at essentially ambient temperatures.

SUMMARY: The above findings are consistent with - if not predicted for - a ballistic ejection of primary crater ejecta followed by a secondary cratering regime and its ensuing debris surge. Excavation and intimate mixing of local materials occurs during secondary cratering as well as during the highly turbulent surge. Turbulence is created by secondary ejecta fragments colliding with ejecta from neighboring events, which may have vastly different azimuthal velocity vectors; but the overall momentum is radially away from the primary crater because more secondary ejecta mass is launched downrange than tangential or even uprange. Average, radial surge velocities are on the order of 100 m/sec for the BB deposit; radial ranges travelled by locally derived components are demonstrably on the order of a crater radius. These processes combine to yield highly chaotic deposits that thoroughly mask and destroy most systematic trends predicted for the purely ballistic phase, e.g., inverted target stratigraphy or annular distribution of various shock levels.

Importantly the BB was deposited at ambient temperatures; by analogy we postulate other large scale continuous deposits to be also emplaced as relatively cool masses. Flow features observed in distal lunar basin deposits and traditionally interpreted as "hot" impact melts, may merely represent flow phenomena associated with a relatively cold, albeit fast moving, debris surge. Even if such "pools" were indeed impact melts, it does not follow that they are of considerable vertical extent (of massive volume) and especially it does not follow that the surrounding, clastic material was of comparable, hot temperature. The structural relationship of "hot" suevite and "cold" BB in the Ries Crater argue very strongly that "hot" and "cold" ejecta have different ejection histories (angles; velocities; launch times) and generally do not mix in the continuous deposits. The majority of thermal energy partitioned during cratering resides within the crater cavity (impact melts, fallback ejecta) and very little is deposited into the continuous deposits.

FIGURE CAPTION: Grain size distribution, modes and shock metamorphic effects as a function of radial range in the continuous deposits of the Ries crater. Thickness of Bunte Breccia is >80, 34, 76, 52, 84, 47, 21 and 17 m, respectively, for cores A through I. Figure A is based on 18,000 individually measured clasts and 220 sieve analyses, originally separated into 16 grain size categories; Figure B and C depict subsets of these data, with each clast categorized into its appropriate stratigraphic horizon; next to grain size analyses, heavy mineral population studies verified the "local" derivation of the matrix. Figure D, unfortunately, is statistically limited: the total crystalline clast population amounted to 98 specimen; the figure includes data of only 84 clasts, because 12 samples were badly weathered.

ACKNOWLEDGMENT: G. B. Banholzer, H. Gall, R. Hüttner, S. Langer, R. H. Morrison, V. R. Oberbeck, R. Ostertag, D. Pratt, D. A. Rainey, R. B. Schaal and D. Stöffler contributed significantly to this study.

"BUNTE BRECCIA" OF THE RIES

Hörz, Fred

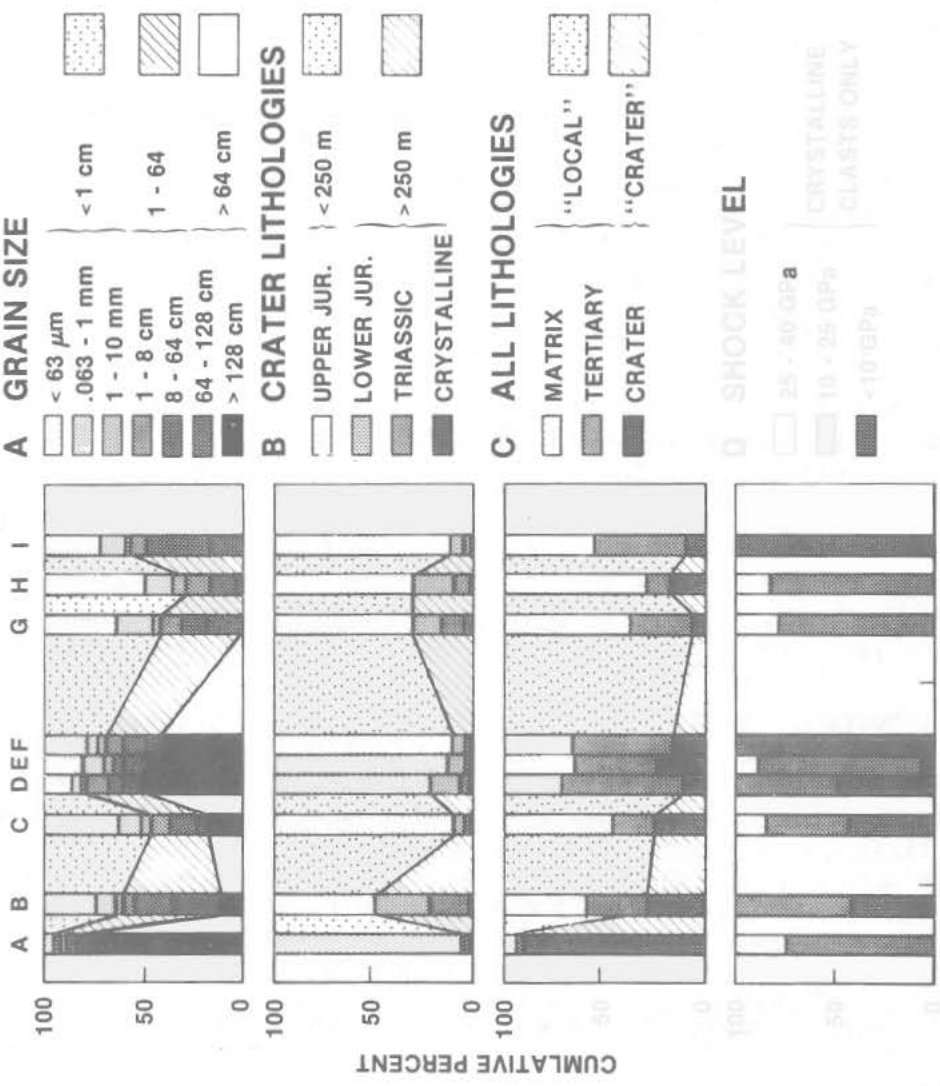

BRECCIA DIKES AND MULTI-GENERATION BRECCIAS: RELATION TO IMPACT CRATER FORMATION AND MODIFICATION. P. Lambert, Center for Meteorite Studies, Arizona State University, Tempe, AZ 85281.

A major aspect of ring basins formation is the crater modification of large size impacts (1). A potential clue to the understanding of this phenomenon is the study of the dikes of breccia commonly reported in the target rocks, below the crater floor limit of deeply eroded terrestrial complex craters (2-7 and others). Their striking development is revealed by drillings (8,9). However there is still no systematic study of these breccias which appear in the literature under different names: dike breccia (10-11) mixed breccia (7), myolisthenites (12), pseudstachylites (13-15). Besides their relationships with impact structures they all feature polymict materials and eventually exhibit evidence of shock metamorphism. Their disposition is complex and does not reflect the summetry of the impact phenomenon.

Two major textures can be distinguished: A: breccias characterized by mainly small, rounded fragments rather sorted and often preferentially oriented, commonly monomineralic (quartz), in a well developed cryptocrystalline matrix often exhibiting a fluidal texture. B: breccias formed by rock, mineral and eventually glass fragments with angular to subrounded edges, widely variable in size, without obvious preferential orientation in a matrix of fine debris of the same material. They are similar to glass-poor or glass-free breccias commonly found inside and outside impact craters. For commodity these two breccia types will be respectively refered to A and B in the following. Among the B breccias those forming cm to m thick, rather straight and continuous dykes can be distinguished from others extremly comples and variable in size and geometry (shart changes in direction partly controlled by the bedrock texture, bifurcations, discontinuities, mm up to m thick but usually thin). The first ones may separate different lithologic units and eventually show striations on the wall while the others do not affect the original disposition of separated blocks.

A remarkable feature is the occurence of A breccias among the clasts of the B breccias. This observation results from the study of breccia dykes issued from Rochechouart (France) Charlevoix, Carswell and State Island (Canada) and Richao Ring (Brasil). The following cases are observed; the A breccia debris are angular or sub-rounded and are not deformed; - they are rounded but still not deformed; - they are deformed, distorted, partially mixed with the B breccia matrix. In Charlevoix several B breccia generations can be infered from the relationships between clast and matrix (5). Interestingly similar debris of A breccia are observed in suevite and polymict breccias ejected from the Ries (Germany) and from Rochechouart.

DISCUSSION. There are two main generations of fracturation leading to the successive formation of A and B breccia dikes. The time period between formation of A and B breccia dikes is large enough to allow A breccias to cool down and consolidate before being reworked by B. Deformed and mixed A breccia clasts in B matrix indicate such condition is not always fulfilled. The evidence of A breccia clasts in rocks deposited in the crater suggests some material is circulating upward in B dikes, from the target to the crater. However material clearly injected from the top is observed in the B breccia dikes of the Ries (10). An alternative explanation is the "assimilation" of the A dikes and surroundings by the downward growth of the crater. Because of the sharp angles made by the small B breccia dikes and because of the

evidence of transported material over long distance in such fortuous way, these dikes are assumed to be caused by a very brief high energy phenomenon. This process is apparently not related to readjustment since there is no relative displacement of separated blocks. It could occur by injection in the expanded target on pressure release while the crater is still growing. The largest B breccia dikes are very likely related to readjustment. In case of Charlevoix they were perhaps discontinuously active, indicative of a re-adjustment by step of the crater. Tentatively the A breccia dikes are assumed to form upon shock loading. If not, their relationship with the shock front must be close in time, and consequently in space, in order to satisfy the timing constraints discussed above.

The results strongly suggest there is a deep fracturation event in the target which is produced by the impact and which occurs before the re-adjustement of the large craters. Depending on the importance of the development of this fracturation, this could be the solution of the strength dilemma in the models of crater modification by gravity (16-17), requiring a low cohesion strength and a small angle of internal friction of the target material after the crater has been formed. More work is needed to appreciate the importance of such fracturation, to determine its original geometry, and to compare to the geometry of the listric slip planes assumed in any model of crater modification.

REFERENCES

1. Roddy, D.J., Pepin, R.O., Merrill, R.B., Editors (1977). Impact and Explosion Cratering, Pergamon Press (N.Y.).
2. Robertson, P.B. (1968). Meteoritics, 4, p. 89-112.
3. Dence, M.R. (1972). Geol. Ass. Canada Spec. paper, 10, p. 7-18.
4. Halls, H.C., Grieve, R.A.F. (1976). Can. J. Earth Sci., 13, p. 1301-1309.
5. Rondot, J. (1980). These d'Universite, Clermont-Ferrand.
6. Lambert, P. (1977). Earth Planet. Sci. Letters, 35 p. 258-268.
7. Wilshire, H.G., Offield, T.W., Howard, K.A., Cummings, D. (1972). U.S. Geol. Survey Prof. Paper, 599-H.
8. Geologica Bavarica (1977), 75, Bayer-Geol. Landesamt.
9. Lmabert, P. (1977). These d'etat, Univ. Paris-Orsay. 513 p.
10. Stoffler, D. (1977). Geologica Bavarica, 75, p. 443-458.
11. Pohl, J., Stoffler, D., Gall, H., Ernston, K. (1977). Impact and Explosion Cratering, p. 343-404.
12. Rondot, J. (1971). Meteoritics, 6, p. 307-308.
13. Dietz, R. (1961). J. of Geology, 69, p. 499-516.
14. Dietz, R. (1964). J. of Geology, 72, p. 412-434.
15. French, N.M. (1968). Shock Metamorphism of Natural Materials, p. 383-412.
16. Melosh, M.J. (1977). Impact and Explosion Cratering, p. 1245-1260.
17. McKinnon, W. (1978). Proc. Lunar Planet. Sci. Conf. 9th, p. 3965-3971.

SPACING AND MORPHOLOGY OF INNER BASIN RINGS IN LUNAR BASINS: CLUES FOR THE ORIGIN OF RIDGE RINGS. Ted A. Maxwell, Center for Earth and Planetary Studies, National Air and Space Museum, Smithsonian Institution, Washington, D. C. 20560

Mare ridge rings in flooded lunar basins define the innermost ring structure of the largest lunar multi-ring basins. Based on spacing relationships with outer basin rings, and the concentric arrangement of these ridge rings, previous studies have considered ridge rings to be the equivalent of the prominent, topographically distinct inner rings of unflooded lunar basins (1,2). Although formation of ridges has been attributed to a volcanic means (3), a genetic link between peak rings and wrinkle ridges has been suggested on the basis of a consistent ratio between ridge ring diameter and basin rim diameter. This relation has been further investigated, and found to have an extremely high degree of correlation based on a semi-logarithmic format (4). However, in recent studies (5,6), it was found that extrapolation of the best-fit linear relation between peak rings and basin rims underestimates the diameter of ridge rings; e.g. that ridge rings occur closer to the edge of the basin than would be expected if they directly overlie a buried peak ring. This observation is important both for models for the origin of multi-ring basins and for tectonic models for the origin of mare ridge systems (7), in that both are dependent on whether the ridge ring truly represents the location of a basin peak ring.

In order to further investigate this relationship, the ring diameters of peak ring basins were measured once again. The diameters of the innermost limit of slumping or terracing, and the outermost limit of visible ring structure for inner basin rings were also measured to provide an estimate of the range of diameters. In addition, the morphologic expression of inner rings was noted for unflooded basins, although this factor is limited by the varied states of preservation. Five basins listed in (8) have not been included in this study because of the difficulty in obtaining realistic estimates of inner ring diameters.

As noted in several previous studies, ring spacing for double-ring basins exhibits a systematic increase with the size of the basin (Fig. 1), although in multi-ring basins the spacing is much more variable. Because of this variability, double-ring basins are herein treated separately from multi-ring basins (Fig. 2). Using ring diameters measured in this study , a linear least squares regression for peak rings vs. the second basin ring in double-ring basins results in: $D_{PR} = 0.452\ D_B + 0.95$ ($r = .96$; dimensions in kms). For multi-ring basins, the best-fit regression for ridge rings vs the next outer ring is: $D_{RR} = 1.343\ D_B - 344$ ($r = .97$), an increase in the ratio over that reported in (7) based on previous ring measurements. If it is assumed that ridge rings are the equivalent of peak rings, then a discrepancy exists between the ratio of inner rings in multi-ring basins as opposed to double-ring basins.

In an attempt to restore an original rim crest by using the innermost extent of slumping of the outer ring (and thus produce a curve closer to that of ridge rings), the slope of the best-fit line decreased. The decrease in ratio resulted from the more degraded state of large double-ring basins and the consequent lack of an estimate for the inward extent of slumping. In actuality, a diameter decrease of approximately 50% for the larger basins would be needed to provide a consistent ratio to that of ridge rings.

Additional evidence for a discrepancy between peak ring and ridge ring location is the existence of ridge rings within double-ring basins. Within

SPACING AND MORPHOLOGY OF INNER BASIN RINGS

Maxwell, T. A.

Figure 1. Peak ring, ridge ring and outer basin ring diameters.

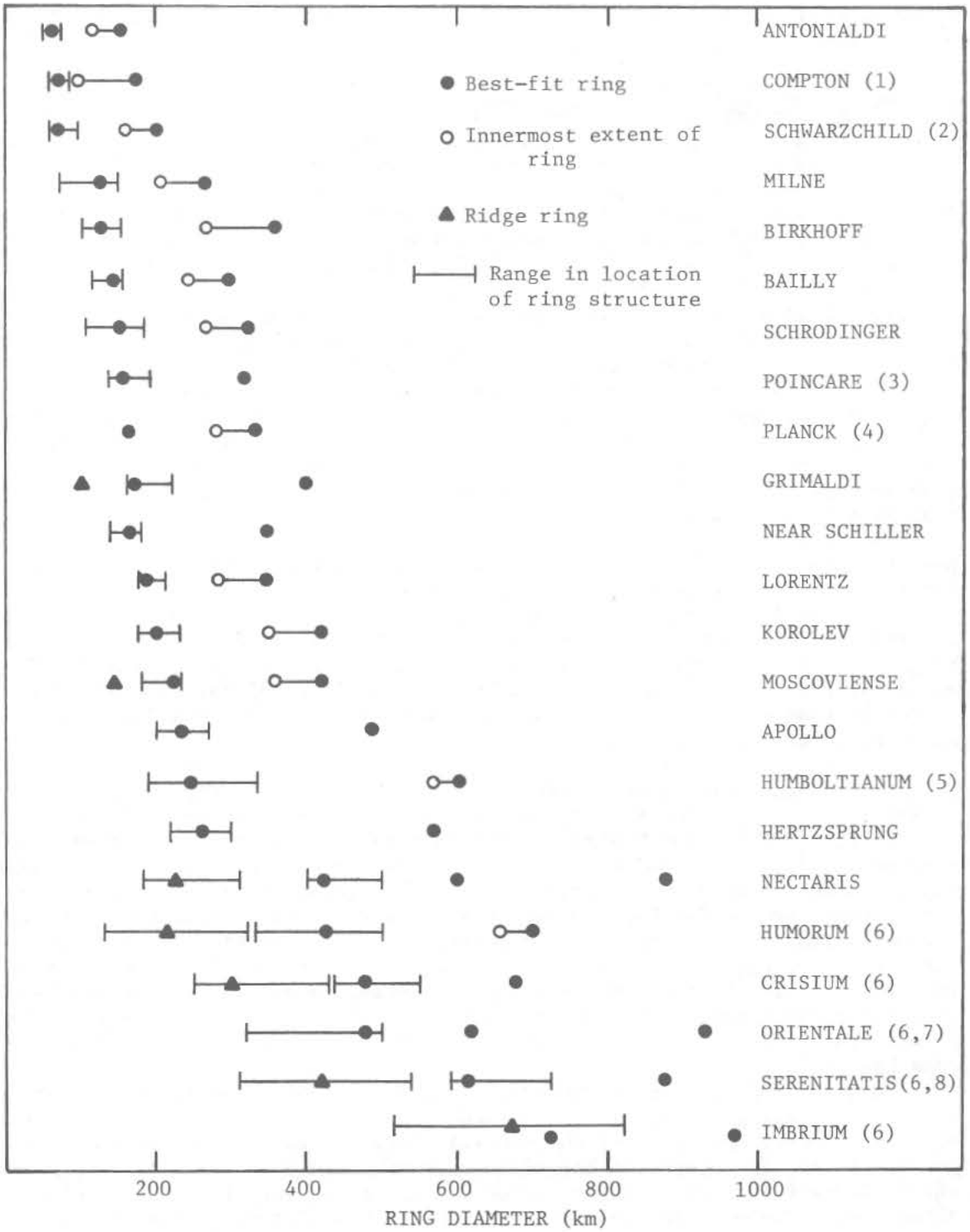

(1) In Compton, there are 2 arcs of a ridge ring within the peak ring; visible on LO V 181 M. (2) The "peak ring" is really an arcuate group of hills

SPACING AND MORPHOLOGY OF INNER BASIN RINGS

Maxwell, T. A.

in the western half of the basin. (3) There is a suggestion of an innermost ring of ridges within Poincaré. (4) No distinct inner ring structure; only suggested by ridges oblique to Prandtl and two other craters within Planck. (5) Topographic bench and mare ridges visible in the western half of the interior of the basin. (6) Additional outer rings have been mapped by Wilhelms and McCauley (1971). (7) See reference (9) for details of Orientale ring structure. (8) See reference (10) for details of Serenitatis outer ring structure.

the inner ring of Moscoviense, a topographic bench and associated ridge system occur around the northern and western edges of the basin, similar to those of lunar multi-ring basins. The inner basin of Grimaldi is bordered by ridges in the southeast and southwest, and even within Compton, two arcs of mare arches and ridges occur inside peak ring segments. In both Poincare and Korolev, a ridge ring is suggested, although not confirmed with existing images.

Consequently, evidence from both ring spacing and ring morphology contradict the previously-held notion that ridge rings in multi-ring basins represent the location of a buried peak ring. Although the influence of pre-mare structure is visible around the edges of basins and in areas of shallow fill, the relationship of inner ring ridge systems to buried peak rings is more complex than a simple overlying model.

(1) D. E. Wilhelms and J. F. McCauley (1971) USGS Map I-703. (2) J. W. Head (1977) in Impact and Explosion Cratering, 563-573. (3) W. K. Hartmann and C. A. Wood (1971) The Moon, 3, 2-78. (4) W. J. Brennan (1976) Proc. 7th, 2833-2843. (5) S. K. Croft (1980) LPS XI, 180-182. (6) T. A. Maxwell and A. W. Gifford (1980) Proc. 11th, in press. (7) S. C. Solomon and J. W. Head (1980) RGSP, 18, 107-141. (8) C. A. Wood and J. W. Head (1976) Proc. 7th, 3629-3651. (9) C. A. Hodges and D. E. Wilhelms (1978) Icarus, 34, 294-323. (10) J. W. Head (1979) Moon and Planets, 21, 439-462.

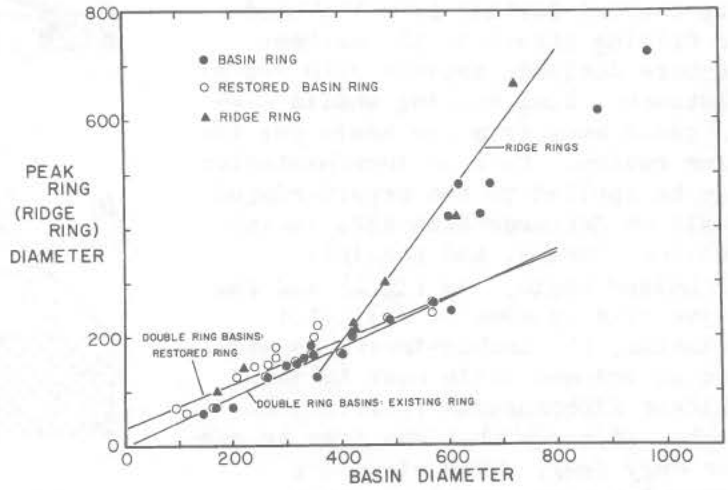

Fig. 2. Peak ring and ridge ring vs. next outer basin ring for double- and multi-ring basins.

ASPECTS OF RING TECTONICS: MERCURY, GANYMEDE, AND BEYOND.

William B. McKinnon, Lunar and Planetary Laboratory, University of Arizona, Tucson, AZ 85721.

The mechanics of multiple ring formation have been shown to be related to the collapse of the transient basin cavity when the excavation depth and lithosphere thickness are comparable (1,2). Fig. 1 illustrates the effects of lithosphere strength and thickness (or more broadly, planetary thermal structure) on the number, spacing, and morphology of such rings. As the gravitational potential of the transient crater supplies the energy for ring tectonics, both density and local g are important parameters. For very thin, weak lithospheres and underlying asthenospheres of sufficiently low viscosity, basin formation is followed by oscillation of the transient cavity region and outward propagation of a gravity wave which catastrophically disrupts the lithosphere (fig. 1a). The required viscosities are generally so low that such oscillations will be confined to the transient crater unless the asthenosphere is truly liquid. An increase in asthenospheric viscosity, such that the system is overdamped, is in keeping with realistic thermal gradients and the time and stress scale of basin relaxation. Thus, extension is solely radial. For thin lithospheres, a multiple set of concentric rings is generated. Morphology (tensional rifts, normal faults, or graben) depends on driving stress, asthenospheric strain, and ring curvature. Generally graben are favored farther from the basin as driving stress in the asthenosphere declines rapidly with radial distance. Ring spacing should also increase away from the basin for the same reason. Such an interpretation may be applied to the crypto-ringed basin on Ganymede (remnants include Galileo, Marius, and possibly Nicholson Regio, see fig.2) and the major ring systems on Callisto: Valhalla, the double-impact Asgard, and an unnamed basin near Adlinda. Thicker lithospheres restrict the number of rings that can form to one (or very few). Such rings are irregular, intersecting, steep

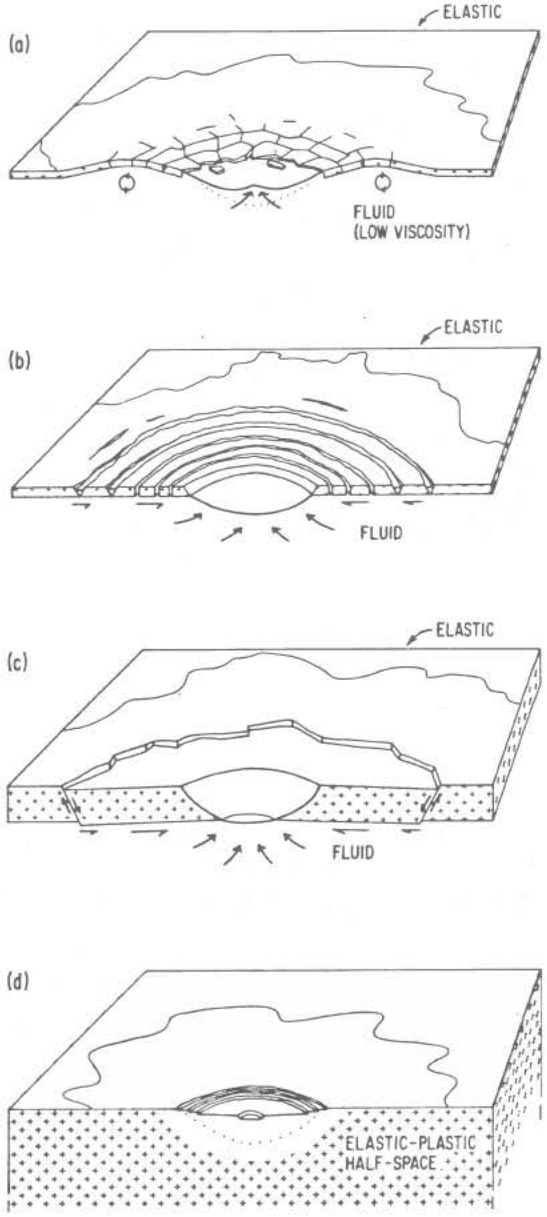

FIGURE 1.

RING TECTONICS

McKinnon, W.B.

inward facing normal faults (fig. 1c). This most likely describes the outer rings on terrestrial bodies such as the Moon (i.e., Cordilleran-type rings) and that of the relatively young basin Gilgamesh on Ganymede. Such *outer ring* formation is suppressed if the lithosphere becomes too thick (fig.1d). Deformation is confined to the crater region and is represented here by the Galilean satellite standard; rim terraces, flat floor, and central pit.

It is clear that the physical criteria of this formation mechanism are not met by the ring structures preserved in terrestrial continental shields. It seems highly probable that terrestrial rings, and peak rings in general, form in a different manner. It is interesting to note that an asteroidal impact into an ocean basin (ignoring possible complications due to ∿5 km of water) could result in multiple rings, forming as described above. The oceanic lithosphere is relatively thin (compared to the continents) and also unstably stratified. If the rings were fractured (along radial planes), the potential exists for blocks to sink into the asthenosphere on a time scale of $\sim 10^5$-10^6 years.

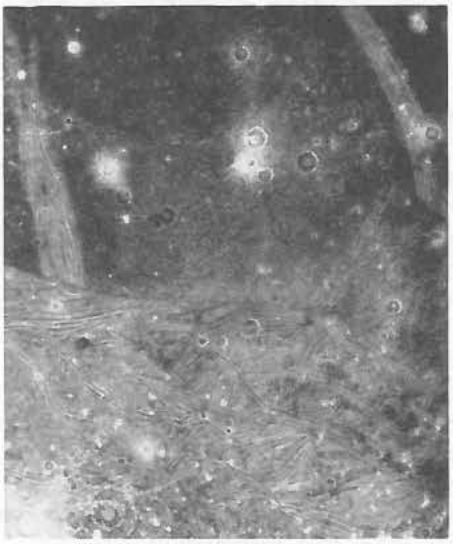

FIGURE 2. A circular albedo feature, ∿450 km in diameter, lies quite close to the site of the basin scale impact proposed to generate the Ganymedian rings (3). The top of the frame includes the southernmost extension of Marius Regio. The blocks of reticulate terrain appear to contain two sets of roughly orthogonal grooves. One strikes parallel to the general trend of adjacent grooved terrain. The other may reflect structural control of an ancient basin. Voyager 2 frame FDS 20636.02

The number and preservation state of large basins on Mercury and the existence of intercrater plains raise questions about the timing of thermal evolution and terminal bombardment (4). As such effects are observable through ring structure on Ganymede and Callisto (2), it is interesting to search for similar effects on Mercury. The only evidence to date on outer rings is derived from Caloris (centered at 31°N, 194° W), Tolstoj (-16°S, 164°W), and a possible basin in western Sobkou Planitia (34°N, 133°W) (5,6). This narrow latitudinal distribution may be a real effect, due to an equator to pole difference in lithosphere thickness. Differential insolation (corresponding to a temperature contrast of almost 600 K) elevates lithospheric isotherms and may thin the equatorial lithosphere by as much as one third with respect to the poles. There does not appear to be an observable latitude dependence for the onset of *peak ring* formation or the crater rim/peak ring ratio (fig.3).

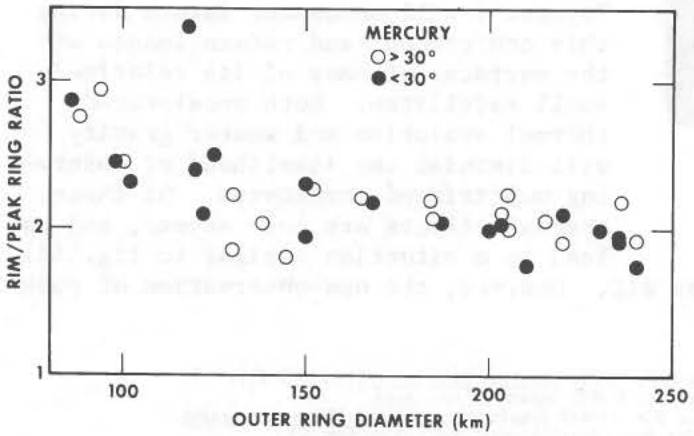

FIGURE 3. Data are from (6).

RING TECTONICS

McKinnon, W.B.

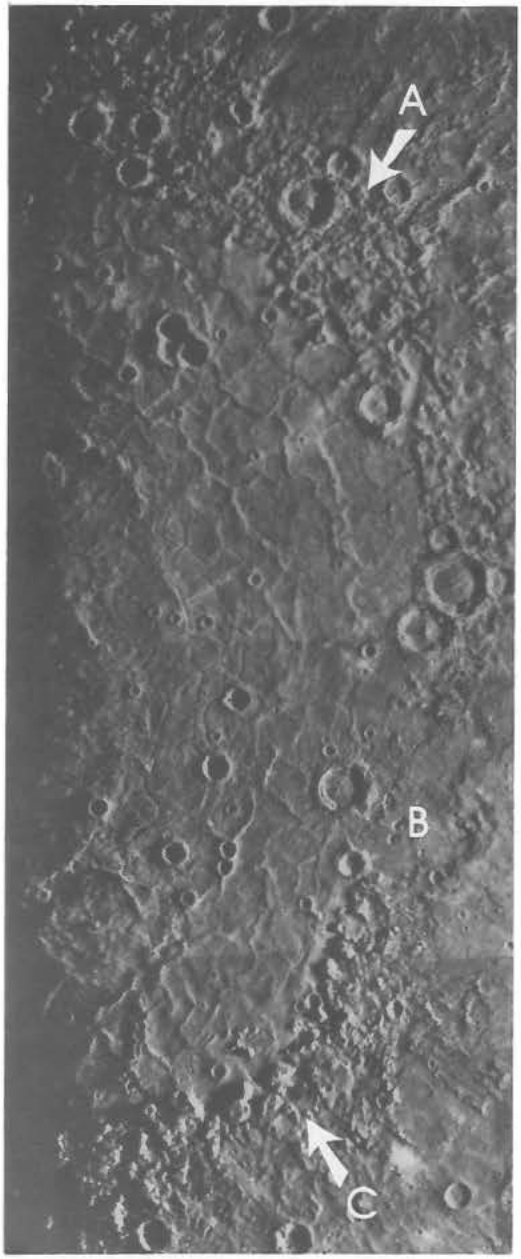

FIGURE 4. Caloris.

Again, formation mechanisms are not expected to be similar, and temperature effects on the generation of peak rings may not be expected in this case.

The ring ratios of Caloris and Tolstoj (<1.4) are such that the lithosphere must be considered as thin. The limited development of the rings may be related to the greater strength of the mercurian lithosphere (7,8) and/or viscosity structure in the asthenosphere. The inter-ring distance serves as an upper limit for the lithosphere thickness, H. Thus $H \lesssim 50$ km for Tolstoj. As Tolstoj is $\sim$300 km in diameter, a non-proportional excavation depth can serve as a lower limit. For Caloris (fig. 4) this upper limit varies from $\sim$120 km in the NE (arrow A) to $\sim$75 km in the SE (arrow C). These limits are consistent with both the expected equator-to-pole thermal variation and with the relative ages of the two basins.

The missing section of the Caloris Montes formation (B) is not readily explained, unless this section of the ring system sank into the mercurian mantle. This leaves open the possibility that the main Caloris scarp lies outside the original rim, and that all interior ring blocks were subducted. The necessary density inversion is plausible but speculative.

It is hoped that the ring tectonic theory will increase in refinement and application to solar system basins. Voyager 1 will encounter Saturn during this conference, and return images of the surfaces of many of its relatively small satellites. Both accelerated thermal evolution and weaker gravity will diminish the likelihood of observing multiringed structures. Of these, thermal effects are more severe, and may lead to a situation similar to fig. 1d. Thus outer rings may not form at all. However, the non-observation of peak rings is considered unlikely.

References
(1) Melosh H.J. and McKinnon W.B. (1978) Geophys. Res. Lett. 5, p. 985-988.
(2) McKinnon W.B. and Melosh H.J. (1980) Submitted to Icarus.
(3) Passey Q.R. and Shoemaker E.M. (1980) Submitted to The Satellites of Jupiter.
(4) Schaber G.G. et al. (1977) Phys. Earth Planet. Int. 15, p.189-201.
(5) Schaber G.G. and McCauley J.F. (1980) U.S. Geol. Surv. Map I-1199.
(6) Croft S.K. (1979) Ph.D. Thesis, U.C.L.A.
(7) McKinnon W.B. (1980) Ph.D. Thesis, Caltech.
(8) Pike, R.J. (1980) Proc. Lunar Planet Sci. Conf. 11th, in press.

A MECHANICAL ANALYSIS OF THE VALHALLA BASIN, CALLISTO

H. J. Melosh*, N. B. McKinnon+, and Anne Remsberg* (*Dept. Earth and Space Sciences, SUNY Stony Brook, Stony Brook, N. Y. 11794. +Lunar and Planetary Laboratory, Univ. of Arizona, Tucson, Ariz. 85721).

The Valhalla basin on Callisto (JIV) is the largest and most complex multiring basin yet discovered. The outer rings of this basin are located some 2,000 km from the basin center -- a distance nearly equal to the 2420 km radius of the satellite. The basin's interior is occupied by a roughly circular patch of high albedo material 600 to 800 km in diameter. This is surrounded by darker terrain which is traversed by bright, roughly concentric ridges. These ridges have an irregular "ropy" appearance similar to mare ridges. They occupy an annulus surrounding the basin center, extending from the edge of the bright interior to 200-300 km outward. Beyond the zone of concentric ridges there is a region of dominantly outward-facing concentric scarps. These scarps are best developed in an annulus about 600 km wide, but individual scarps (especially to the NE of the basin center) can be seen as far as 2,000 km from the center. Near the inner edge of this zone a few inward-facing scarps and graben occur. A light-colored hummocky plains unit appears to have been extruded at the foot of many of these escarpments. The crater density is relatively low on the dark terrain within about 300 km of the edge of the bright basin center, suggesting obliteration of the original crater population by ejecta from the basin-forming impact. Farther away from the basin center the escarpments cut older heavily cratered terrain. Numerous examples of craters cut by the escarpments may be observed. The down dropped portion of several such craters appears to have been innundated by the light hummocky plains unit.

It has been proposed (1) that asymmetric multiple rings are caused by the fracture of the lithosphere as the underlying fluid asthenosphere flows toward the transient crater cavity. When the lithosphere is relatively thick (or strong) compared to the transient cavity depth (or overburden pressure relief), then only one or two inward-facing ring scarps develop. When, as appears to be the case for Callisto, the lithosphere is thin compared to the transient crater depth, it suffers multiple fragmentation (2) In this case the elastic analysis of (1) is no longer appropriate. A plastic analysis, in which general yielding is assumed to have occured in a large region, is a better approximation.

We have performed a preliminary plastic analysis of the situation shown in Fig. 1. A thin elastic-plastic lithosphere of thickness t overlies a fluid asthenosphere. The lithosphere is punctured by a crater of radius R and depth d. The asthenosphere then flows inward toward the crater, exerting a shear stress $\sigma_b = -S \left(\frac{R}{r}\right)^4$ on the base of the lithosphere. Stresses σ_{rr} and $\sigma_{\phi\phi}$ are thus induced in the lithosphere. For low values of σ_b these stresses do not cause general yielding. At most, an extensional failure occurs where σ_{rr} reaches its maximum value (at $r_{max} = 1.5R$).

VALHALLA BASIN

H. J. Melosh

However, when σ_b is large compared to the strength of the crust two types of plastic solution must be introduced. Yielding begins at the inner lip of the crater, where $\sigma_{rr} - \sigma_{\phi\phi} = \tau_c$ ($\tau_c \equiv$ yield strength). This failure first occurs when the dimensionless strength parameter $\gamma = \frac{SR}{\tau_c t}$ reaches a value of 2.40.

The plastic solution corresponds to strike slip faulting, with a vertical intermediate principal axis. Figure 2 shows the failure mode as a function of γ and distance away from the crater run. The vertical dashed line in the elastic region shows where σ_{rr} is maximum. When plastic yielding begins this radius of maximum extension shifts slightly. As γ becomes larger eventually $\sigma_{rr} = \tau_c$, $\sigma_{\phi\phi} = 0$ and the strike slip solution is no longer valid. This occurs when $\gamma > 5.75$. The intermediate principal axis becomes horizontal and concentric normal faults form. A region of strike slip faulting must still intervene between this concentric normal fault province and the elastic solution, but strains are small far from the crater and it is questionable that this region could be observed with low-resolution images.

The limitations of this model are that it is only valid for a flat plate, whereas a planet's lithosphere should be treated as a spherical shell, and that it ignores the interdependence of applied shear stress and yielding: the actual basal stress is reduced as soon as inward flow begins. However, the general structure of the solution seems to accord roughly with the Valhalla basin. The inner concentric ridges may be interpreted as the traces of vertical strike-slip faults (or perhaps material extruded along them). The outer scarps form in the concentric normal fault zone. The fact that the scarps face outward is perhaps due to the lateral transmission of stress through the plastic lithosphere: The inward basal drag falls off rapidly away from the crater rim. However, since the extensional σ_{rr} stresses are transmitted many crater radii from the rim, at large distances the lithosphere's inward motion is retarded by drag in the asthenosphere rather than driven by it. In this case, the force couple on crustal blocks tends to rotate their tops inward, producing outward-facing scarps with gently inward dipping backslopes. Closer to the crater the basal drag is in the opposite sense and (as in lunar multiring basins) inward facing scarps form. The occurrence of opposed scarps (graben) at intermediate distances in Valhalla tends to support this concept.

References

(1) Melosh, H. J. and W. B. McKinnon, Geophys. Res. Lett. 5, 985-988 (1978)
(2) McKinnon, W. B. and Melosh, H. J., Icarus, in press (1980)

VALHALLA BASIN

H. J. Melosh

FIG. 1

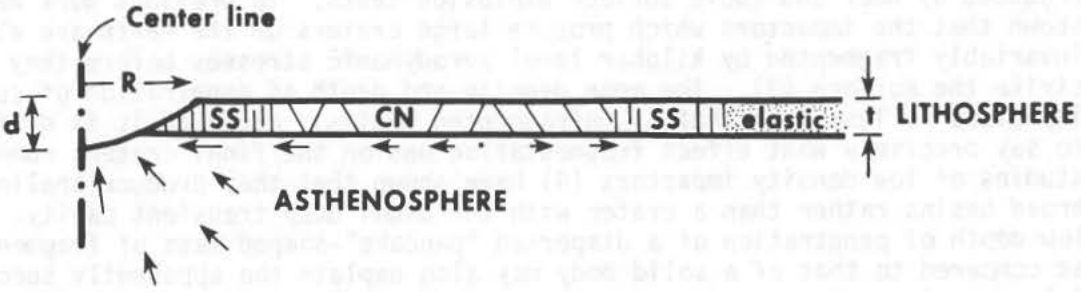

FIG. 2

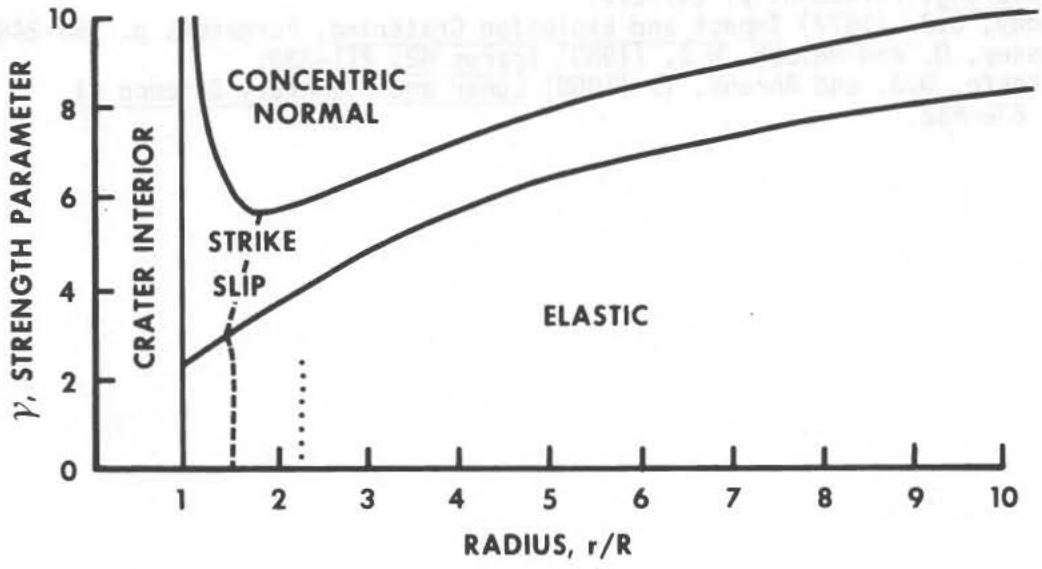

ATMOSPHERIC BREAKUP OF TERRESTRIAL IMPACTORS H. J. Melosh, Dept. Earth & Space Science, SUNY Stony Brook, Stony Brook, NY 11794 and Q. Passey, Div. Geol. & Planetary Sci., Caltech, Pasadena, CA 91125

A number of terrestrial impact craters in the size range 3-50 km have frequently been used as analogues of multiring basins (1,2). Furthermore, Roddy (2) has demonstrated a similarity between these craters and the craters produced by near and above surface explosion tests. In previous work we have shown that the impactors which produce large craters on the earth are almost invariably fragmented by kilobar level aerodynamic stresses before they strike the surface (3). The mean density and depth of penetration of such impactors is less than that of unfragmented bodies. Although it is difficult to say precisely what effect fragmentation has on the final crater, numerical studies of low density impactors (4) have shown that they produce shallow, broad basins rather than a crater with the usual deep transient cavity. The low depth of penetration of a dispersed "pancake"-shaped mass of fragments as compared to that of a solid body may also explain the apparently successful comparison of such terrestrial craters as Flynn Creek and Ries (2) with craters produced by surface explosions. In view of these considerations, the comparison of terrestrial impact craters with craters on airless bodies (or even on Mars) must be approached with extreme caution. It seems possible that large terrestrail impact structures may have little to tell us about large craters on other planets, since they were formed by a very special (aerodynamically fragmented) type of projectile. Further investigation of the effects of fragmentation upon final crater form is thus necessary in interpreting terrestrial craters.

REFERENCES

(1) Dence, M.R., Grieve, R.A.F., Robertson, P.B. (1977) Impact and Explosion Cratering, Pergamon, p. 247-275.
(2) Roddy, D.J. (1977) Impact and Explosion Cratering, Pergamon, p. 185-246.
(3) Passey, Q. and Melosh, H.J. (1980) Icarus 42, 211-233.
(4) O'Keefe, D.J. and Ahrens, T. (1980) Lunar and Planetary Science XI, p. 830-832.

MORPHOLOGICAL FEATURES OF THE SUDBURY CRATER;
Gordon G. Morrison and Geological Staff, Inco Metals Company, Copper Cliff, Ontario, Canada, P0M 1N0.

The Sudbury structure has, for the past fifteen years, been suspected of being an impact crater. These suspicions are based on the presence of various features which have a strong correlation with impact craters but nonetheless are termed "circumstantial" and "debatable" by those opposed to the existence of such impacts. These features are shock metamorphism of minerals, shatter cones and the voluminous amounts of breccia within the wall rocks. Also, there is the perennial debate over the genesis of the Onaping Formation -- ash flow tuff or fallback breccia?

The above features, although convincing to a large number of geologists, are not conclusive proof. This is why an in-depth comparison of the morphological features of the Sudbury structure with those of documented impact sites was undertaken. The major morphological features of fresh craters the size of the original Sudbury crater are: 1) a polygonal outline, 2) terraces along the crater wall, 3) a shallow crater wall angle which dictates a maximum crater depth of less than 10 km and 4) flat floor and central peaks.

1) The polygonal outline. A study of lunar and other planetary craters indicates that a number of large craters have a common symmetry to their polygonal outlines. Terrestrial craters such as Manicouagan and Charlevoix have polygonal outlines with similar symmetries to those observed for lunar craters. The reconstruction of the polygonal outline of the Sudbury crater yields this strikingly familiar symmetry.
2) Terraces. The walls of the Sudbury crater are definitely a rubble zone or megabreccia penetrating for thousands of feet into the surrounding country rocks. The inner face of this rubble zone is terraced. The terraces, in certain areas, repeat at regular depth intervals of about 1,000 feet. The terraces are the traps in which the concentrations of copper-nickel sulphides are found.
3) Shallow crater wall angle. The shape of the Sudbury terraces as compared to those within lunar craters and also the position of the ores within the Sudbury terraces indicate that the present steep contact angles at Sudbury are a deformational feature and that the original crater wall angle at the time of deposition of the sulphides was near 15° rather than the present 45° - 60°. Recent paleomagnetic work supports these observations.
4) Flat floor and central peaks. The evidence indicates that the Sudbury crater is endogenically modified and that considerable subsidence of the central position of the crater occurred after intrusion of the triggered magma. Therefore, the original flat floor and central peaks have probably been destroyed.

MORPHOLOGICAL FEATURES OF THE SUDBURY CRATER

G. G. Morrison et al

References:

1) Currie, K. L. (1972): Geology and petrology of the Manicouagan resurgent caldera, Quebec; G.S.C. Bulletin 198.

2) Dence, M. R. (1972): Meteorite impact craters and the structure of the Sudbury Basin; in New Developments in Sudbury Geology (J. V. Guy-Bray, ed.); Geol. Assoc. Can. Spec. Pap. 10, 7 - 18.

3) Head, J. W. (1976): Origin of outer rings in lunar multi-ringed basins; in Impact and explosion cratering (Roddy, Pepin and Merrill, editors).

4) Melosh, H. J. (1976): Crater modification by gravity; in Impact and explosion cratering (Roddy, Pepin and Merrill, editors).

5) Morris, W. A. (1979): Tectonic and metamorphic history of the Sudbury norite: the evidence from paleomagnetism; E. M. & R. internal report.

6) Murtaugh, J. G. (1975): Geology of the Manicouagan cryptoexplosion structure; Ph.D. thesis, Ohio State University.

7) Pattison, E. F. (1979): The Sudbury sub-layer, Can. Min., vol. 17.

8) Rondot, Jehan (1971): Les breches d'impact de Charlevoix (abs.); Meteoritics 6, 307 - 308.

9) ——— (1972): Geologie de la structure de Charlevoix; Congr. Geol. Int. 24^{e} Sess. Sect. 15, 140 - 147.

10) ——— (1979): Reconnaissance geologiques dans Charlevoix - Saguenay, Ministere des Richesses Naturelles du Quebec, DPV-682.

SCHIAPARELLI BASIN, MARS: MORPHOLOGY, TECTONICS AND INFILLING HISTORY. P.J.Mouginis-Mark, and V.L.Sharpton, Dept. Geological Sciences, Brown Univ., Providence, R.I. 02912; and B.R.Hawke, Hawaii Inst. Geophysics, Honolulu, HI 96822

Introduction : Analyses of the distribution and morphometry of martian basins (1,2) have demonstrated that, compared to the Moon and Mercury, Mars possesses significantly fewer basins per unit surface area. Although superficially resembling lunar basins of comparable size (1), the problem of interpreting the morphology and style of basin ejecta emplacement on Mars is handicapped by this small number of basins, the eroded nature of the larger examples (e.g. Argyre, Hellas and Isidis), and the lack of complete high-resolution photography for many of the basins. While more degraded than lunar basins such as Orientale and Imbrium, the 470 km dia. martian basin Schiaparelli (3S, 343W) (Fig.1) is not subject to these limitations and affords the opportunity of identifying remnants of the original basin structure, interpreting basin infilling processes and comparing its tectonic history to the inferred evolution of lunar basins(3).

Fig. 1: Mosaic of oblique images showing the prominent features within Schiaparelli (3S, 343W). Basin diameter is 470 km. Viking frames 655A45-53.

Morphology of interior units : Five main morphological units can be identified within Schiaparelli (Fig.2). At least two units that are probably related to the original basin geometry exist: remnants of a peak ring (partially modified by an old crater in the SW) measuring approx. 230 km in diameter and 10-40 km wide; and "furrowed material" interpreted to be original wall segments of the basin. The "rugged ridged material" may also

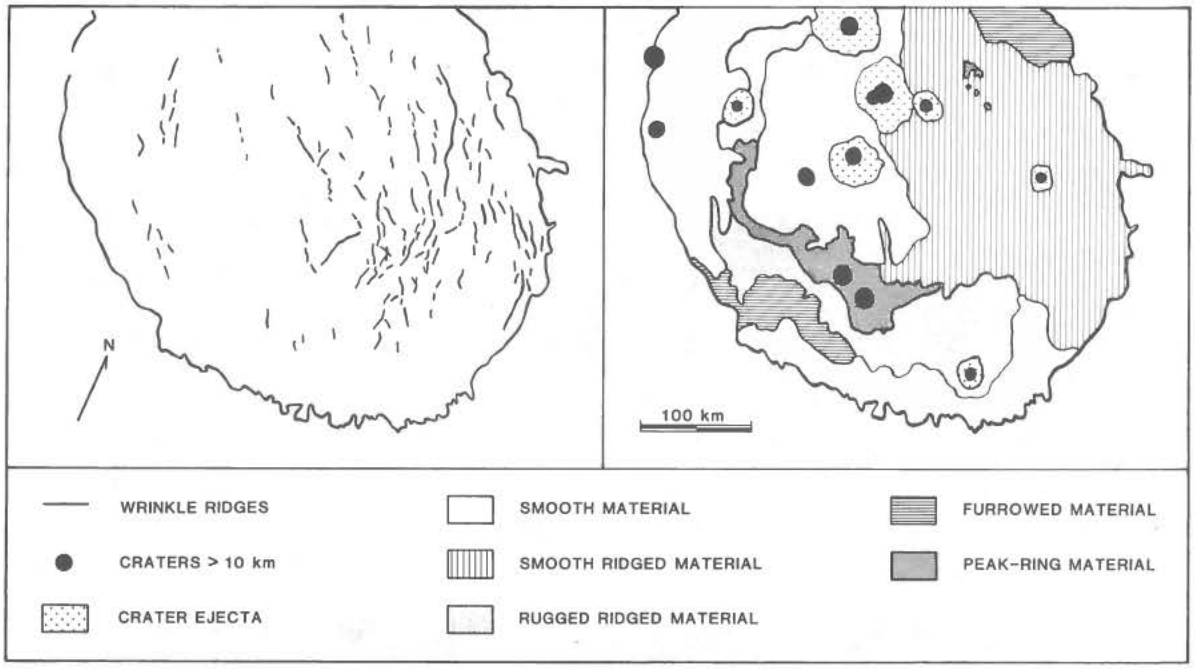

Fig.2: Morphological maps of Schiaparelli showing the distribution of wrinkle ridges and surface units described in the text. Base map same as Fig.1.

represent early basin floor material that was subsequently tectonically deformed in situ or buried by a thin layer of coherent material. The "smooth ridge material" is believed to post-date the period of basin formation, due to the presence of several buried craters outlined by the ridge elements. The morphometry of these wrinkle ridges may also indicate that lunar mare-type volcanism (5) has occurred in this martian basin. The areas mapped as "smooth materials" appear to be of relatively recent origin and are interpreted to be the products of multiple periods of eolian deposition. Independant evidence that supports the presence of such deposits within Schiaparelli also exists, because Earth-based radar measurements made in 1976 (6) failed to produce returns from the basin floor, indicating the possible existence of very porous material over an extensive area.

Basin tectonics from wrinkle ridges : Both the "smooth" and "rugged ridged materials" (Fig.2), interpreted here to overlie the original basin topography, possess numerous examples of wrinkle ridges (Fig.1). By analogy to lunar basins (3,4), the presence of these ridges implies that the surface units on the eastern side of the basin floor are composed of cohesive, brittle materials that have undergone tectonic deformation. Many ridge locations appear to be related to the position of the buried peak ring, but a strong NW-SE trend to the ridge elements also exists. This ridge orientation may in part be due to sampling limitations as a consequence of the eolian mantle on the western floor, but it also suggests that a regional stress pattern existed at the time of ridge development. Such a regional stress field is also locally corroborated by the occurrence of two large normal faults at 25S, 340W and 25S, 25W that both have NE-SW orientations.

SCHIAPARELLI BASIN, MARS

P.J.MOUGINIS-MARK ET AL.

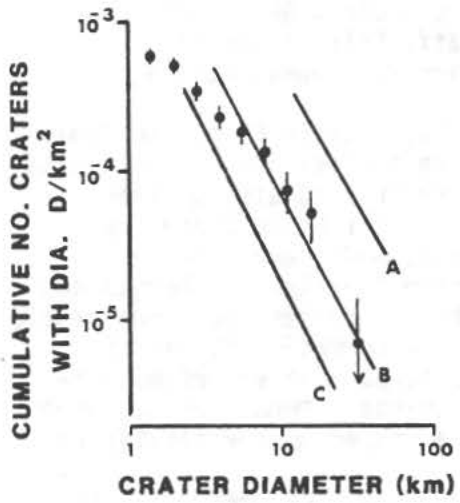

Fig.3: Cumulative size/frequency distribution for Schiaparelli. A: cratered upland. B: Lunae Planum. C: Solis Planum

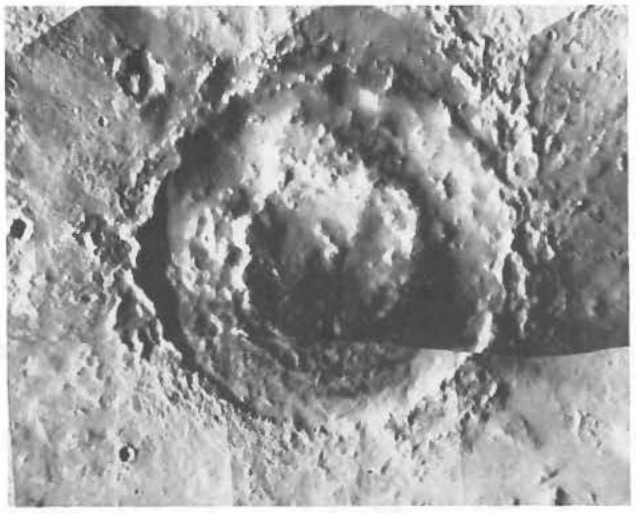

Fig.4: 190 km Lyot (50N, 330W) may be a good analogue to the pre-filled Schiaparelli. Part of JPL mosaic 211-5819.

Basin history: Fig.3 presents a size/frequency curve for 78 craters larger than 2 km dia. identified within Schiaparelli.Comparisons of this curve with those for cratered uplands (7), Lunae Planum (7) and Solis Planum (8) indicate that Schiaparelli predates the formation of Lunae Planum but is considerably younger than the cratered uplands. This relative age may, however, be an underestimate due to the loss of craters buried beneath the "smooth ridged material". For craters less than 10 km, eolian mantling also appears to be important because extensive areas of "smooth material" are devoid of such craters. From the existence of the buried craters beneath the "smooth ridged material", it is clear that an extended time period existed between basin formation and infilling by (presumed) volcanics.

A possible analogue to the pre-infilling morphology of Schiaparelli may exist in the 190 km basin Lyot (50N, 330W). Lyot (Fig.4) has a broad peak ring with extensive wall deposits that may be similar to the "furrowed material" in Schiaparelli. The existence of an extensive secondary crater field for Lyot (9) indicates the basin's relative youth, but there is no indication whether the absence of volcanic infilling and tectonic deformation is a product of the smaller size of Lyot, target characteristics, or lithospheric thickening with time comparable to that identified on the Moon (3).

References: 1) D.E.Wilhelms (1973) J.Geophys.Res. 78, 4084. 2) C.A.Wood & J.W.Head (1976) PLSC 7th, 3629. 3) S.C.Solomon & J.W.Head (1980) Rev. Geophys.Space Phys. 18, 107. 4) W.R.Muehlberger (1974) PLSC 5th, 101. 5) V.L. Sharpton & J.W.Head (1980) LPS XI, 1024. 6) G.S.Downs et al. (1978) Icarus 33, 441. 7) G.Neukum & D.E.Wise (1976) Science 194, 1381. 8) P.J.Mouginis-Mark et al. (1980) LPS XI, 762. 9) B.R.Hawke & P.J.Mouginis-Mark (1980) this volume.

EXPLOSION CRATERING AND THE FORMATION OF CENTRAL UPLIFTS AND MULTI-RINGS

David J. Roddy, U.S. Geological Survey, Flagstaff, Arizona 86001
G.H.S. Jones, Scientific Adviser, Emergency Planning Canada, Ottawa, Ontario, Canada.

Three explosion experiments, called Snowball, Prairie Flat, and Dial Pack, formed large flat-floored craters with both central uplifts and multi-ring structures. The surface morphologies of the craters also displayed either prominent central mounds or multirings. In all three cratering trials, the charge type, charge energy, and target media were the same. However, the use of both hemispherical and spherical explosion charges and the nature of their different energy coupling to the target had a noticeable effect on the specific morphology and structural deformation developed at each crater. These explosion data imply that a comparable set of morphological and structural effects may occur in large-scale impact events when projectile and target conditions are varied in a scaled manner similar to the changes in explosion conditions.

The three explosion trials were conducted within a kilometer of one another on the Watching Hill Test Site at the Defense Research Establishment Suffield, Alberta, Canada (1,2). Each cratering event was completed in the same stratigraphic units of interbedded clays, silts and sands overlying saturated clay; the water table was $\sim$ 7 m depth. The Snowball Crater, formed by a 500-ton TNT hemisphere lying on the ground, is a flat-floored crater, $\sim$ 83 m in apparent diameter, with a large central mound (Figs. 1a, 1b, 4). The Prairie Flat and Dial Pack Craters were both formed by 500-ton TNT spheres lying tangential on the ground, and are flat-floored craters, $\sim$ 60 m in apparent diameter, with low central mounds surrounded by radial ridges and troughs and multirings (Figs. 2a,b; 3a,b; 5, 6). The remarkable topographic and structural similarities between the Prairie Flat and Dial Pack Craters uniquely demonstrate that large-scale cratering events do yield very similar results when the initial conditions are well matched.

In the most general sense, both the hemispherical and spherical charges detonated at or near the ground surface formed broad flat-floored craters surrounded by low rims and continuous ejecta blankets. Both types of charges also formed craters with major subsurface uplift and inward movement of deeper water-saturated clay under the entire floor of each crater. The hemispherical Snowball charge formed the largest crater because it was detonated at the center of the charge on the ground surface, i.e., zero height-of-burst. It coupled a high-pressure shockwave directly into the target soils beneath the entire TNT charge. The spherical Prairie Flat and Dial Pack charges formed smaller craters, in part because the detonation point in the center of the charge was above ground. Consequently, the detonation pressure was transferred to the ground only along the contact at the base of the sphere. Beyond the contact area, shock pressures were greatly reduced because of attenuation of the TNT gas pressures prior to interaction with the ground. Therefore, less total energy was coupled downward due to the shape of the spherical charge and the small contact area with the ground. (S. Schuster, CRT, personal comm., 1980).

Cratering induced by the hemispherical charge with zero height-of-burst produced structural uplift beneath the entire crater floor and the most prominent central mound. Concentric and radial anticlinal/synclinal folds were formed on the flanks of the uplifted clay, but were not uplifted enough to affect the topography of the crater floor. Cratering induced by the spherical charges with a raised height-of-burst also produced uplift beneath the entire crater floor. The uplift, however, contained prominent

EXPLOSION CRATERING

RODDY, D.J. and JONES, G.H.S.

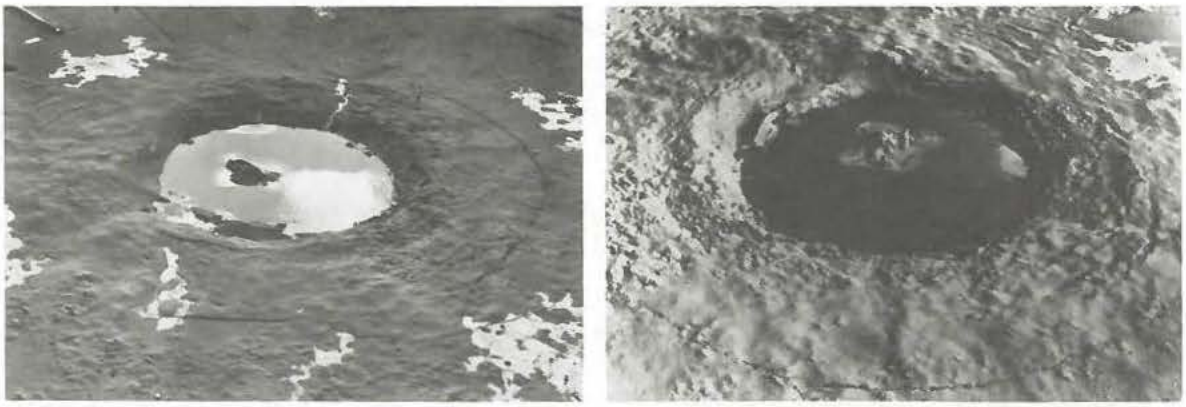

Fig. 1a,b. Snowball explosion crater one day after formation (from 2).

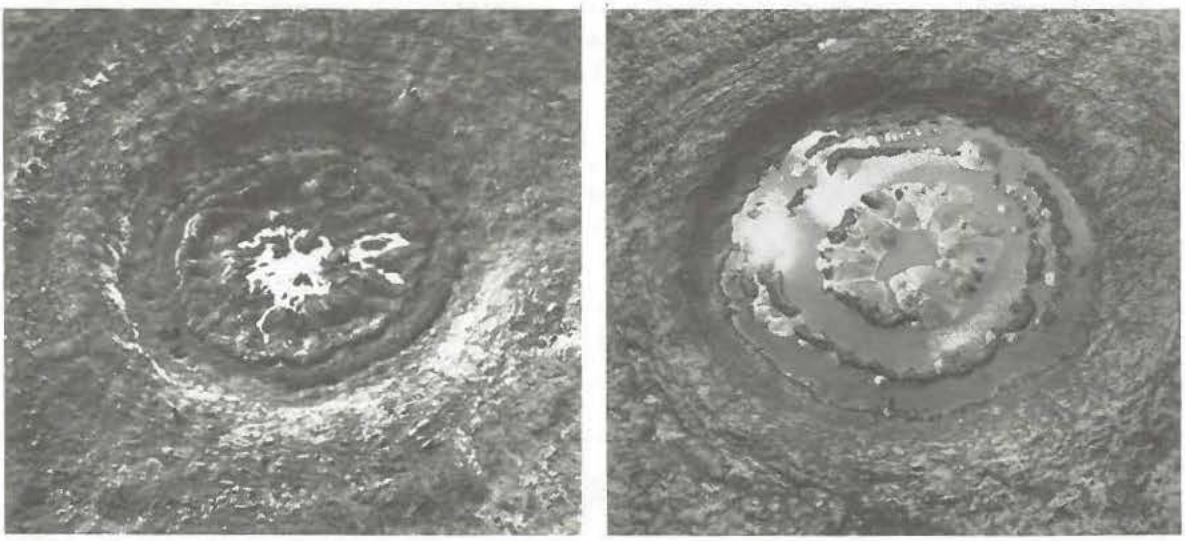

Fig. 2a,b. Prairie Flat explosion crater one hour after formation (a) and one day after formation (b) with groundwater flooding (from 2).

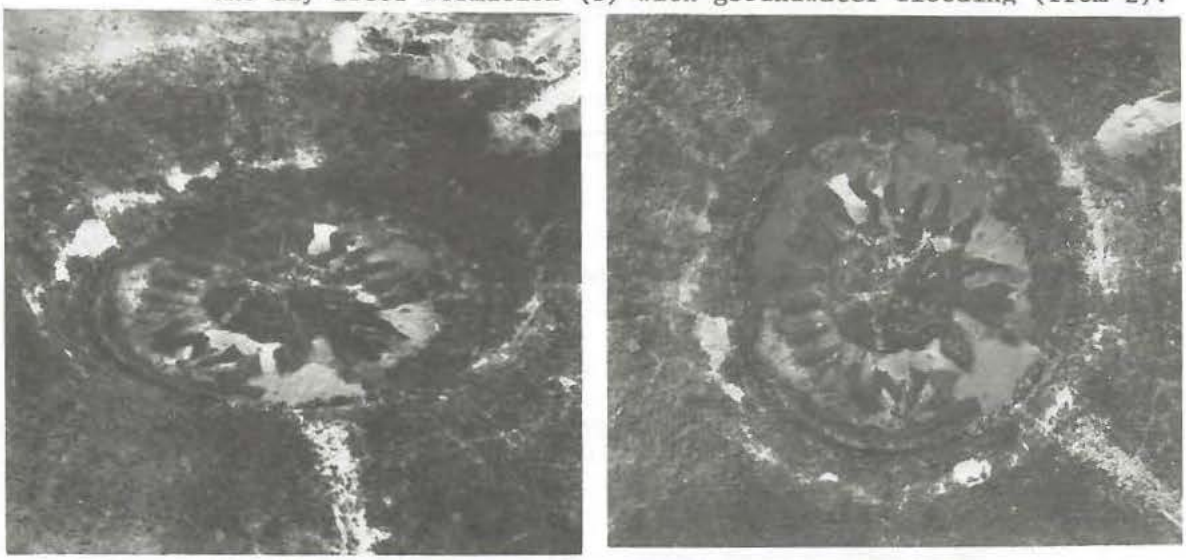

Fig. 3a,b. Dial Pack explosion crater one day after formation with groundwater flooding.

anticlinal/synclinal folds that formed both radial ridges and troughs and multiring topography surrounding a very low, flat, central mound. These structural and topographic features are a direct consequence of the charge yield, charge configuration, height-of-burst, nature of energy coupling, and highly compressible target soils over less compressible, mobile, water-saturated clay.

Qualitative application of the explosion analog data suggests that energy coupled by impacting bodies at or near the target surface should be effective in forming central uplift and multiring craters. Furthermore, a narrow range in the height-of-burst appears critical to the development of central peaks versus multiring structure and topography. These explosion analog conditions could be met, in part, by extensive vaporization of the projectile upon impact, thereby insuring maximum surface transfer of energy with minimum target penetration. Such impact conditions are plausible with low-density bodies, such as comets, as suggested in recent calculations by (3) and (4). In addition, layered targets with fluid-like properties, such as those of shallow, hot, mantle rocks, should greatly enhance uplift and multiring structure and topography. The complexity of these conditions, as well as the specific roles of impact energy, impacting body type, layering, target material responses, gravity, and other initial cratering parameters, suggest that numerical code work is essential to studies of the formation of the largest impact craters and basins.

(1) Jones, G.H.S., 1977, Complex craters in alluvium, in Roddy, D.J., and others, eds., Impact and Explosion Cratering, Pergamon, N.Y., 162-184.
(2) Roddy, D. J., 1977, Large-scale impact and explosion craters: Comparisons of morphological and structural analogs, in Roddy, D.J., and others, eds., Impact and Explosion Cratering, Pergamon, N.Y., 185-246.
(3) O'Keefe, J.D., and Ahrens, T.J., 1980, Cometary impact calculations: Flat floors, multiring and central peaks: Proc. Lunar Planetary Sci. Conf. 11th, Abstracts, P. 3, 830-832.
(4) Roddy, D. J., Kreyenhagen, K., Schuster, S., and Orphal, D., 1980, Theoretical and observational support for formation of flat-floored central uplift craters by low-density impacting bodies: Proc. Lunar Planetary Sci. Conf. 11th, Abstracts, P. 3, 943-945.

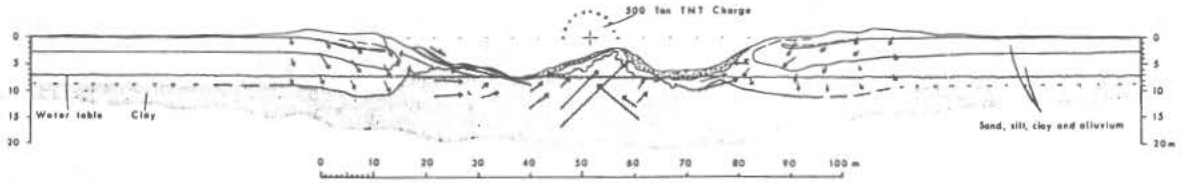

Fig. 4. Generalized geologic cross-section of Snowball explosion crater (2).

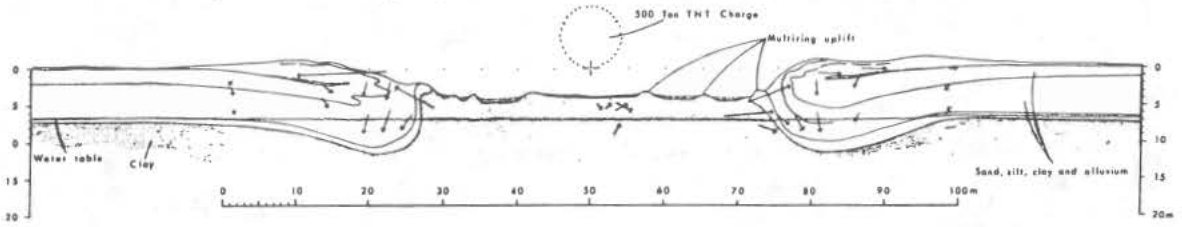

Fig. 5. Generalized geologic cross-section of Prairie Flat explosion crater (2).

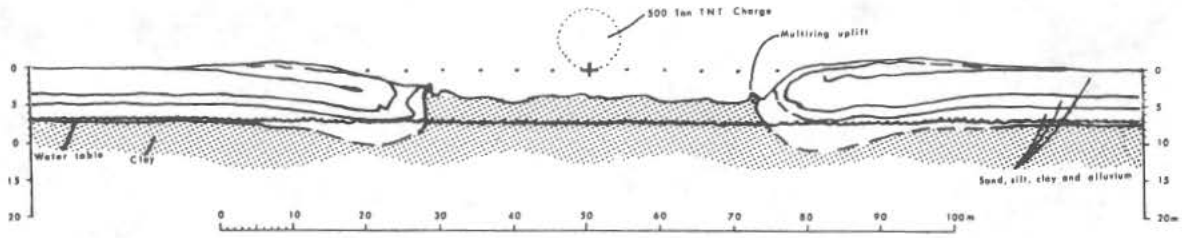

Fig. 6. Generalized geologic cross-section of Dial Pack explosion crater.

CENTRIFUGE SIMULATION STUDY OF THE PRAIRIE FLAT MULTI-RING CRATER*

R. M. Schmidt, Shock Physics Lab, M/S 42-37,
Boeing Aerospace Co., Seattle, WA 98124

K. A. Holsapple, Dept. of Aeronautics and Astronautics,
University of Washington, Seattle, WA 98195

A. J. Piekutowski, University of Dayton Research Institute,
Dayton, OH 45469

A model of the PRAIRIE FLAT site stratigraphy was devised to investigate the feasibility of reproducing the morphology of a multi-ring crater at subscale on a centrifuge. This in turn would allow a method to systematically determine which features of the stratigraphy model lead to a particular morphology.

A first-order soil model of the PRAIRIE FLAT stratigraphy was used for the subscale centrifuge simulation. Two important elements were tested: the depth to the water table and the depth to the competent sublayer. A 12.8-gram PETN spherical explosive charge was used dictating a linear scale factor of 1/395 with corresponding increased gravity equal to 395 G. The choice of scale for the test was influenced by both the charge size as well as the soil container size. The finite depth of the soil container to the thick aluminum baseplate was used to approximate the depth to the sandstone bedrock, 13.0 cm x 395 = 51 m. (For purposes of comparison each centrifuge subscale test dimension is multiplied by 395, thereby giving an equivalent prototype dimension.) An unconsolidated Ottawa "BANDING" sand medium was used for the initial testing. The sample was centrifuged at 395G to achieve equilibrium before the explosive was detonated.

*This work supported by NASA Planetary Geophysics and Geochemistry, Contract No. NASW-3291.

PRAIRIE FLAT CENTRIFUGE STUDY

Schmidt, R. M. et al.

The simulated depth to the water table on the first shot was 8.1 m. The resulting crater showed no rings and was of a characteristically different shape than that produced in the PRAIRIE FLAT event. The crater was too deep and the flat floor appeared to coincide with the water table depth. For the second shot, the water table was located at 5.1 m. The charge was detonated and the resulting crater showed better agreement with the bulk dimensions of the PRAIRIE FLAT crater, (see Table 1). In addition, three discernable discontinuous concentric rings were observed. The approximate radii were 0.2 R, 0.4 R and 0.7 R (where R is the apparent crater radius).

Table 1. Comparisons between centrifuge-scaled prototype and PRAIRIE FLAT event.

	395G Prototype	PRAIRIE FLAT
Water table depth (m)	5.1	6.7
Depth to "bedrock" (m)	51	60
Diameter (m)	71	61
Depth (m)	6.7	5
Volume (m^3)	13,800	13,000 (est.)
Radius/depth	5.3	6.1
Ring locations		
1st	0.2 R	0.28 R
2nd	0.4 R	0.52 R
3rd	0.7 R	0.61 R
4th	--	0.71 R

The fact that the geometries only approximately correspond to the field event can be attributed to numerous approximations in the centrifuge model. What is important, however, is that multi-ring features as well as the approximate crater bulk dimensions were reproduced in this very simplified stratigraphy model. Further sensitivity studies are anticipated to refine the technique, and then to evaluate the importance of water table depth, soil type, bedrock type and depth, charge size, and gravity.

The relative success of this experiment indicates that the centrifuge dynamic scaling which has been proven valid for dry and moist soils may also be applicable for saturated soil. Elevated gravity subscale tests appear promising to determine, at least qualitatively, the role of the site stratigraphy on complex morphology.

MULTI-RING BASIN FORMATION: POSSIBLE CLUES FROM IMPACT CRATERING CALCULATIONS, P. H. Schultz[1], D. Orphal[2], B. Miller[1], W. F. Borden[2] and S. A. Larson[2]. [1]Lunar & Plan. Inst., 3303 NASA Road 1, Houston, TX 77058, and [2]Calif. Res. and Techn., Inc., 4049 First St., Suite 135, Livermore, CA 94550.

Continuum mechanics computer code calculations of relatively low energy impacts (10^{23}, 10^{24} ergs) have been carried to late times and permit evaluating the generation and distribution of impact melt at different impact velocities.

The approach and imputs for the calculations are reported in detail by Orphal *et. al.* (1). Two calculations were performed for identical impactors (spherical iron, 10^{12} g) into identical targets (gabbroic anorthosite) but at different velocities, 5 km/s (NASA-1) and 15.8 km/s (NASA-2) producing craters about 900 m and 2000 m in diameter, respectively, as determined from ballistically extrapolating the cratering flow field at about one second. Although additional calculations are needed before extrapolations can be made to other energy and momentum ranges, these two examples reveal aspects of crater growth and ejecta distribution that may be significant for understanding impact phenomenology associated with basin formation.

CALCULATIONAL RESULTS

Crater Growth. Transient crater growth is discussed in detail by Orphal in ref. (1). Figure 1 shows the volume of material ejected (V_e) relative to the total ejected volume (V_E) for the two calculations. During most of crater growth, material is ejected as a function of $(X/R)^3$, which may be idealized as hemispherical growth, where X is the radius of the growing crater and R is the final transient crater radius. After reaching maximum penetration, d, crater growth approaches a cylindrical approximation or $(X/R)^2$. About 80% of the total ejected mass leaves the cavity prior to the cylindrical growth stage although the crater has reached nearly 75% of its final radius. Figure 1 shows that NASA-1 and NASA-2 are slightly displaced. This reflects the larger size of NASA-2 and the effects of gravity.

The amount of material ejected from a crater is significantly less than the amount defined by the transient crater (2,3,4). The present calculations indicate that only 57% and 43% of the "missing" mass defined by the transient cavity is actually ejected for NASA-1 and NASA-2, respectively. Figure 2 reveals that most of this "missing" mass represents material displaced downward and outward, a phenomenon described in impact experiments (2,5), explosion-cratering theory (4,6), and other impact-cratering calculations (7). Tracing selected particle paths suggests that material about 200 m (NASA-1) and 300 m (NASA-2) below the original ground surface are not ejected from the crater. These values correspond to approximately 60% of the maximum crater depth.

Ejecta Distribution. Figure 3 shows the distribution of ejecta around NASA-2; results from NASA-1 are similar. Thicknesses represent the mass per unit area arriving at a given range and no correction has been introduced for secondary cratering processes. The results are referenced to the thickness value at 1.5 R_c (R_c=radius of crater at the original ground surface) in order to minimize effects of rim uplift. The data have been smoothed by a running mean (window of r/R_c=0.1). The relative thickness decreases with relative range as $(r/R)^{-4}$ near the rim but approaches $(r/R)^{-2.5}$ at larger distances. This ejecta decay approximates the -3 slope suggested by McGetchin *et al.* (8), but results in significantly more ejecta at larger ranges. The change in the power-law decay reflects the effect of ejection position within the cavity (9). For comparison, an analytical prediction of ejecta decay used in (9) is shown for terrestrial gravity.

The calculations were designed to permit analyzing the distribution of shocked materials. Figure 4 reveals that materials arriving at any range

CRATERING CALCULATIONS

Schultz, P. H. *et al.*

display a wide range in peak shock pressures experienced prior to ejection. Impact melt occurs within a crater radius of the crater rim (NASA-2) but is mixed with ejecta having very low peak pressures. As discussed in (1), 47% of the melt is actually retained in the final NASA-2 crater, in contrast with no retained impact melt in NASA-1.

POSSIBLE IMPLICATIONS FOR BASIN FORMATION

The extrapolation of these calculations to basin size is clearly a precarious game; nevertheless, there are several notable trends. If it is *assumed* that the transient crater of a basin impact resembles the calculated transient craters, then the amount of material ejected from an impact cavity is less than half of the volume represented by the transient cavity and is derived from depths nearly half of the transient cavity depth. This result and its implications have been discussed by Croft (4,10). (It should be noted, however, that unusually low density projectiles may produce much shallower transient crater cavities.) Under lunar gravity, ejecta are more widely dispersed (Fig. 3), thereby reducing the power-law decay of ejecta thickness from a near-rim relation of $(r/R)^{-3}$ approaching $(r/R)^{-2}$ at large distances. As the limit of gravity-controlled excavation reduces relative to the limit of strength-controlled disruption, the total arrival of mass/unit-area reduces but the rapid fall-off implied by previous models reduces significantly. For a spherical body, ejecta thicknesses at large distances (>5R) exhibit an even slower decay, $(r/R)^{-1}$. Consequently, the effects of near-rim ejecta characterizing 50 km-diameter craters may be extended to larger distances around major basins.

Extrapolating the results of Fig. 4 suggests that a wide range of shock levels can be anticipated at a given range. The specific values depend on both impact velocity and impact energy, and on the average increase with increasing range. The minimum peak shock pressures for both NASA-1 and NASA-2 are similar at a given range, but the typical and maximum values are significantly greater. Owing to re-zoning and averaging during the calculations, however, specific shock-pressure histories (with the exception of the melted and partially melted materials) must be treated with caution. The observed trends also must be considered in the context of gravity-limited growth for basin-size events where only the higher velocity materials with higher peak shock pressures can escape the transient cavity (11).

Further calculations bracketing different combinations of impact velocity and impact energy are necessary to resolve some of the trends inferred from NASA-1 and NASA-2. Nevertheless, current trends suggest (a) relatively shallow excavation depths; (b) ejecta volumes that are nearly one-half of the transient-crater volume; (c) cylindrical crater growth at later stages; (d) less rapid thinning of ejecta mass with distance and (e) a wide range in peak shock pressures at a given range but much higher typical pressures than might be inferred directly from the current calculations.

References: 1. Orphal D. L. *et al.* (1980) *Proc. Lunar and Planet. Sci. Conf. XI* (in press). 2. Stöffler D. *et al.* (1975) *J. Geophys. Res. 80*, 4062-4077. 3. Dence M. R. *et al.* (1977) *IEC**, p. 247-275, Pergamon, NY, 1296 pp. 4. Croft S. K. (1980) *Proc. Lunar and Planet. Sci. Conf. XI* (in press). 5. Gault D. E. *et al.* (1968) In *Shock Metamorphism of Natural Materials* (B. M. French and N. M. Short, eds.), p. 87-100, Mono, Baltimore. 6. Orphal D. L. (1977) In *IEC**, p. 907-917. 7. Austin M. G. *et al.* (1980) *Proc. Lunar and Planet. Sci. Conf. XI* (in press). 8. McGetchin T. R. *et al.* (1973) *Earth Planet. Sci. Lett. 84*, 7669-7687. 10. Croft S. K. (1979) *Impact Craters from Centimeters to Decameters*, Ph.D. Dissertation, UCLA, 264 pp. 11. Schultz P. H. and Mendell W. (1978) *Proc. Lunar and Planet. Sci. Conf. IX*, 2857-2883.

*In *Impact and Explosion Cratering* (D. J. Roddy, R. O. Pepin and R. B. Merrill, eds.), Pergamon, NY. 1296 pp.

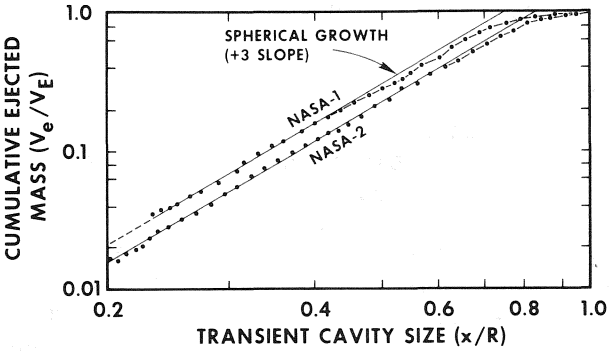

Fig. 1. Volume (mass fraction ejected relative to the total volume ejected at a given stage in crater growth.

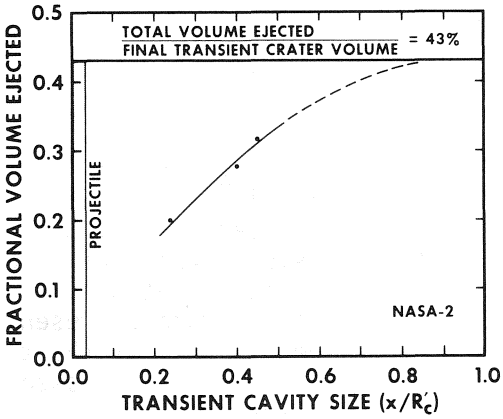

Fig. 2. Volume (mass) fraction ejected relative to transient cavity volume (mass) for NASA-2.

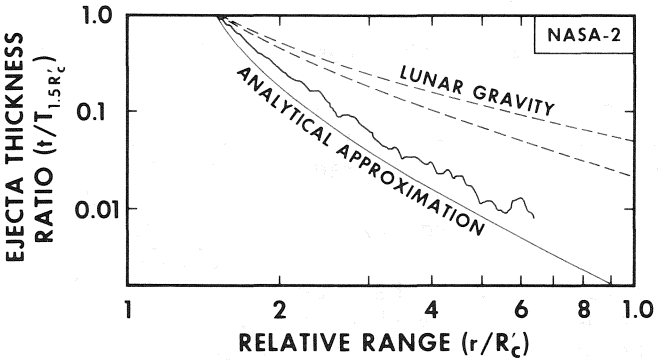

Fig. 3. Distribution of mass/unit-area (thickness) referenced to value at 1.5 R'_C (R'_C = strength-controlled radius) for NASA-2 under terrestrial and lunar gravities. Upper broken curve is for large lunar basin (300 km diameter) with a spherical moon.

Fig. 4. Distribution of peak pressures at a given range from the crater (R_C = gravity-controlled radius; R'_C = strength-controlled radius). Fig. 3a. NASA-1 calculation for 5 km/s iron impactor resulted in R'_C = 450 m with all impact melt ejected from the cavity. Fig. 3b. NASA-2 calculation for a 15.8 km/s iron impactor resulted in R'_C = 1000 m with 45% of the melt retained in the impact cavity and 55% ejected throughout the ejecta deposit.

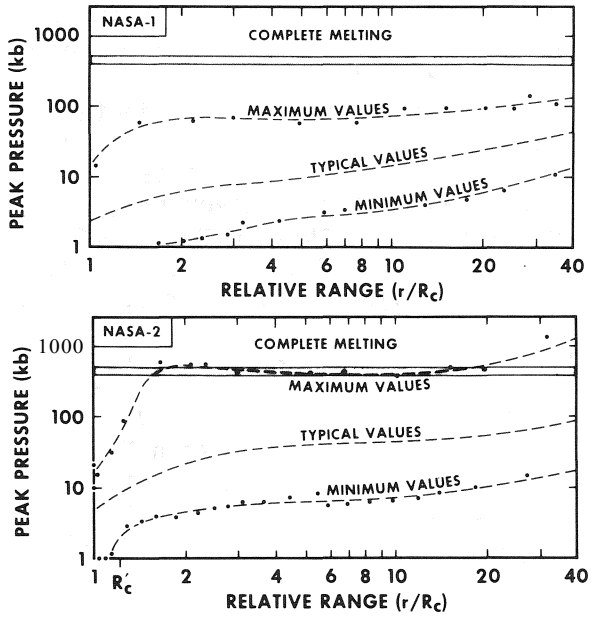

ANCIENT IMPACT BASINS ON MARS, by P. H. Schultz and R. A. Schultz, Lunar and Planetary Institute, 3303 NASA Road 1, Houston, TX 77058.

The record of impact basins on Mars generally appears to be deficient relative to Mercury and the Moon (1, 2, 3, 4). This deficiency has been attributed to a fundamental difference in the production rate of martian impact basins (3, 4) or the additional process of planetary resurfacing, thereby removing the early episodic/cataclysmic record (3). However, several extremely subdued impact basins have been identified with multi-ringed patterns resurrected by endogenic processes related to the chaotic and fretted terrains (5). Five examples have been selected for detailed further comparison (Table I).

Ladon basin was first recognized by earth-based radar profiling (6) but its full dimensions and relation to the nearby chaotic terrains were not recognized until later (5). Ladon displays three well-defined rings. The innermost ring is poorly defined, but corresponds to a subtle scarp crossing the interior plains. The second ring is expressed by massifs, scarps, drainage channels, and concentration of floor-fractured craters. The massifs form two closely spaced concentric rings, perhaps in analogy with the Inner and Outer Rook Mountains of the Orientale Basin. The third ring is less well defined by massifs, but is clearly expressed by a discontinuous scarp and control of drainage to the south. The southern boundary of Eos Chasma forms an arc correlating with the extrapolated outer ring to the north. An additional but very poorly defined fourth ring may be present: again delineated by changes in drainage, a few scarps, further structural control of Eos Chasma, and floor-fractured craters. A smaller multi-ringed basin (600 km diameter) overlaps Ladon to the southwest. Chaotic terrains and major channel/valley source regions originate along the inner and outer rings of both basins. Widespread erosion, however, is most pronounced outside the third ring of Ladon. Ladon is the least endogenically modified basin of the group, but has clearly undergone extensive erosion and infilling. Ejecta scour and impact-related features other than the massifs are generally absent.

Aram Chaos is a well-known region of chaotic terrain, but is also a multi-ringed basin (5) in a more degraded and more endogenically modified state than Ladon. Three and possibly four concentric rings can be identified. The circular region called Aram Chaos is bounded by an irregular rim/scarp and narrow moat that marks the second and most prominent ring. Within this boundary, a wide region of fractured plains partly encircles a complexly modified crescent-shaped region at lower elevation. The inner boundary of the fractured plains on the west also has small massifs and floor-fractured craters delineating the innermost ring. The orderly concentric sequence (proceeding inwards) of scarp, moat, fractured plains, massifs, and inner chaotic zone is poorly expressed in the eastern sector where a breach in the scarp links with Ares Valles.

Concentric with Aram Chaos are two other major regions of chaotic terrains: Iani Chaos to the southeast and Hydaspis Chaos to the west. Between the boundary scarp of Aram Chaos and these peripheral chaotic regions, the lightly cratered plains form a distinctive concentric zone of relatively unmodified terrain. The chaotic terrains of Iani and Hydaspis are the source regions for major channels/valleys, Iani being the primary source for Ares Valles. Both channels veer around Aram Chaos and merge to the north to form a single major channel. As around Ladon, extensive erosion and ground deterioration typically occurs along or outside the third ring.

It is proposed that the region of Aram Chaos represents the inner modified zone of an "Aram Basin" controlling and contributing to the development of chaotic terrains and major erosional channels. The regions of

greatest modification are expressed as low-lying knobby and smooth terrains concentric with the basin center and seemingly analogous to the regions of mare flooding in the Orientale Basin on the Moon. Within the innermost ring, modification is highly complex and exhibits evidence for multiple stages of fracturing, erosion, and deposition; this region may correspond to the central zone of basalt fill of Mare Orientale. Surrounding the central core is a fractured but relatively intact zone, including the innermost massif remnants, that indicates uplift/subsidence but comparative stability; the proposed Orientale analog is the region between Mare Orientale and the arc of mare ponds within the Outer Rook Mountains. The concentric moat of chaotic terrain indicates the second zone of extensive modification bounded by the basin scarp/rim, proposed to be analogous to the mare ponds at the interior base of the Outer Rook Mountains. The wide zone of stable plains bordered by regions of chaos to the southeast and southwest but controlling the paths of Ares Valles and another channel most likely corresponds to the knobby terrains of Orientale bounded by the Cordillera scarp. This latter analogy is strengthened by the highly localized occurrence of both chaos (Aram Basin) and maria (Orientale Basin). An additional ring around Aram Basin is identified on the basis of concentric fractures and floor-fractured craters -- perhaps represented as a concentric pattern of mare and graben around Orientale.

The last three examples occur along the fretted terrain and exhibit notable similarities and significant differences with Ladon and Aram. A 300 km-diameter circular structure was first mapped by Lucchitta (7), but also can be interpreted as the interior remnant of a major 500 km-diameter basin that has been buried, resurrected by differential erosion, and now half-destroyed along the fretted terrain (5). Shadow measurements of remnant relief clearly reveal the steplike profile of an impact basin including probable massif remnants. The concentric zones of fracturing, stability, and scarps bear close resemlance to the better preserved Aram Basin. Although chaotic terrains are generally absent, regions of most extensive erosion again occur exterior to the major rings. This is in direct contrast with the last two examples 700 km to the west within Deuteronilus Mensae. Here, ground deterioration has preferentially destroyed the basin interior leaving concentric hills, mesas, and arcuate scarps encircling a small central hummocky zone interpreted as exposures of the central uplift. These examples, therefore, present an inverted topography with respect to Aram and Ladon.

Figure 2 permits direct comparison of the major terrains and processes associated with the selected multi-ringed structures. Two important aspects of basin structure emerge. First, the concentric rings are not simply uplifted relief but correspond to long-lasting and deep-seated faults that become progressively less well defined away from the basin center. Second, localization of endogenic activity in these zones is not necessarily associated with low-lying areas but occur where faults occur, as previously stressed for the Moon (8). Results of detailed mapping of terrains and processes for Ladon, Aram, and the unnamed basin along the fretted terrain has four additional implications. First, the martian impact basin record may be comparable to other planets but has been largely removed by erosion and deposition. Second, the resurrection of ancient basins often occurs in a systematic manner that can reveal fundamental clues for original basin structure. Third, major outflow channels commonly originate in chaotic terrains linked to basin structures and develop episodically rather than continuously or in a single catastrophe. Fourth, the most extensive regions of erosion occur along or outside the third ring where, it is proposed, that the ejecta deposits are highly permeable (and therefore more saturated with water/ice) and are easily eroded.

ANCIENT IMPACT BASINS ON MARS

Schultz, P. H., et al.

References: 1. Mutch T. A. et al. (1976) The Geology of Mars, 400 pp., Princeton Un. Press, New Jersey. 2. Wilhelms D. E. (1974) J. Geophys. Res. 79, 529-537. 3. Malin M. (1976) Proc. Lunar Sci. Conf. 7th, 3589-3602. 4. Wood, C. A. and Head J. W. (1976) Proc. Lunar Sci. Conf. 7th, 3629-3651. 5. Schultz P. H. and Glicken H. (1979) J. Geophys. Res. 84, 8033-8047. 6. Saunders et al. (1978) NASA TM-79729, 157-159. 7. Lucchitta B. K. (1978) Geologic Map of the Ismenius Lacus Quadrangle of Mars. USGS Inv. Series I-1065 (MC-S). 8. Schultz P. H. (1976) Moon Morphology, U. Texas Press, Austin, 626 pp.

TABLE I

RING STRUCTURE	LOCATION (DEGREES)	RING DIAMETERS (km)*	REGIONAL SETTING
Ladon	29W, 18S	(270-S), 470-M/580-M, 975-F	Cratered plateau materials below eastern extension of Valles Marineris
Aram	21.5W, 2.7N	(53-S), 140-S, 250-M, 440-M, 550-F	Cratered plateau materials surrounded by chaotic terrains
Unnamed	322W, 41.6N	(60-S), 145-S, 260-F, 480-SM, 570-F	Plateau material along fretted terrain
Deuteronilus (A)	342W, 44N	44-S, 80-S, (100-S, 170-S) 220-SM, 280-S	Plateau material along fretted terrain
Deuteronilus (B)	338W, 42.5N	55-M, 201-SM, (250-S)	Plateau material along fretted terrain

*Notation: S=scarp, M=massif, F=major fracture

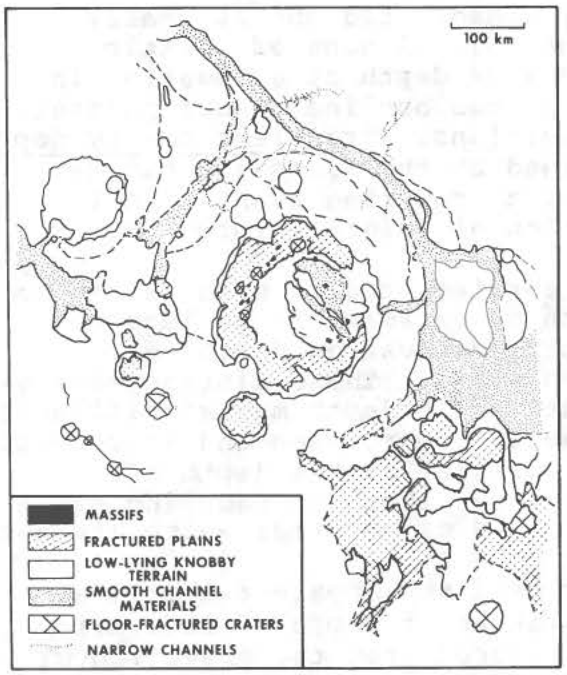

Figure 1. An abridged terrain map of Aram Chaos region. Aram Chaos is the central region of a multi-ringed basin delineated by remnant massifs, arcuate scarps, and concentric arrangements of chaotic terrain and floor-fractured craters. Igneous intrusions localized by long-lasting and deep-seated fractures resurrected the largely erased multi-ringed basin plan.

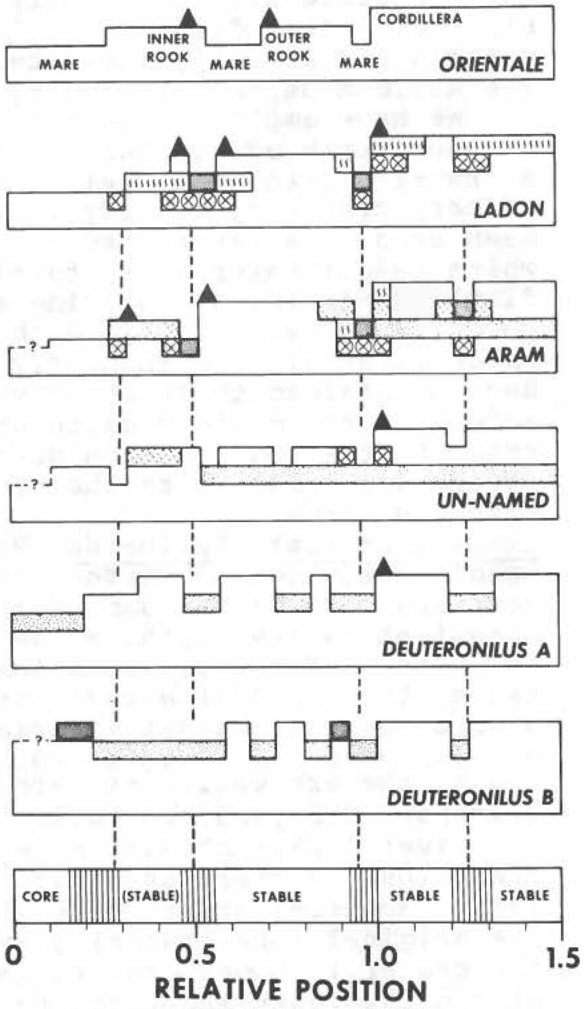

Figure 2. Stylistic comparison of profile and terrains associated with ancient martian impact basins. Distance is referenced to the major ring diameter underlined in Table I.

DEPTH OF EXCAVATION OF BASIN-SIZED CRATERING EVENTS ON THE MOON: A REVIEW OF CURRENT UNDERSTANDING. Mark Settle, Office of Space and Terrestrial Applications, Code ERS-2, NASA Headquarters, Washington, DC 20546 and James W. Head, Dept. of Geological Sciences, Brown University, Providence, RI 02912

Definition of Terminology The term 'depth of excavation' has been used in different contexts by various investigators to generally describe the subsurface penetration of impact craters. It is important to note that a crater's transient cavity expands through the dual processes of excavation and plastic deformation, which operate simulataneously during the so-called excavation stage of crater formation. The maximum depth at which target material is actually excavated may not necessarily correspond to the maximum depth attained by the crater's transient cavity [1].

We have employed the term sampling depth to refer to the maximum depth of crustal material ejected beyond the rim crest of a crater's transient cavity (equivalent to maximum depth of primary crater ejecta [2]). The term depth of excavation has been used in a restricted sense to refer to the maximum depth at which target material is forcibly dissociated and laterally displaced during a cratering event [3]. A zone of plastic deformation extends beyond the maximum depth of excavation in which material is permanently displaced but individual particles have maintained their relative positions. Transient cavity depth refers to the maximum depth attained by the transient cavity prior to the modification stage of a cratering event. (All depths are relative to the elevation of original (pre-crater) ground surface.)

Excavation Depth Estimates Many earlier studies have failed to specifically define whether 'depth of excavation' estimates correspond to crater sampling depth, excavation depth, or transient cavity depth, as defined above. These distinctions are important. For example, transient cavity depth may significantly exceed the depth of excavation due to compression and structural displacement of target material. Similarly, the depth of excavation may be significantly greater than the sampling depth due to the excavation of large volumes of material which are not transported beyond the cavity rim.

Several past studies have employed the apparent depths of fresh lunar craters as direct estimates of depth of excavation [4]. (Apparent crater depth is measured from the elevation of the original (pre-crater) ground surface to the observed floor of the crater.) Lunar craters smaller than 15 km in diameter form within the lunar megaregolith, which consists of highly comminuted and brecciated material [5]. Compression and lateral flow of megaregolith materials may play a major role in the formation of small sized lunar craters. If this is the case, the apparent depths of these craters would significantly overestimate the crater's true depth of excavation. The apparent depths of small craters may, however, provide a reasonable estimate of transient cavity depth, provided that wall slumping during the terminal stages of crater formation does not significantly alter the morphometry of the transient cavity.

Lunar craters greater than 15 km in diameter exhibit

BASIN-SIZED CRATERING EVENTS ON THE MOON

Settle, M.

pervasive morphologic evidence of modification during the latter stages of crater formation. There is a general consensus that large scale crater cavities are enlarged and infilled during the terminal stages of the event through some combination of processes. The principal modification processes are inferred to be rim slumping, floor rebound, and ejecta fallback [6,7].

Past estimates of the depth of excavation of large scale lunar cratering events have been obtained in two very different ways. One method involves extrapolation of the observed morphometry of small sized craters. This method generally assumes that: (i) depth of excavation and transient cavity depth are equivalent, (ii) the observed depth of small, fresh lunar craters is approximately equal to transient cavity depth and (iii) transient cavity shape (i.e. depth/diameter ratio) remains constant over a wide range of cavity size. The latter assumption implies that the observed decrease in the depth/diameter ratios of large lunar craters is due solely to the increased efficacy of cavity modification processes during large scale events. The other method of estimation employs morphologic and morphometric observations of large lunar craters to directly infer the original size or shape of their transient cavities. This method uses observational evidence and mechanistic models of cavity modification processes to reconstruct the configuration of transient crater cavities and ejecta source regions. This method involves no a priori assumptions concerning the relative efficacy of excavation and modification processes within craters of different size.

Estimates of the depth of excavation of basin-sized cratering events based upon the morphometric extrapolation method range up to 80-120 km for Orientale and Imbrium, respectively [8,9]. The sampling depths of these two cratering events have been inferred on the basis of primary ejecta volume estimates [2]. Maximum estimates of ejecta sampling depths for Orientale and Imbrium range up to 20 and 27 km, respectively. No attempt has been made to mechanistically reconstruct the transient cavities of basin-sized craters. This is due primarily to our lack of understanding of how wall failure and floor rebound processes operate at basin-sized scales. Recent studies of rim slumping and ejecta fallback [10] mechanisms have been conducted for craters up to 140 km in diameter. These studies indicate that rim slumping is a major agent of transient cavity modification, whereas fallback plays a minor role in modifying lunar crater cavities. Extrapolation of the results of the rim slumping study to basin-sized structures suggests that transient cavity depth for the Orientale and Imbrium events was on the order of 35 to 50 km, respectively.

In summary, morphometric extrapolation models indicate that transient cavities formed by basin-sized cratering events extended far below the 60 km seismically-defined lunar crust. Estimates of depth of excavation based upon these models suggest that significant volumes of subcrustal material were disaggregated and presumably ejected from basin-sized cavities. In contrast, cavity reconstruction models indicate that basin-sized impacts produced initial cavities with depths on the order of 50 km or less. Material ejected from these cavities is

expected to originate from approximately the upper half of the seismically-defined crust.

The single piece of 'ground truth' evidence which can be used to identify a preferred range of excavation depth estimates is the general lack of deep seated crustal rocks within the lunar sample collection. A few select samples exhibit geochemical and petrographic features which are indicative of in situ crustal formation at depths ranging up to 20-30 km. However, there is no widely recognized suite of samples which formed at depths greater than 30 km. In fact, the number of samples inferred to originate from depths of 10-30 km is quite limited. This evidence is generally consistent with depth of excavation estimates based upon cavity reconstruction methods.

Key Problems for Future Research

1) Compressional Effects in Small Lunar Craters

A critical assumption of the morphometric extrapolation model concerns the equivalency between depth of excavation and transient cavity depth. As mentioned above, small lunar craters form within highly compressible materials. Laboratory cratering experiments in quartz sand have shown that substrate compression can account for up to one-half of apparent crater depth [11]. The ratio of excavation depth to transient cavity depth should logically increase with increasing crater size due to the lower compressibility of deeper crustal materials. If the fractional volumes of excavated and plastically deformed target material vary significantly as a function of cavity size, then small crater depth/diameter ratios cannot be used to directly infer the maximum depth of excavated material.

2) Rebound Effects in Large Lunar Craters

Cavity reconstruction models which can account for basement rebound mechanics during the modification stage of crater formation have not been developed to date. Cavity reconstruction models have shown that rim slumping cannot be solely responsible for the morphometric transition from small, bowl-shaped craters to large, saucer-shaped craters greater than 100 km in diameter [3]. However, cavity reconstruction methods have not yet disproved the hypothesis that transient cavity shape remains constant over a wide range of crater size. Models demonstrating the combined effects of wall failure and basement rebound must be constructed to determine whether the observed morphometry of large lunar craters is due completely to the expanded role of modification processes in large scale cratering events.

REFERENCE [1] Dence, M. et al. (1977) in Impact and Explosion Cratering, p.247. [2] Head, J.W. et al. (1975), 6th LSC, p. 2805. [3] Settle, M. and J.W. Head (1979), JGR v.84, p. 3081. [4] Horz, F. et al. (1976), Proc. 7th LSC, p. 2931. [5] Head, J.W. (1976), Proc. 7th LSC, p. 2913. [6] Quaide, W.L. et al. (1965), Ann. N.Y. State Acad. Sci. v. 123, p. 563. [7] Grieve, R.A.F. et al. (1977), in Impact and Explosion Cratering, p. 791. [8] Dence, M. et al. (1974) in Lunar Science V, p. 165. [9] Moore, H.J. et al. (1974), Proc 5th LSC, p. 71. [10] Settle, M. (1980), Icarus v. 42, p.1. [11] Stoffler, D. et al. (1975), JGR v. 80, p 4062.

PETROLOGY OF THE APENNINE FRONT, APOLLO 15: IMPLICATIONS FOR THE GEOLOGY OF THE IMBRIUM IMPACT BASIN. Paul D. Spudis, U.S. Geological Survey, 2255 N. Gemini Dr., Flagstaff, AZ 86001 and Dept. of Geology, Arizona State University, Tempe, AZ 85281

Introduction and Geologic Setting

The Apollo 15 mission was targeted for one of the most geologically diverse of the Apollo landing sites, the Hadley-Apennine region (26°N, 4°E). The site is on a mare plain near the Montes Apenninus chain, which marks the southeastern topographic rim of the Imbrium basin. The primary highland sampling objectives of the Apollo 15 mission were to characterize the nature of Imbrium ejecta and to sample the pre-Imbrian section that may be exposed in the Apennine scarp (1). Of principal scientific interest were the petrology and chemistry of Imbrium ejecta in this region and radiometric dating of Imbrium-related samples to help establish the absolute age of the Imbrium impact. Results of these studies have significant implications for the location and dimensions of the original Imbrium crater and also help constrain theories of the origin of lunar multi-ringed basins.

The Imbrium basin is one of the largest and youngest of the large lunar basins and the geology of the Apollo 15 landing site has been strongly influenced by its formation and that of two pre-Imbrian basins: Serenitatis and an old degraded basin centered near Copernicus (2). The Apennines are an arcuate chain of highlands that display chaotic dune-like topography in the south and massif/domical terrain in the north, near the landing site (2,3). Extensive slump blocks occur along the basin-facing scarp of the Apennines together with bright, fresh talus slopes around most of the massifs. The highlands sampled by Apollo 15 are represented by the Hadley Delta massif, an equant mountain block about 15 by 20 km in plan. The relief, about 3400 m above the mare plain, well exceeds the thickness of Imbrium ejecta (about 1 km) expected at the crest of the Apennine scarp (4). The possibility that an extensive pre-Imbrian section is exposed within the massif enhances the probability that ejecta from pre-Imbrian basins, particularly that of Serenitatis, was sampled.

Petrology of the Apennine Front

The most abundant type of rock returned from Hadley Delta, collected at all front stations, consists of vitric matrix breccias of varying degrees of coherence. These rocks appear to be single-generation breccias with clasts of local mare basalt, a non-mare basalt type with medium-K KREEP composition, glass and mineral fragments of various types, and minor amounts of granulated anorthositic clasts. The proportions of these components vary widely: some samples consist entirely of mare basalt/KREEP basalt clasts in a glassy matrix (e.g. 15205; 5) whereas in others the clast population is almost entirely dominated by anorthositic rock types (e.g. 15459; 6). The incorporation of large amounts of local, post-basin debris, and the saturation of solar wind gases in the glassy matrices of these breccias (7), strongly suggest that these rocks are lithified soils, probably unrelated to the Imbrium ejecta component at the site (8). However, some vitric-matrix breccias with a high proportion of exotic lithic clasts may represent Imbrium ejecta, although none have been identified to date.

The other rocks collected at the front are microcrystalline matrix breccias of two types. The station 6A boulder, represented by 15405, consists of a KREEP-rich melt enclosing clasts of KREEP basalt, KREEP granites, and a unique quartz monzodiorite (9). The breccia assembly age for

this rock is about 1.25 AE (10), which in addition to the unique petrology of the rock suggests that 15405 is exotic and not related to the local Apennine front composition. The other type is represented by 15445 and 15455, the "black and white" breccias, representative of the 1-m boulder on the rim of Spur crater (1). These rocks consist of an aphanitic melt matrix of Mg-rich, low-K Fra Mauro (LKFM) basalt composition that encloses pristine noritic and troctolitic lithic clasts and abundant mineral debris (8). The lithic clasts include a norite dated at 4.52 AE, one of the oldest lunar rocks known (11), and unique spinel cataclasites that appear to have equilibrated at great depths (>50 km) in the lunar crust (12). These breccias apparently were assembled at about 3.92 AE (13). These rocks have been interpreted as fragments of the Imbrium basin impact melt sheet (8,14); if so, they are the best samples of primary Imbrium ejecta in the Apollo collection.

Anorthosite is sparse at the Apennine front, and study of front soils and glasses confirms that the dominant composition is LKFM basalt (15,16). This dominance suggests that the Imbrium ejecta component at the front is of LKFM composition, and the paucity of anorthosite in the Imbrium component is confirmed by the clast population of the "black and white" rocks, which contain norites and troctolites (mafic ANT) (8,17). The anorthosite 15415 may be a pre-Imbrian sample of Serenitatis or other basin ejecta, an interpretation supported by its great age ($\sim$ 4.2 AE; 18). Other anorthosite fragments from the front may have a similar origin.

Agglutinitic glasses of LKFM composition are abundant in soils from the Apennine front (15). It might be expected that these glasses are the products of regolith formation on the Imbrium ejecta component within the massif. The chemistry of the Apollo 15 LKFM glasses more closely resembles the Apollo 17 melt sheet than the Imbrium melt sheet ("black and white" breccias), (Fig. 1). Moreover, the glasses cannot be produced by mixing of the chemically distinct "black" and "white" portions of the Imbrium melt rocks, because they do not fall on a mixing line between these components. This suggests that the Apollo 15 LKFM glasses may be derived from a unit exposed within the massif having bulk chemistry similar to the Apollo 17 melt rocks. Geologic studies (3,4) have suggested that uplifted, pre-basin rocks may be exposed within the Apennines; thus the Apollo 15 LKFM glasses may have been derived, at least in part, from a section of Serenitatis ejecta exposed within the Apennine front. Although large rock samples of probable Serenitatis origin have not yet been identified in the Apollo 15 collection, some rake samples (e.g. 15359; 19) have bulk chemistry and petrology compatible with such an origin.

The LKFM glasses are probably polygenetic; at least some are generated by mixing of components in Apennine front soils (20). Chemical variation in these glasses (15) demonstrates some to be clearly related to the Imbrium melt component (MgO 14-16%), although the majority have MgO of 9-11% and are probably related to Serenitatis.

Other rock types in the Apennine front collection are volcanic KREEP basalts (21), probably derived from the post-Imbrium Apennine Bench Formation (22,23), and numerous red, yellow and green glass spheres (24,25), probably of post-basin volcanic origin (26,27).

Implications for Imbrium basin geology The probable geologic relations among Apollo 15 front samples are summarized in Fig. 2. A considerable section of pre-Imbrium basin rocks is apparently exposed within Hadley Delta, an exposure consistent with ejecta thickness estimates based on theoretical calculation (28) and photogeologic interpretation (3,4). In

addition, Imbrium impact melt is present, probably as discontinuous patches on the upper slopes of the massif. Purely clastic Imbrium ejecta has not been identified but it probably exists within fines from the front. The Imbrium ejecta at Apollo 15 is certainly of crustal origin (14), and no evidence of lunar mantle materials is found in the Apollo samples (29). These facts place a severe constraint on models that would equate the Apennine ring with the rim of the Imbrium transient cavity (30,31); they imply an extensively wide and shallow cavity. A more likely explanation involves smaller initial craters that excavate deeper (32), although not necessarily proportionally so (33). In this interpretation, the Apennines represent a basin structure outside the crater of excavation (3,4,32, and others). It is possible that none of the present Imbrium rings reflect the location of the initial cavity, particularly if considerable post-impact structural modification has occurred (34). The considerable exposure of pre-Imbrian material in the massif, relative thinness of Imbrium ejecta, absence of deeply (> 50 km) derived ejecta, and preservation of pre-Imbrian topography in the Apennines (3) all suggest a relatively small transient cavity, located within the Apennine ring.

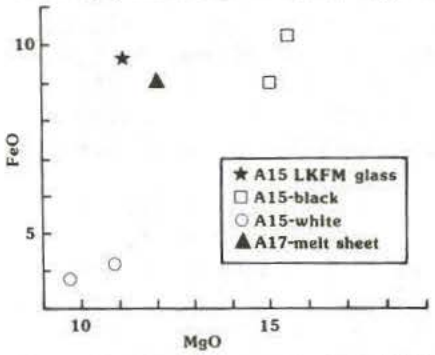

Fig. 1. FeO-MgO variation diagram for Apollo 15 LKFM glasses and black and white breccias and the Apollo 17 melt sheet. Data from 14, 15, 16, 17.

References

(1) Swann, G. et al. (1972), NASA SP-289, 5-1. (2) Wilhelms, D. and McCauley, J. (1971) USGS Map I-713. (3) Spudis, P. and Head, J. (1977) PLSC 8, 2785. (4) Carr, M. and El-Baz, F. (1971) USGS Map I-723. (5) Synek, R. et al. (1974) PLSC 5, 235. (6) Ridley, I. (1975) LS VI, 671. (7) Husain, L. (1972) Apollo 15 Lun. Samples, 374. (8) Ryder, G. and Bower, J. (1977) PLSC 8, 1895. (9) Ryder, G. (1976) EPSL 29, 255. (10) Bernatowicz, T. et al. (1977) LS VIII, 97. (11) Nyquist, L., et al. (1979) Conf. Lun. Highlands, 122. (12) Herzberg, C. (1978) PLPSC 9, 319. (13) Alexander, E. and Kahl, S. (1974) PLSC 5, 659. (14) Ryder, G. and Wood, J. (1977) PLSC 8, 655. (15) Reid, A. et al. (1972) Meteoritics 7, 395. (16) Taylor, R. et al. (1973) PLSC 4, 1445. (17) Ridley, I. et al. (1973) J. Geol. 81, 621. (18) Husain, L. et al. (1972) Science 175, 428. (19) Dowty, E. et al. (1973) Univ. New Mexico SP-8. (20) Ridley, I. (1977) Phil. Trans. Roy. Soc. 285, 105. (21) Dowty, E. et al. (1976) PLSC 7, 1833. (22) Spudis, P. (1978) PLPSC 9, 3379. (23) Hawke, R. and Head, J. (1978) PLPSC 9, 3285. (24) Cuaide, W. (1973) LS IV, 606. (25) Ridley, I. et al. (1973) PEPI 7, 133. (26) Hawke, R. et al. (1979) PLPSC 10, 2995. (27) Delano, J. (1979) PLPSC 10, 275. (28) McGetchin, T. et al. (1973) EPSL 20, 226. (29) Taylor, R. (1975) Lunar Science. (30) Wilhelms, D. et al. (1977) Imp. Expl. Cratering, 539. (31) Hodges C. and Wilhelms, D. (1978) Icarus 34, 294. (32) Dence, M. (1976) Imb. Consort. I, 147. (33) Croft, S. (1980) LPS XI, 182. (34) Schultz, P. (1979) Conf. Lun. Highlands, 141.

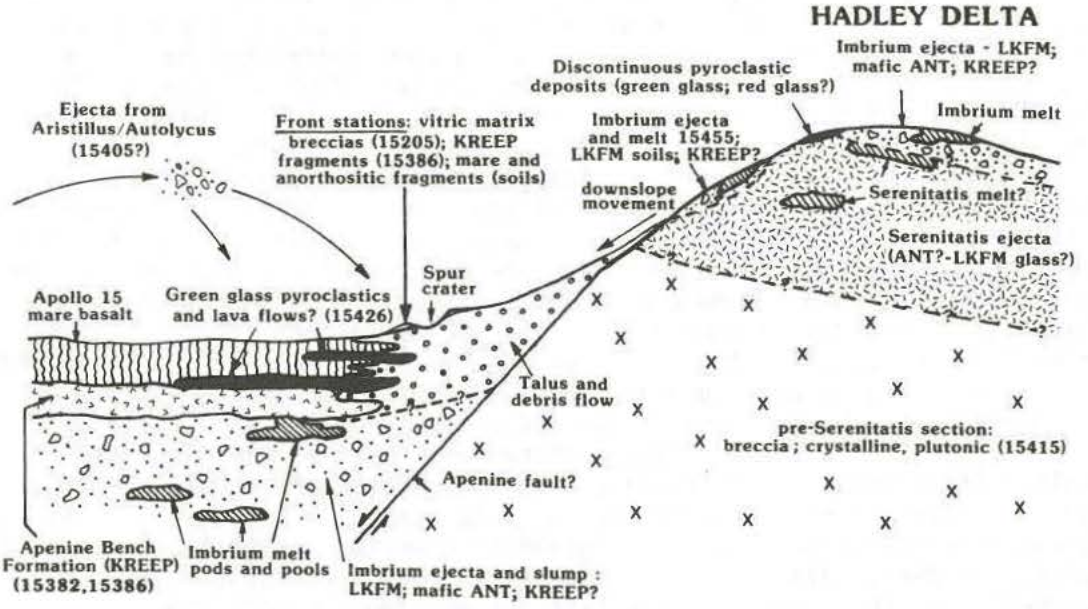

Fig. 2. Schematic cross section showing inferred relationships between rock types at the Apollo 15 landing site.

APOLLO 17 IMPACT MELTS AND THE GEOLOGY OF THE TAURUS-LITTROW HIGHLANDS. Paul D. Spudis[1] and Graham Ryder[2]. 1. U.S. Geological Survey, 2255 N. Gemini Dr., Flagstaff, AZ 86001 and Dept. of Geology, Arizona State University, Tempe, AZ 85281, 2. Northrop Services Inc., P.O. Box 34416, Houston, TX 77034.

A melt sheet produced by the Serenitatis event is generally considered to be represented by the poikilitic, impact-produced melt breccias that dominate the highlands samples collected at Taurus-Littrow (1,2,3). These poikilitic melts comprise Boulders 2 and 3 at Station 2; the Station 6 boulders; the Station 7 boulder; and several smaller rocks. Aphanitic melt breccias, commonly lighter in color (Boulder 1, Station 2; 73215;73235; 73255) have also generally been considered samples of the melt sheet (4,5,6,7) because of their "overall similarity" (4) to the poikilitic breccias. However, as outlined below, the aphanitic breccias are actually significantly different from the poikilitic breccias. We contend that these differences indicate that the aphanitic breccias are not directly related to the Serenitatis basin-forming event.

THE APOLLO 17 MELT ROCKS

Clast Populations: The aphanitic breccias contain a more varied and distinct clast population than do the poikilitic breccias (6,8). Felsite (granitic) clasts are common in the aphanitic breccias and absent in the poikilitic breccias. Mare-like basalts and basaltic impact melt clasts, abundant in the aphanitic breccias, are rare in the poikilitic breccias. The latter contain mostly mafic plutonic and granoblastic clasts of lower crustal origin.

Chemistry: Figure 1 demonstrates that the poikilitic melts form a chemically homogeneous group, with a dispersion a little greater than that of the terrestrial Manicouagan melt sheet (9). In contrast, the aphanites as a group have considerable scatter. Samples 73215 and 73235 are similar, and distinct from sample 73255. The Boulder 1, Station 2 aphanites show a wider dispersion, though the extremes are all from one sample, 72275. All are distinct from the poikilitic breccias.

Petrographic Features: The aphanitic breccias are mainly accretionary; the Boulder 1, Station 2 aphanites are commonly rounded inclusions or form rinds on lithic clasts around which they have been wrapped (8,10). Similar structures form samples 73215 and sample 73235 (5,11) and 73255 is a single accretionary melt bomb (6). The poikilitic breccias generally lack such accretionary characteristics.

Discussion: The aphanitic melts are not only distinct from the poikilitic melts but are markedly distinct from one another. Meteoritic signatures (12) also suggest that the Boulder 1, Station 2 aphanites and one sample of 73215 are distinct from the others. Ar-Ar plateau ages for poikilitic and aphanitic melt rocks are similar, but samples 73215 and 73255, at least, may be younger. ($\sim$ 3.88 AE) (13) than the poikilitic rocks ($\sim$ 3.96 AE) (14), if the latter completely outgassed during formation and their plateau ages accurately reflect crystallization ages.

Obviously, the aphanitic rocks had a cooling history distinct from the poikilitic melts, but all of the differences cannot simply be a result of cooling histories. The differences indicate a distinct, shallower source for the aphanitic rocks. Wood (4) suggested that the Boulder 1, Station 2 aphanites formed from an early, high-angle ejection during the Serenitatis event. However, this model requires that the entire crustal depth penetrated by the event was roughly low-K Fra Mauro composition (5), an unlikely proposition (15). The evidence is consistent with smaller-scale

APOLLO 17 IMPACT MELTS

Spudis, P.D. and Ryder, G.

(compared to Serenitatis) impact events into shallow-level source materials for the origin of the aphanitic breccia.

REGIONAL GEOLOGY

The Apollo 17 landing site was selected to provide access to both young volcanics and ancient highlands (16). Numerous pre-mission geologic studies showed that the Serenitatis basin would be a likely source for many terra rocks with an additional uncertain Imbrium contribution (16,17). Post-mission studies have tended to emphasize similarities and correlation with the better preserved Orientale basin (7,18,19), equating the Apollo 17 massifs with the Outer Rook ring and the Sculptured Hills unit with the knobby Montes Rock Formation (7). In these interpretations, all highland samples from Apollo 17 are directly related to Serenitatis basin ejecta, and the landing site is considered very near the rim of the Serenitatis transient crater.

A major problem with these interpretations is illustrated in Fig. 2. The Sculptured Hills unit displays varied morphology, with knobby (k), smooth (s) and lineated (arrow) facies; the lineated terrain is probably Imbrium related (20). If the Sculptured Hills is equivalent to the Montes Rook Formation of Orientale, it should be contemporaneous with the Serenitatis basin. As shown in fig. 2, however, the Sculptured Hills unit overlies the rim of the crater Littrow (L). This crater postdates the Serenitatis ring structure; therefore the Sculptured Hills may not be analogous to the Montes Rook Fm. as defined (18). Either of two possibilities may explain this relation: 1) the Sculptured Hills is a facies of Serenitatis material, deposited on pre-Serenitatis craters; the transient cavity of the Serenitatis crater would therefore lie well within the presently defined topographic basin (see 21); 2) The Sculptured Hills is a post-Serenitatis terra unit, deposited on the massifs and craters of the Serenitatis rim; a possible source could be the Alpes facies of Imbrium basin ejecta (20,22).

These observations suggest that the Taurus-Littrow highlands may not be dominated solely by Serenitatis material. A complex, multiple-impact history involving basins and smaller local impacts seems required to explain the regional geology. Particularly intriguing are the craters Littrow (30 km dia.; 50 km range to landing site) and Vitruvius (30 km dia.; 80 km range to landing site); these craters probably contributed ejecta to the Apollo 17 site ($\sim$ 4.7 and 1.1 m average ejecta thickness respectively, from equations of McGetchin et al. (23)). The impact target for these craters would be Serenitatis basin ejecta, with, in the case of Vitruvius, some Imbrium basin material possibly admixed. Littrow's irregular shape (Fig. 2) may indicate that it is an Imbrium secondary crater, related to other Imbrium secondaries abundant in this region (24). If so, Littrow probably resulted from a relatively low velocity impact (25) that would not have generated much melt, but would rather have redistributed existing local material. The melt-bomb nature of sample 73255 (6) and its relatively young age (13) are consistent with its generation as melt ejecta from Vitruvius, which appears to be an Imbrian-age primary impact crater.

CONCLUSIONS

Geologic, chemical, petrographic, and age data indicate that the Apollo 17 highlands have experienced a complex, multiple-impact history. In contrast to prevailing opinion (6,7), we suggest that these highland rocks are not all derived from the Serenitatis basin impact. Specifically, the aphanitic breccias collected at Stations 2 and 3 appear to represent distinct, non-Serenitatis impact events that may both predate ($\sim$ 4.0AE

APOLLO 17 IMPACT MELTS

Spudis, P.D. and Ryder, G.

(26); Boulder 1, Station 2) and postdate (~ 3.88 AE (13); 73255) the Serenitatis basin melt sheet (~ 3.96 AE (14); poikilitic boulders).

The data suggest that the aphanitic breccias are not directly related to Serenitatis, but might be from another basin, or might result from local impacting into the melt sheet and partial mixing with other incompletely identified components. We recommend a critical re-examination of the contributions of both smaller local impacts (Littrow, Vitruvius) and of the Imbrium basin itself to the geology of the landing site.

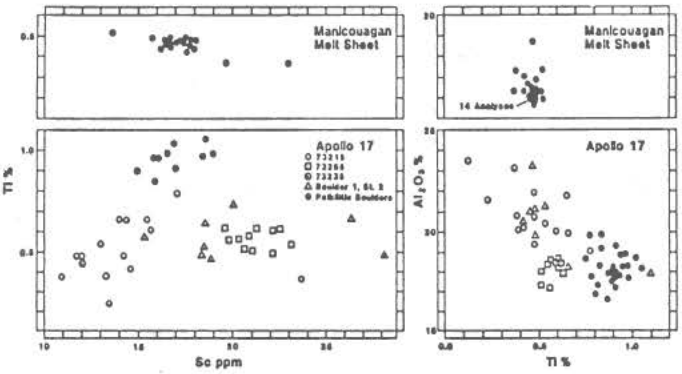

Figure 1. Chemical variation of Apollo 17 melt breccias and Manicouagan melt sheet for three significant refractory elements. Apollo 17 data: all published chemical data. Manicouagan data from (9).

Figure 2. The Apollo 17 landing site (A) and environs. The Sculptured Hills unit displays both knobby (K) and smooth (S) facies, gradational with Imbrium-related lineated terrain (arrows); it also overlies the rim of the crater Littrow (L). Local craters possibly contributing ejecta to the landing site include Littrow, Vitruvius (V), and Maraldi (M). Area shown is about 200 km square; north at top; AS 17-594.

References

(1) Warner, J. et al. (1976) PLSC 7, 2233. (2) Winzer, S. et al. (1977) EPSL 33, 389. (3) Dymek, R. et al. (1976) PLSC 7, 2335. (4) Wood, J. (1975) Moon 14, 505. (5) Dence, M. et al. (1976) PLSC 7, 1821. (6) James, O. et al. (1978) PLPSC 9, 789. (7) Wolfe, E. et al. (1980) USGS Prof Paper (in press). (8) Ryder, G. et al. (1975) Moon 14, 327. (9) Floran, R. et al. (1978) JGR 83, 2737. (10) Marvin, U. (1975) Moon 14, 315. (11) James, O. (1976) PLSC 7, 2145. (12) Hertogen, J. et al. (1977) PLSC 8, 17. (13) Staudacher, Th. et al. (1979) PLPSC 10, 745. (14) Cadogan, P. and Turner, G. (1976) PLSC 7, 2267. (15) Ryder, G. and Wood, J. (1977) PLSC 8, 655. (16) Scott, D. and Carr, M. (1972) USGS Map I-800. (17) Head, J. (1974) Moon 9, 355. (18) Wolfe, E. and Reed, V. (1976) J. Res. USGS 4, 171. (19) Head, J. (1979) Moon and Planets 21, 439. (20) Scott, D. and Pohn, H. (1972) USGS Map I-799. (21) Schultz, P. (1979) Conf. Lun. Highlands, 141. (22) Wilhelms, D. and McCauley, J. (1971) USGS Map I-713. (23) McGetchin, T. et al. (1973) EPSL 20, 226. (24) Wilhelms, D. (1980) USGS Prof Paper 1046-A. (25) Oberbeck, V. (1975) RGSP 13, 337. (26) Leich, D. et al. (1975) Moon 14, 407.

CRATERING EXPERIMENTS IN NONCOHESIVE AND WEAKLY COHESIVE SAND: EXCAVATION MODE AND EJECTA CHARACTERISTICS Stöffler, D.*, Gault, D.E.†, Reimold, W.U.* *Lunar and Planetary Institute, Houston, TX 77058 and Institute of Mineralogy, University of Münster, D-44 Münster, Germany †Murphys Center of Planetology, Murphys, CA 95247

Experiments. Aluminum spheres and Lexan (plastic) cylinders of 0.3 - 0.4 g were fired vertically into sand targets at 5.9 to 6.9 km/s in the light gas gun facility of NASA Ames Research Center. Two types of targets were used: (1) loose, dry quartz sand, and (2) slightly cohesive sand of glass beads. The target region to be cratered was marked by various geometries of colored sand. In one type of target, 5 horizontal (9 mm thick) layers of differently colored sand were on top of clear sand. In a second type of target, a single 9 mm thick horizontal layer of sand of concentric annuli with different colors was positioned at 0, 9, 18, and 27 mm depth in the target, respectively. Details of the experimental conditions and the crater parameters are given in Table 1 and Fig. 1.

Ejecta were collected around the craters within at least two 45° sectors on the reference ground plane and in vertical catchers at a radial distance of about 7 crater radii following previous procedures (1). Mass; color of sand grains; grain size-distribution; mass, types, and color of shock-metamorphosed grains; and presence of projectile material on grains were determined for each sample.

Results. Bowl-shaped craters with smooth rims, 30 to 33 cm in diameter and 5.3 and 7.4 cm in depth, were produced in all experiments with loose, dry sand targets (1). The rims and the continuous ejecta blankets form perfectly developed overturned flaps with inverted target stratigraphy in all cases.

Craters with blocky rims and blocky ejecta blankets were formed in two shots with slightly cohesive sand of glass beads. The blocks, up to 6 cm in size at the rim, gradually decrease in size with radial range. They extend to about 7 crater radii. The blocks near the rim are either horizontally displaced, tilted or overturned and consist of the upper two layers (18 mm thick) of the target. With increasing range the blocks are primarily derived from only the uppermost 9 mm target layer. Noncohesive ejecta from deeper layers originating from as deep as 36 mm are discontinuously distributed between cohesive blocks in a zone of at least 2 crater radii. Results of quantitative analyses of the ejecta collected quantitatively from inside and outside the craters can be summarized as follows: (1) The average ejecta thickness as a function of range can be expressed by the following decay function for experiments in quartz sand:

$$t \text{ (ejecta thickness)} = T \left(\frac{r}{R}\right)^{-3.26} ,$$

where T is the rim thickness corrected for uplifting, r is the range, and R is the crater radius. The decay of ejecta thickness is actually steeper near the rim. Separate regression analyses in the range from 1.0 to 1.6 crater radii yield exponents of the decay function of -4.3 to -6.2. (2) The boundary line (dashed line in Fig. 1) above which sand was excavated and ejected beyond the crater rim is rather shallow. It deviates from a simple bowl-shaped cavity, having a shoulder at about 0.3 crater radius. A larger volume of the final crater is produced by downward, lateral, and oblique upward flow and compaction of sand. (3) The mass distribution of shock metamorphosed particles (melt particles, shock-lithified breccia particles and comminuted quartz grains) which amount to about 4% of the total displaced mass, is distinctly different from the distribution of the total displaced mass. About

85% of the total shocked mass is confined to the crater itself. Within the ejecta blanket the percentage of shocked mass increases from below 0.1% near the rim to about 8% in the far distant ejecta. (4) The type, color, and distribution of melt and shock-lithified breccia particles in the ejecta permit defining corresponding zones of shock pressure produced by the impact. Peak pressures at point of impact range from 47-51GPa for the shots with Al-projectiles and are at about 30GPa for the shots with the Lexan projectiles. If it is assumed that a lower limit of 3-5GPa produces lithified breccia (1,2), then the peak pressure at the point of impact attenuated an order of magnitude within the two shock zones shown in Fig. 1. This limits the zone of shock melting and shock lithification to about 0.15 (0.1 - 0.2) crater radius. (5) Shock-fused projectile material forms a thin crust on the glassy side of melt agglutinates. Such particles are found inside and outside the crater within the complete radial range of ejecta. In the case of aluminum projectiles only very minor mixing between the fused metal and the adjacent, vesiculated silica glass was observed.

REFERENCES

(1) Stöffler, D., Gault, D.E., Wedekind, J.A., and Polkowski, G. (1975) J. Geophys. Res. 80, 4062.

(2) Kieffer, S.W. (1975) The Moon 13, 301.

Table 1. Experimental conditions and crater parameters for hypervelocity impacts into sand targets.

Projectile			
size (cm)	0.79 x 0.51 (cylinder)	0.636 (diameter spheres)	0.79 x 0.51 (cylinder)
type	Lexan	Aluminum	Lexan
mass (g)	0.27 - 0.31	0.38	0.30
velocity (km/sec)	6.4 - 6.9	5.9 - 6.5	6.7
kinetic energy (ergs)	6.3 - 7.2 x 10^{10}	6.2 - 8.1 x 10^{10}	6.6 x 10^{10}
Target			
type	loose quartz sand (0.06 - 0.25 mm)	loose quartz sand (0.06 - 0.25 mm)	glass-beads sand* (slightly cohesive)
markers	colored horizontal 9 mm layers	concentric annuli of colored 9 mm layers at variable depth	colored horizontal 9 mm layers
peak pressure (GPa)	~ 30	42 - 51	~ 30
crater diameter (cm)	30.5 - 32.8	31.8 - 33.1	~ 30 - 32
crater depth (cm)	5.9 - 7.4	5.3 - 6.4	~ 5
crater volume (cm^3)	1167 - 1467	1168 - 1583	?

*grain size: 0.125 - 0.3 mm.

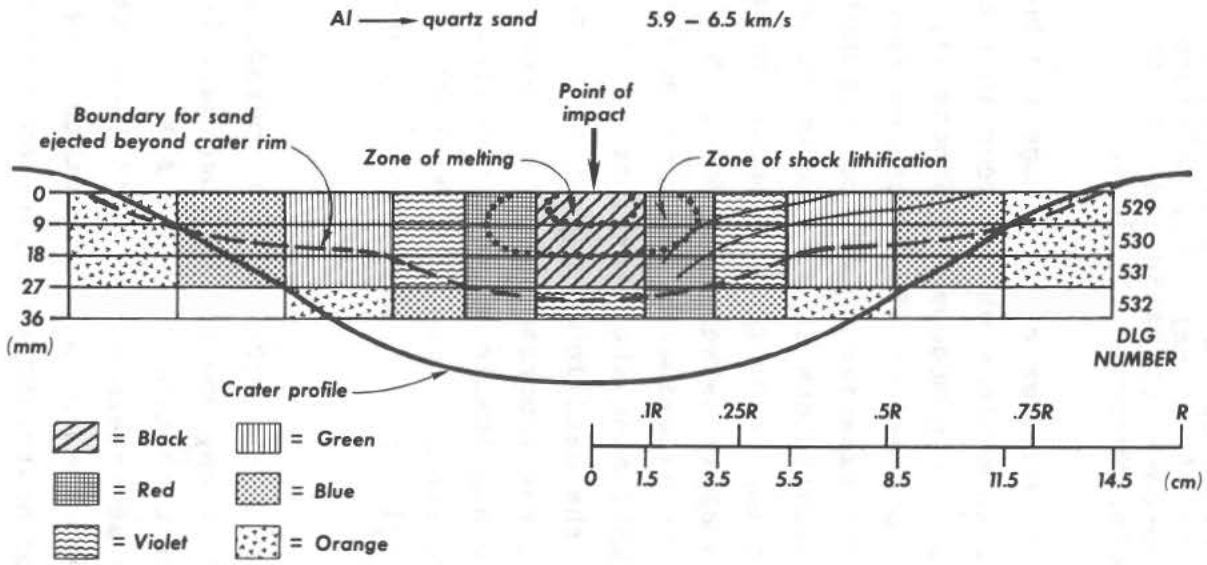

Fig. 1. Cross section through target and average crater profile for a series of 4 experiments (DLG 529-531) in quartz sand with the layer of concentric annuli of differently colored sand at variable depths. Two thin, solid lines indicate excavation volumes ejected beyond 2 and 7 crater radii, respectively.

THE DETAILED APPLICATION OF MAXWELL'S Z-MODEL TO LABORATORY-SCALE IMPACT CRATERING CALCULATIONS

Thomsen J.M., Austin M.G., and Ruhl S.F., Physics International Co., San Leandro, CA 94577; Orphal D.L., California Research and Technology, Inc., Livermore, CA 94550 and Schultz P.H., The Lunar and Planetary Institute, Houston, TX 77058.

Finite-difference computer calculations can be used to simulate target material motions which occur in realistic hypervelocity impacts into homogeneous targets (1, 2, 3, 4) and layered targets (5). Our effort (6, 7) concentrates on laboratory-scale impact experiments and corresponding finite-difference computer simulations in an attempt to understand the basic dynamics of the impact process. Concurrent with these efforts is an effort to apply Maxwell's Z-Model (8, 9) to impact cratering. Because the experiments can confirm (or deny) the results, thereby establishing the limits of credibility of the theoretical efforts, the detailed application of this analytic model should begin at the laboratory scale. Eventually, the detailed model may be applicable to some specific features of the process of basin formation, including (10) growth of the transient cavity, origin of excavated material, and transient and permanent rim uplift.

We previously found that the Z-Model characterizes the cratering flow field at any one time in our calculation, but that Z generally increases with time (7) from $Z \cong 2.1$ at early times (18 μsec) to $Z \cong 2.8$ at intermediate times (600 μsec). This finding destroys the notion of a steady-state flow field as previously applied to near-surface explosion cratering calculations. To assess the effect of Z(t) more quantitatively, we plotted the paths of selected Lagrangian zones (streamlines) from our two-dimensional calculational results. We then compared these streamlines to those computed with Equations 1 and 2--the

steady-state Z-Model streamline relations (8)--using the reported early time (Fig. 1) and intermediate time (Fig. 2) values of $Z(\theta)$ reported by Austin et al. (7). The flow-field strength parameter, α, and the flow-field center (6) were held constant at 0.1 $cm^{Z+1}/\mu sec$ and 0.6 cm, respectively. Neither set of Z values fits the streamlines generated by the calculation very well.

$$R(t) = \left[(Z+1)\alpha t + R_o^{Z+1}\right]^{1/Z+1} \qquad (1)$$

$$\theta(t) = \cos^{-1}\left[1 - \left(\frac{R(t)}{R_o}\right)^{Z-2}(1-\cos\theta_o)\right] \qquad (2)$$

Analyses to date suggest that $Z(\theta)$ derived at any single time in the calculation will not well match the entire streamline pattern observed in the target material. The computed streamline pattern (at least for material which is not ejected) can be fit, however, with Equations 1 and 2 using constant (time-independent) values of $Z(\theta)$. This match is accomplished by calculating various streamlines using Equations 1 and 2 with different values of Z until a best-fit is achieved (Fig. 3). Construction of a time-independent Z-flow flow field in this way essentially averages the time dependence of Z, thereby providing a reasonable--but not exact--overall fit.

Investigation of the detailed application of the Z-Model has, at this time, yielded the following results: the steady-state Z-Model appears to be able only to describe the time-integrated cratering flow field in an average sense, and $Z(\theta)$ must be chosen by a tedious process of fitting streamlines derived from a complete finite-difference calculation. These results apply only to one set of impact conditions and may be different if the momentum of the impacting projectile were varied over reasonable limits.

APPLICATION OF Z TO IMPACTS

Thomsen, J. M. et al.

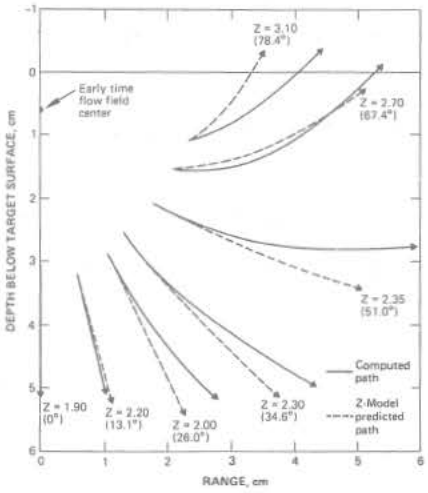

Fig. 1 Computed paths compared with Z-Model predicted paths using early time (18 μsec) Z values.

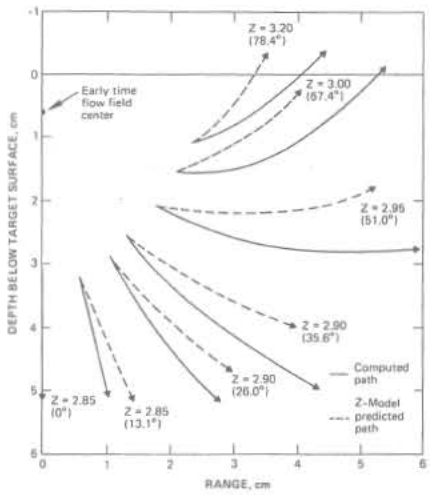

Fig. 2 Computed paths compared with Z-Model predicted paths using late time (600 μsec) Z values.

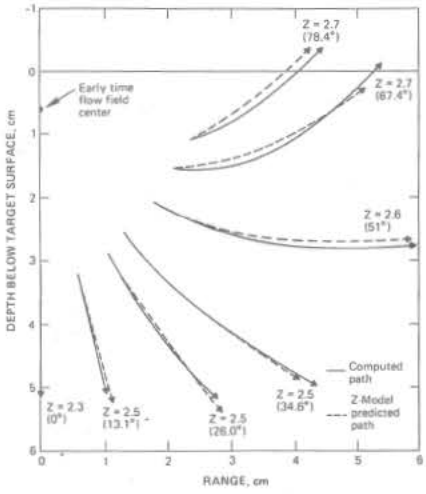

Fig. 3 Computed paths compared with Z-Model predicted paths using best-fit Z values.

Acknowledgement - This work was supported by NASA under contract NASW 3168.

References - 1.) Bjork R. L. (1961) J. Geophys. Res. 66, p. 3379-3387. 2.) O'Keefe J. D. and Ahrens T. J. (1975) Proc. Lunar Sci. Conf. 6th, p. 2831-2884, Pergamon. 3.) Bryan J. B. et al. (1978) Proc. Lunar Planet. Sci. Conf. 9th, p. 3931-3964, Pergamon. 4.) Orphal D. L. et al. (1980) Proc. Lunar Planet. Sci. Conf. 11th (in press). 5.) Roddy D. J. et al. (1980) Proc. Lunar Planet. Sci. Conf. 11th (in press). 6.) Thomsen J. M. et al. (1979) Proc. Lunar Planet. Sci. Conf. 10th, p. 2741-2756, Pergamon. 7.) Austin M. G. et al. (1980) Proc. Lunar Planet. Sci. Conf. 11th (in press). 8.) Maxwell D. E. (1977) In Imp. and Expl. Cratering (Roddy, Pepin and Merrill) p. 1003-1008, Pergamon. 9.) Orphal D. L. (1977) In Imp. and Expl. Cratering, p. 907-917, Pergamon. 10.) Croft, S. K. (1980). Proc. Lunar Planet. Sci. Conf. 11th (in press).

"BP" STRUCTURE, SOUTHEAST LIBYA: A TERRESTRIAL MULTI-RING BASIN.
James R. Underwood, Jr., Department of Geology, Kansas State University, Manhattan, KS 66506

The "BP" meteorite impact structure, which lies some 165 km northeast of Kufra Oasis at lat 25°19' N and long 24°20' E (Fig. 1), consists of a central block 0.6 km in diameter surrounded by two discontinuous rings of low hills, 2 km and 2.8 km in diameter (Fig. 2). Approximately 80 km almost due south of the "BP" structure is the "Oasis" structure, 11.5 km in diameter and centered at lat 24°35' N and long 24°24' E. The multi-ring character of this structure is not as clearly expressed as is that of the "BP" structure. The structures lie in the Kufra structural basin; they and the country rock are composed of Nubia Sandstone, which in Libya has been considered to be part of the Lower Cretaceous Series (2) but which in southern Egypt has been determined by Klitsch et al. (3) to be part of the Upper Cretaceous Series.

The concentric rings of disturbed strata of the "BP" structure are in striking contrast with the typical landforms of the region, i.e. buttes, mesas, and northwest trending ridges. The beds in the outer ring dip inward at angles ranging from 3° to 15°, and the beds of the inner ring dip generally outward at angles of 20° to 40°, thus creating a rim syncline. The outer ring rises as much as 20 m above the surrounding desert plain, the inner ring extends some 30 m above the plain, and the central block has a maximum height above the surface of about 38 m. The inner ring structurally is more complex than the outer and contains numerous gently plunging folds whose axes are tangent to the structure and whose limbs dip as much as 70°. The south half of the central block is deeply eroded, complexley folded, and composed of light-colored sandstone, probably the oldest rock exposed in the structure. The folds there are gently plunging, 3-15 m from limb to limb at the surface, and randomly oriented. The high standing north half of the central block is intensely jointed and heavily impregnated with iron oxide. Although not chaotic, bedding of the rock there is difficult to discern; measured dips of 45° - 70° may not be valid. Faults in the "BP" structure are inconspicuous (4).

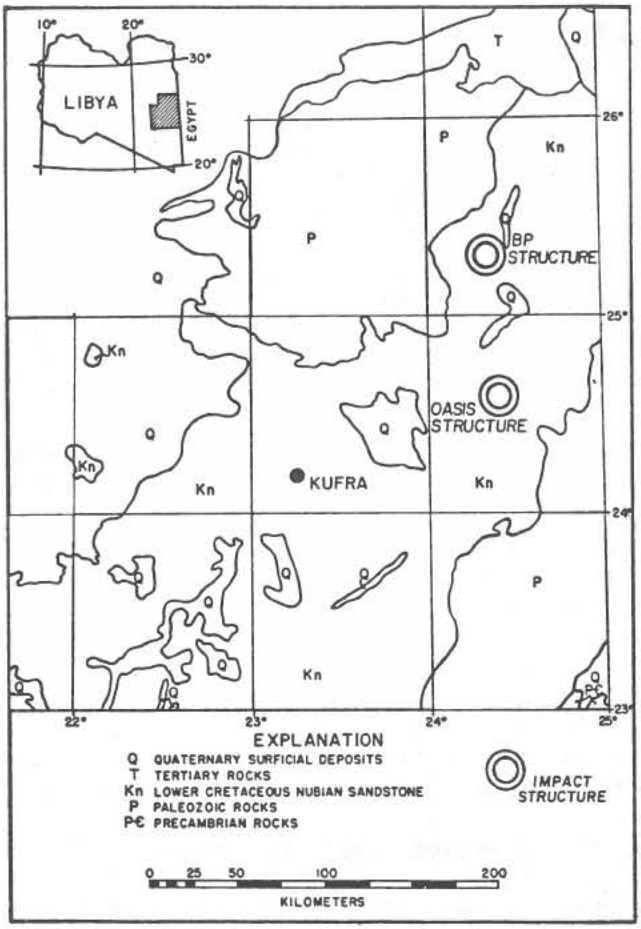

Figure 1. Generalized geologic map of Kufra region, showing localities of impact structures northeast of Kufra oasis. Modified from Conant and Goudarzi (1964)(1).

Kohman et al. (5) first reported the circular structures, having noticed them on air photographs; the larger "Oasis" structure they also recognized on Gemini orbital photographs. The low albedo of the rocks, both of the structures and of the surrounding buttes, mesas,

"BP" STRUCTURE, LIBYA

Underwood, J.R., Jr.

Figure 2. "BP" structure; diameter of outer ring of low hills is 2.8 km, of inner ring, 2.0 km, and of central block, 0.6 km. South half of central block eroded to level of interior plain. Top of photograph is north; grid drawn on original photograph by exploration geologists.

and ridges, prompted Kohman et al. to interpret the structures and associated rocks as volcanic. Although on the ground and at close range the rocks appear to be volcanic, the low albedo and the black color of much of the rock of the structures and of the region is the result of intense impregnation of the Nubia Sandstone by hematitic iron. Martin (6) suggested that the "BP" structure might be of impact origin and that it could be, in some way, connected with the distinctive Libyan Desert glass, discovered in SW Egypt in 1932 only 150 km east of the "BP" structure (7, 8, 9).

Following a neccesarily brief two-day field study in 1970, it was considered likely that the structures were created by diapiric intrusion, although incompetent rocks likely to produce such features are not known in the Kufra basin. Neither igneous volcanic nor plutonic rocks crop out in the area, although both occur some 200 km to the south in or near Jebel Arkenu and Jebel Awenat, where granite plutons (Paleozoic or younger) and Tertiary volcanic rocks are exposed (2). Examination of thin sections of rocks of both circular structures, however, revealed abundant shock metamorphic features that indicated that the structures were created by meteorite impact.

French et al. (10, 11) identified the two circular structures northeast of Kufra oasis as impact structures because of their: (1) geometry, (2) style of deformation, and (3) microscopic evidence of high-pressure shock metamorphism of quartz grains. No meteorite fragments, shatter cones, magascopic breccia, Ne-Fe spherules, or impact glass were found at the sites.

Quartz grains of the medium- to coarse-grained Nubia Sandstone composing both structures show widespred microscopic cleavage and shock lamellae with prominent orientations in the {0001}, {1122}, and {1011} planes and less prominent orientations in the {1013} and {1012} planes; the larger quartz grains characteristically are shattered and fractured and surrounded by a matrix of small, angular fragments of quartz. Extinction in many grains is irregular and mosaic-like. Interstitial brown glass occurs in some samples (10, 11).

All that can be said of the age of the impact event that produced the "BP" structure is that the event was post-Early to Late Cretaceous. If the origin of Libyan Desert glass is in some way connected to the event that produced the "BP" structure, it may be 28.5 million years old, the age of the glass determined by fission-track analysis (12). One could imagine that the impact event produced a depression not unlike Meteor Crater in northern Arizona and that the absence of obvious surface indications of meteoritic origin is explained by the subsequent lowering of the land surface several hundred meters. Thus today we examine only the basement or the roots of the

structures, below the level, for example, where shock pressure would have been sufficiently intense to produce shatter cones.

Recent intensive core drilling by Roddy at Flynn Creek and the study of large-scale, man-made explosion structures at various test sites has indicated, however, that multi-ring basins may be formed initially and are not necessarily the result of prolonged erosion that eliminates a broad and deep cavity. The key requirement is that, with only shallow penetration, the kinetic energy of the bolide be transformed into shock-wave energy that affects the surface and near-surface rocks (D.J. Roddy, personal communication, 1980).

The origin of multi-ring basins on planets other than Earth has been considered by many investigators, most of whom favor a magaterrace model that involves vertical or rotational slumping along concentric faults. An opposing view has been put forward by Hodges and Wilhelms who argued for a nested-craters model wherein the outermost ring represents the rim crest of the transient cavity and the concentric rings may result from "... differential excavation of lithologically diverse layers (13, 14)." A critical question to ask about the "BP" structure is: "Are the strata that compose the outer ring also the strata that compose the inner ring?" Although the question cannot be answered with certainty, the impression is that they are the same. If, in fact, this is true, the geology of the "BP" structure seems to contradict the nested-craters model of Hodges and Wilhelms and support the megaterrace model of many other investigators.

REFERENCES: (1) Conant, L.C. and Goudarzi, G.H. (1964) U.S. Geol. Survey Misc. Inv. Map, MI-350A, 1:2,000,000. (2) Goudarzi, G.H. (1970) U.S. Geol. Survey Prof. Paper 660. (3) Klitzch, E., Harms, J.C., Lejal-Nicol, A., and List, F.K. (1979) AAPG Bull. 63(6), 967-974. (4) Underwood, J.R., Jr., and Fisk, E.P. (1978) Abs. Second Symp. on Geol. of Libya, Tripoli, 61-62. (5) Kohman, T.P., Lowman, P.D., Jr., and Abdelkhalek, M.L. (1967) Abs. 30th Ann. Meteorit. Soc. Meeting, Moffett Field, CA. (6) Martin, A.J. (1969) Nature 223, 940-941. (7) Clayton, P.A. and Spencer, L.J. (1934) Mineral. Mag. 23(144), 501-508. (8) Barnes, V.E. and Underwood, J.R., Jr. (1976) Earth and Planet. Sci. Letters, 30(1), 117-122. (9) Underwood, J.R., Jr. (1979) NASA Tech. Memo. 80339, 87-90. (10) French, B.M., Underwood, J.R., Jr., and Fisk, E.P. (1972) Geol. Soc. America Abs. 4(7), 510-511. (11) French, B.M., Underwood, J.R., Jr. (1974) Geol. Soc. America Bull. 85(9), 1425-1428. (12) Störzer, D. and Wagner, G.A. (1971) Earth and Planet. Sci. Letters 10, 435-440. (13) Hodges, C.A. and Wilhelms, D.E. (1976) Abs. 25th Int. Geol. Congress, Sydney, 2, 612-613. (14) Hodges, C.A. and Wilhelms, D.E. (1978) Icarus 34, 294-323.

NATURE AND ORIGIN OF BASIN-FORMING PROJECTILES G.W. Wetherill, Dept. of Terrestrial Magnetism, Carnegie Institution of Washington, Washington, DC 20015

The formation of multi-ringed basins can be considered from two points of view: as the result of physical processes and as historical events. In this presentation a summary will be given of our understanding of how these historical events fit into the general picture of the evolution of the solar system. This is of interest as a scientific problem in its own right, and also provides the context in which hypothesized physical processes occurred and may even provide some constraints on these processes.

Lunar exploration, photogeology, and radiometric dating have provided a good understanding of the principal features of the bombardment history of the moon. These are: (1) A period of heavy bombardment, extending from the time of lunar formation until 3.9 ± .1 b.y. ago. At the end of this period, the lunar mass flux was ~10^3 to 10^4 times the present lunar and terrestrial value. Most of this mass was represented by the basin-forming projectiles. All the major lunar basins were formed during this period, which ended quite suddenly after the formation of the Imbrium and Orientale basins. (2) A transitional period between 3.9 and 3.2 b.y. ago during which the mass flux declined from ~10 times the present value to a flux within a factor of 2 of the present impact rate. (3) The period subsequent to 3.2 b.y. ago characterized by an average flux similar to the present lunar and terrestrial value.

In a sufficiently general way this history can be understood in terms of theories for the evolution of the small body population of the solar system (1-5). At the present time and for the last 3 b.y. the projectiles have come from sources with dynamic lifetimes comparable to or greater than the age of the solar system: the asteriod belt and the Oort cloud of comets in the outermost solar system. The earliest period represents the depletion of residual planetesimals from dynamically shorter-lived (~10^8 yr) regions of the solar system. These regions can be plausibly identified with the zone of the terrestrial planets and that of Uranus and Neptune. The transitionally cratered surfaces may represent the observable record of transfer of residual small bodies from the early short-lived regions to the present long-lived source regions.

A fairly quantitative discussion has been given of the evolution of the ~10^{26} gram planetesimal swarm that remained after the growth of the Earth and Venus was 99% complete (2). At first the near-Earth concentration of this material declined rapidly (~30 m.y. half-life). At later times this decline was dominated by a long-lived "tail", representing bodies that were transferred to purely Mars-crossing orbits by Mars perturbations and secular resonances. These objects slowly diffused back into Earth-crossing orbits by the inverse of these processes, resulting in the ~150 m.y. decay period observed at 3.9 b.y. This population would be depleted in small bodies relative to large (100-500km) projectiles by collisional events. Termination of basin formation at ~3.9 b.y. would then be a consequence of the loss of the last of a small and discrete number of large projectiles. Some of this loss may represent transfer of this material to the Flora region of the innermost asteroid belt, which is consistent with the unusual size distribution observed in that region (6).

Quantitative agreement of this chain of events with the observed record of basin formation requires the occurrence of several phenomena described below. Although there is nothing particularly unnatural about these, our present level of understanding is insufficient to guarantee that they actually took place:

(1) In order that the abrupt nature of the termination of basin formation

BASIN-FORMING PROJECTILES

Wetherill, G.W.

be statistically probable, it is necessary that ~50 m.y. long episodes of basin formation resulted from the breakup of 200-500km diameter bodies by tidal disruption following encounters within ~3 planetary radii of Earth and Venus. Such encounters are themselves inevitable. However, it has not been demonstrated that tidal disruption will actually occur during <1 hr. interval during which the projectile was within the tidally unstable zone. Generation of bursts of ~50km diameter basin-forming projectiles in heliocentric orbits by this process would also result in simultaneous ~50 m.y. long basin-formation episodes on all the terrestrial planets and would be consistent with radiometric chronology indicating near-simultaneity of formation of many near-side basins (7). This process would result in the final ~3.9 b.y. episode being a "marker horizon" throughout the terrestrial planet region.

(2) Data from terrestrial craters show that only a small fraction of the ejecta is metamorphosed sufficiently to clearly reset radiometric ages. For this reason it is difficult to understand quantitatively the high frequency of 3.9 b.y. $^{39}Ar - ^{40}Ar$ ages in the lunar highlands. It is likely that this will require derivation of much basin material from depths sufficiently great to exceed the ~350°C isotherm (8).

(3) The high concentration of siderophile elements found in highland breccias is not consistent with their being derived from single impacts of bodies in heliocentric orbit (9). If the chain of events described here actually occurred, it appears necessary that these concentrations resulted from multiple additions of this material to a megaregolith. It is necessary to reconcile this requirement with evidence for heterogeneity in the spatial distribution of these elements.

(4) A number of authors have suggested that water, inert gases, organic matter, and other volatile materials were added to the Earth by bombardment of the terrestrial planets by projectiles chemically similar to comets during the basin-forming period prior to 3.9 b.y. In a general way, this would be expected if the Oort cloud was populated by transfer of bodies from the region of Uranus and Neptune (1). However it must be remembered that we have insufficient knowledge of the size distribution and dynamics associated with this process to argue very persuasively that it agrees with the observed basin formation record, particularly its abrupt termination. When this question is considered quantitatively, it does not appear likely that more than a few percent of the Earth's water was added subsequent to 4.3 b.y., although the contribution of more depleted elements, e.g., the inert gases, could be much more significant.

REFERENCES

(1) Wetherill, G.W. (1975) Late heavy bombardment of the moon and terrestrial planets. Proc. Lunar Sci. Conf. 6th, p. 1539-1559.

(2) Wetherill, G.W. (1977) Evolution of the earth's planetesimal swarm subsequent to the formation of the earth and moon. Proc Lunar Sci Conf. 8th, p. 1-16.

(3) Chapman, C.R. (1976) Chronology of Terrestrial Planet Evolution: The Evidence from Mercury. Icarus 28, 523-536.

(4) Hartmann, W.K. (1975) Lunar "cataclysm": A misconception? Icarus 24, 181-187.

(5) Wetherill, G.W. (1976) Comments on the paper by C.R. Chapman: Chronology of terrestrial planet evolution--The evidence from Mercury. Icarus 28, 537-542.

(6) Zellner, B. (1979) Asteroid taxonomy and the distribution of the compositional types. In Asteriods (T. Gehrels, ed.), p. 782-806. Univ. Arizona Press, Tucson.

(7) Turner, G. (1977) Potassium-argon chronology of the moon. Phys. Chem. of the Earth 10, 145-195.

(8) Huneke, J.C., Jessberger E.K., Podosek, F.A., and Wasserburg, G.J. (1973) $^{40}Ar/^{39}Ar$ measurements in Apollo 16 and 17 samples and the chronology of metamorphic and volcanic activity in the Taurus-Littrow region. Proc. Lunar Sci. Conf. 4th, p. 1725-1756.

(9) Morgan, J.W., Ganapathy, R., Higuchi, H., Krähenbühl, U., and Anders, E. (1974) Lunar basins: Tentative characterization of projectiles from meteoritic elements in Apollo 17 boulders. Proc. Lunar Sci. Conf. 5th, p. 1703-1736.

THE LUNAR PROCELLARUM BASIN

E. A. Whitaker, Lunar and Planetary Lab., Univ. of Arizona, Tucson, AZ 85721

On the basis of the distribution of net radioactivity on the lunar surface (1), Cadogan postulated the existence of a large, ancient basin (the "Gargantuan Basin") whose boundaries coincided with the shoreline of Oceanus Procellarum on the west, the N. shoreline of M. Frigoris on the north, the S. shoreline of M. Nubium on the south, and the E. shore of M. Vaporum on the east (2). Using a suitable lunar frontside map (3), I found that Cadogan's circular boundary did not fit the shoreline arcs at all closely; they all tended to make small angles with the supposed boundary.

It is known from the other circular maria, and especially M. Imbrium, that the major ridge systems closely follow the locations of buried rings. The mare ridge systems for the entire lunar nearside were therefore traced onto an overlay, together with the relevant shorelines and a few scarp-like features that appeared to be related. This procedure revealed the existence of not one, but three discrete, concentric rings, none of which was complete even though the separate arcs were clear enough.

The innermost ring is marked mainly by a definite shoreline arc running from Lalande to Menelaus; this arc is one of topography rather than an albedo boundary. The arc continues N and W across M. Serenitatis as ridges. The middle ring is marked by the system of very strong ridges that run westwards from Opelt, around the Flamsteed ring, past Reiner to the N. shore of M. Frigoris, where the arc continues as a shoreline to a point near Protagoras. Other arcs of this ring are marked by the very strong ridge system running through Lamont and Jansen in M. Tranquillitatis, and weaker systems in both Lacus Mortis and Lacus Somniorum.

The outer ring is marked by the western shoreline of Oceanus Procellarum from a point near Xenophanes almost to the crater Billy, with a "bay" occuring at Struve. It continues as a weak scarp across the M. Humorum ejecta ring, is lost under that mare, but becomes visible again at Hippalus as a scarp, proceeds through Campanus and Mercator, continuing as the S. shoreline of M. Nubium. Weaker segments can be traced across eastern M. Tranquillitatis and elsewhere.

All three rings are centered within a degree or two of lat. 26°N, long. 15°W, closely west of Timocharis, and have surface diameters of 1700, 2400 and 3200 km respectively. The event that produced this basin may have been largely responsible for the generally greater thickness of crustal deposits on the farside. Presumably it occurred about 4.2 - 4.3 BY ago, at which epoch the transient crater would have been relatively rapidly replaced by asthenospheric materials through isostatic adjustment. Since the Imbrium impact occurred in these materials rather than in "average" lunar surface, any discussions of the Imbrium event and its effects, including sample and surface compositions, should allow for this modifying factor.

THE LUNAR PROCELLARUM BASIN

E. A. Whitaker

REFERENCES:

1. Lunar Orbital Data Maps, Plate II, (1973). Proc. 4th Lun. Sci. Conf. 1.
2. Cadogan, P. H. (1974). Nature 250, p. 315-316.
3. Rükl, A. (1972). Maps of Lunar Hemispheres, 1.

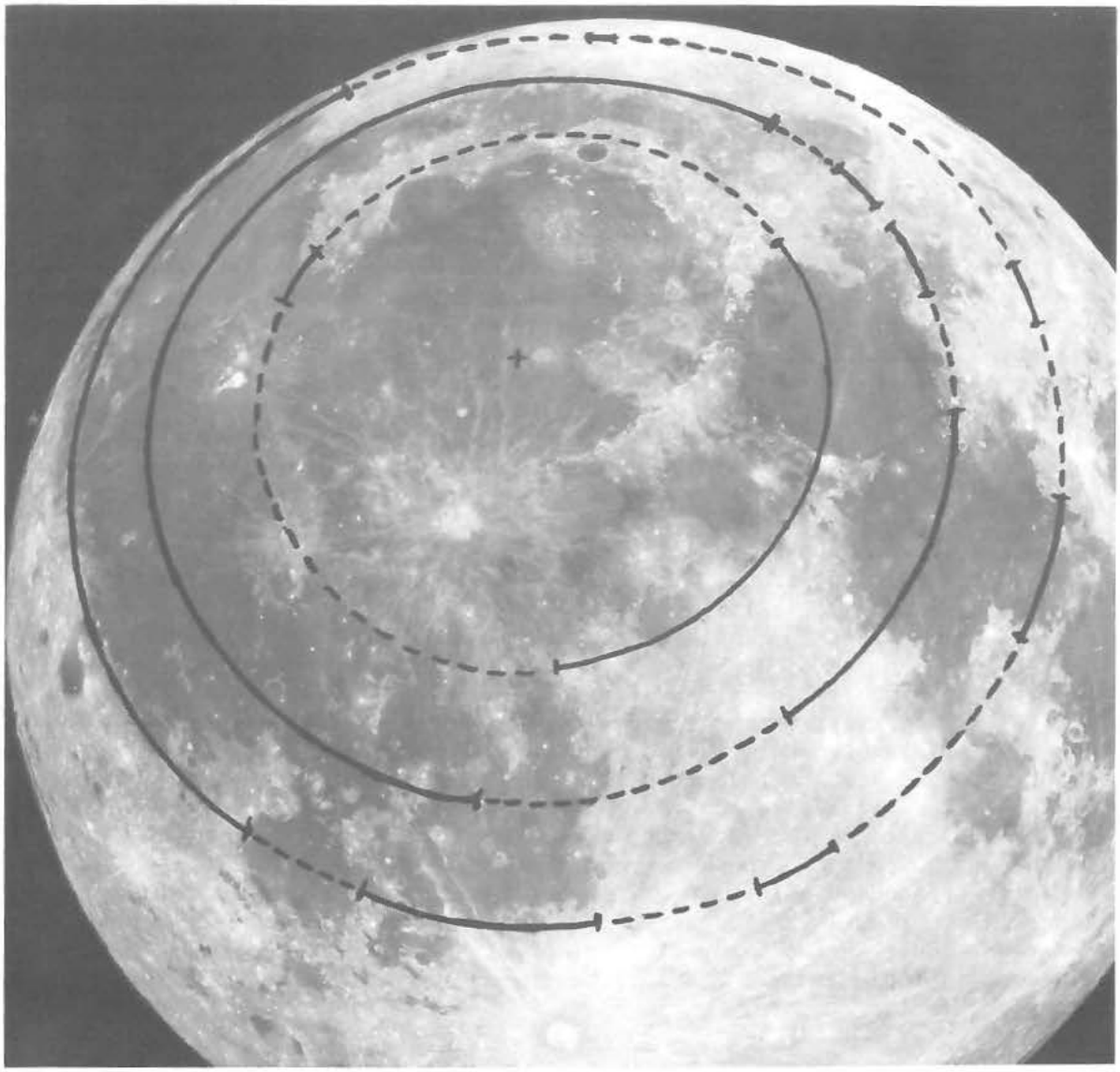

Figure 1. Photograph of full Moon with the three Procellarum Basin rings indicated. Full lines represent smoothed topographic arcs; dashed lines signify the absence of any obvious topographic expression.

IMBRIUM: THE RING UNBROKEN. J.L.Whitford-Stark, 501 Turner #5, Columbia, Missouri 65201.

Various authors (1-4) have attempted to construct rings for the Imbrium basin which either become grossly distorted to the north or connect through areas which only become correlatable in that they fall along the line of a presupposed ring rather than possessing equatable morphologic characteristics. Within and around the Imbrium basin there is extensive evidence for post-impact, vertical crustal motion; a few examples include the abrupt linear termination of the southwestern end of the Apennine Bench, the Alpine Valley (5), and the Sirsalis E - Tobias Mayer W lineament (6). Furthermore, Mason et al (7) hypothesized that many lunar linear rilles had directions inherited from fractures induced by the Imbrium impact.

The concept of a horizontal component of lunar crustal motion has been invoked predominantly to account for the construction of specific rings (e.g,8). It is here proposed that horizontal crustal motion can also result in the destruction of previously-formed rings. Several years ago it was hypothesized (9) that the two sides of Mare Frigoris were originally contiguous and that movements of massive crustal blocks resulted in the formation of the western Frigoris cavity. Several possible mechanisms to account for this were proposed. In the light of more recent work (10), the most probable scenario for the peculier ring development in northern Imbrium appears to have resulted from the translational motion of large crustal blocks into the Imbrium impact cavity after ejecta emplacement. Figure 1a. shows the geologic units,mapped by the U.S.Geological Survey (11,12),that were the product of the Imbrium impact. Figure 1b. shows these same units in their hypothesized pre-movement positions. The locations of the rings have been omitted for the purposes of clarity but it can be seen that the mountain chains in northeast Imbrium become continuous and align with the northern boundary of Mare Frigoris. The advantages of such a reconstruction are that a) the Imbrium basin becomes more nearly regular, b) there is no radial repetition of units in northeast Imbrium, c) the Alpes and Fra Mauro Formations no longer occur inside of the third ring and d) linear trends on each side of Frigoris become aligned.

References:

1) Wilhelms,D.E. and McCauley,J.F.(1971) U.S.Geol.Survey Misc. Inv.Ser.Map I-703.
2) Dence,M.R.(1976) Interdisciplinary Studies by the Imbrium Consortium,Vol.1.Cambridge,Mass. 147-155.
3) Wilhelms,D.E.(1980) NASA TM-81776, 25-27.
4) Hartmann,W.K.and Kuiper,G.P.(1962) Comm.L.P.L.Univ.Ariz.51-66.
5) Mutch,T.A.(1972)Geology of the Moon.Princeton Univ.Press.391p.
6) Pieters,C.M. et al.(1980) J.Geophys.Res.85, 3913-3938.
7) Mason,R.et al.(1976) Proc.Geol.Ass. 87, 161-168.
8) Head,J.W.(1974) The Moon, 11, 327-356.
9) Whitford-Stark,J.L. and Fryer,R.J.(1975)Icarus, 26, 231-242.
10)Whitford-Stark,J.L.(1980) Ph.D.Thesis,Brown University.
11)Lucchitta,B.K.(1978)U.S.Geol.Surv.Misc.Inv.Ser.Map I-1062.

IMBRIUM: THE RING UNBROKEN

Whitford-Stark,J.L.

12)Scott,D.H.et al.(1977)U.S.Geol.Surv.Misc.Inv.Ser.Map I-1034.

Figure 1a. Geologic map of the units around Mare Imbrium(after 1,11,and 12). Solid shading is mountains, dots the Fra Mauro Formation,horizontal the Alpes Formation,vertical the Apennine Bench Fm,

IMBRIUM: THE RING UNBROKEN

Whitford-Stark,J.L.

Figure 1b Geologic map of the Imbrium region reconstructed after (9). The units are the same as in fig 1a.

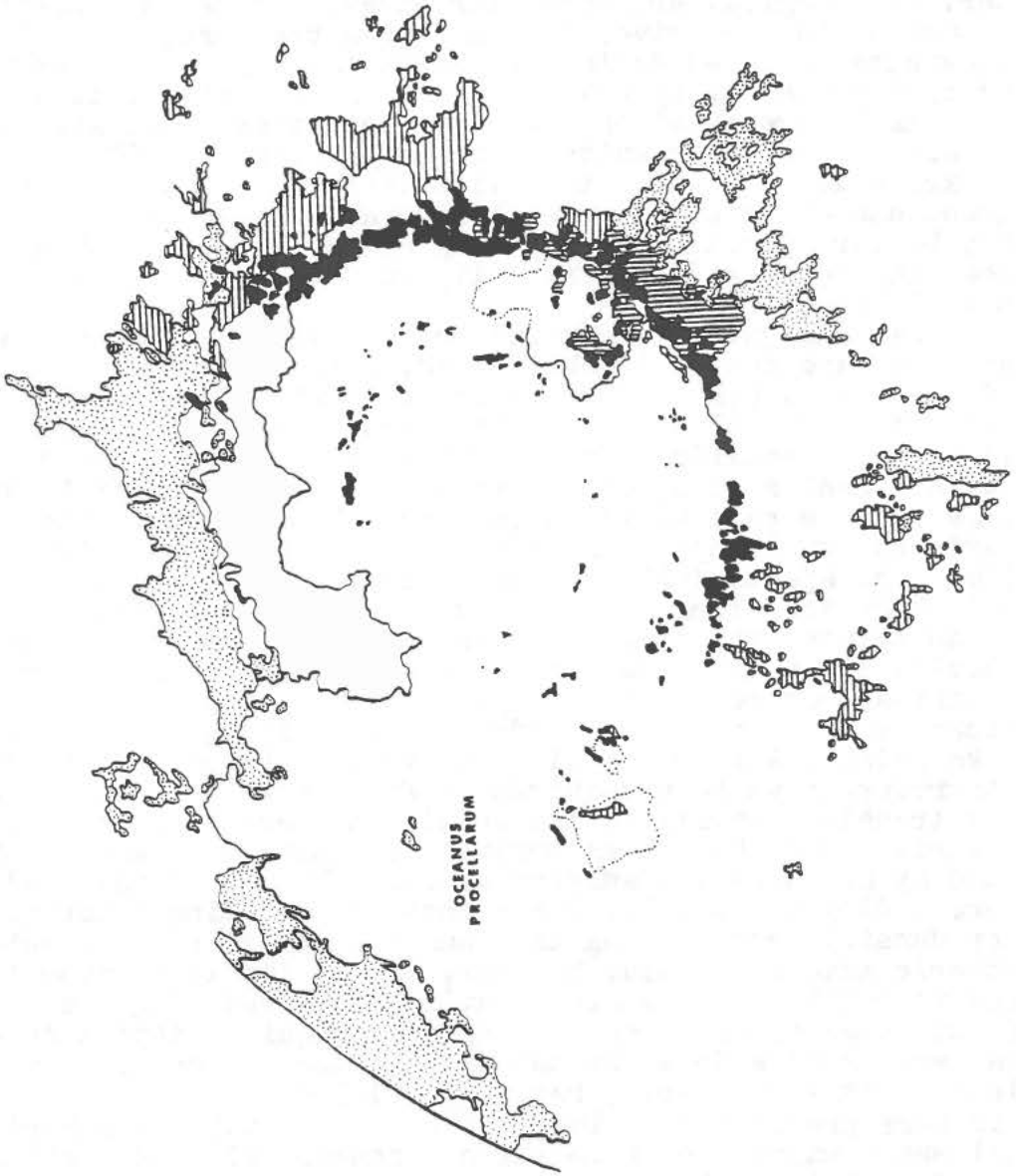

LUNAR BASIN FORMATION AND SUBSEQUENT CRUSTAL MODIFICATION. J.L.Whitford-Stark, 501 Turner #5, Columbia, MO.65201.

Most current models for the impact formation of large craters and basins envisage the production of a transient cavity and its subsequent, almost instantaneous modification by collapse, rebound, and infilling. The only geometric parameters of basins that can be directly measured are the dimensions as they appear at present. Some estimates of the original volumes of transient cavities of basins have been attempted and range from about 0.2 to 2.0 x 10^7 km ^{3} (1 - 5) for Orientale and Imbrium-sized basins, implying excavation depths of from 6 to about 120 km depending on the assumed crater shape and transient cavity diameter. Petrological arguments for excavation depths appear to be somewhat inconclusive, though it has been proposed (6) that fragments produced during the Serenitatis impact event were derived from depths of approximately 60 km. Assuming this value to be the maximum excavation depth for Serenitatis and scaling to the Imbrium cavity, results in a 100 km deep and 480 km radius excavation for the latter transient cavity. Approximating the dimensions of this cavity with a parabaloid shape (which probably better approximates the original cavity shape than a spherical cap geometry) indicates its volume to be of the order of 3.5 x 10^7 km^3.

The present height differential between the Imbrium mountain ring and the mare center is about 7 km, while reasonable estimates of the fill depth at the center of Imbrium fall in the range of 3 to 8 km (7 - 10). In the present model, the post transient cavity modification of Imbrium led to a multi-ring basin with a radius of about 670 km and a depth of about 15 km. Again, assuming a parabaloid shape, the volume of this multi-ring basin cavity is approximately 1.0 x 10^7 km^3. Neglecting the effects of ejecta fallback, lunar curvature, and appreciating that these are order of magnitude estimates, the volume difference between the Imbrium transient cavity and multi-ring basin cavity is of the order of 2.5 x 10^7 km^3. This enourmous volume corresponds to a circular plate with a radius of 1000 km and thickness of 8 km or a cylindrical plug with a 480 km radius and 38 km height. A substantial quantity of subsurface material would therefore have been required to facilitate the transition from the transient cavity to the multi-ring basin morphology. This material could have been derived from directly beneath the basin and by horizontal transport of sublithospheric material from surrounding areas (11). Phase changes producing materials of lower density accompanying the change in depth of this sublithospheric material would, however, lessen the total amount required to infill the transient cavity. Even reducing the volume estimates by an order of magnitude requires that a substantial volume of endogenous material is associated with the transient cavity- multi-ring basin transition.

It is here proposed that the motion of this sublithospheric material was a major factor in the horizontal (12) and vertical (13) modification of the upper lunar crust around the Imbrium basin. The relative importance of the impact event and the pre-

BASIN FORMATION AND CRUST MODIFICATION

Whitford-Stark,J.L.

impact crustal structure in determining the resulting basin and circum-basin topography is difficult to judge. The fact that Imbrium is not a perfect, circular multi-ring basin has been noted by many authors (see 14). For example, the Caucuses do not align with the Alps and there are gaps in the outer ring in the western,southern, and eastern sectors. One problem is, do these anomalies result from such factors as an original variable rim height as is observed at smaller lunar craters (15) or have, as is here proposed, the local lithospheric conditions played an important role in determining the Imbrium multi-ring basin morphology ?

One such influence might be the prior existence of other multi-ring basins within the Imbrium area. To the east of Imbrium lies the Serenitatis basin and to the south the proposed (16) south Imbrium basin. To the west there is little evidence for any large pre-Imbrium basins though one such has been proposed (17) on the basis of six basalt thickness data points. There are no large basins to the immediate north of Imbrium(18), however, it is in this region that the basin structure has suffered the most intensive post-formational impact modification (Iridum and Plato). In general terms, these pre-existing basins appear to have been only a minor influence on the Imbrium ring structure. For example, only about 70 km of the Imbrium ring is missing where it intersects the Serenitatis basin and only about 100 km missing where it intersects the south Imbrium basin. The effects of the proposed basin to the west of Imbrium appear to have been more pronounced, however the reality of such a basin can be called to question. The prior existence of the extremely large "Gargantuan Basin" (19) with a proposed diameter of 2400 km could have exerted a profound effect on the Imbrium ring structure but, again, the evidence for such a basin can be explained by other processes(13).

A further control on basin morphology could have been the variability of the elastic lithosphere thickness. Such thickness variations appear to be independent of local basin history (20). An anomalously thin elastic lithosphere has been proposed (21) for the Procellarum area and this lithosphere apparently thickens to the east of Imbrium (22). This appears to have been an important influence on the morphology of the Imbrium basin possibly by enhanced viscoelastic relaxation in areas of thin lithosphere(21). The combined effects of the transient cavity - multi-ring basin transition and variable lithosphere thickness is believed to contribute in part to the asymmetry of multi-ring basin morphology and may contribute to the formation of the large-scale topographic lows now filled by basalts and grouped collectively as the irregular maria.

References:

1) Croft,S.K.(1978) Proc.Lunar Planet.Sci.Conf.9th,3711-3733.
2) Head,J.W. et al.(1975) Proc.Lunar Sci.Conf.6th, 2805-2829.
3) Hodges,C.A. and Wilhelms,D.E.(1978) Icarus 34, 294-323.
4) Short,N.M. and Forman,M,L,(1972) Modern Geology 3, 69-91.
5) Dence,M.R.(1976) Interdisciplinary Studies by the Imbrium Consortium,Vol.1. Cambridge,Mass. 147-155.
6) Warner,R.D.et al.(1978) Proc.Lunar Planet.Sci.Conf.9th.941-

958.
7) Thurber,C.H. and Solomon,S.C.(1978) Proc.Lunar Planet.Sci. Conf.9th. 3481-3497.
8) Baldwin,R.B.(1963) The Measure of the Moon, Univ.Chicago Press, 488p.
9) Head,J.W.(1979) Lunar and Planetary Science X,(abstract) The Lunar and Planetary Institute,Houston,Texas.516-518.
10) Whitford-Stark,J.L.(1980) Lunar and Planetary Science XI, (abstract) The Lunar and Planetary Institute,Houston,Texas. 1242-1244.
11) Hulme,G.(1974) Nature, 252, 556-558.
12) Whitford-Stark,J.L. and Fryer,R.J.(1975)Icarus,26,231-242.
13) Whitford-Stark,J.L.(1980) Ph.D.Thesis, Brown University,371p
14) Whitford-Stark,J.L.(1980) This volume.
15) Whitford-Stark,J.L.(1978)(abstract) Meteoritics,13,668.
16) Wilhelms,D.E. and McCauley,J.F.(1971) U.S.Geol.Surv.Misc. Inv.Ser.Map I-703.
17) De Hon,R.A.(1979) Proc.Lunar Planet.Sci.Conf.10th.2935-2955.
18) Lucchitta,B.K.(1978) U.S.Geol.Surv.Misc.Inv.Ser.Map I-1062.
19) Cadogan,P.H.(1974) Nature 250, 315-316.
20) Solomon,S.C. and Head,J.W.(1980) Rev.Geophys.Space Phys. 18,107-141.
21) Head,J.W.et al.(1980)Lunar and Planetary Science XI,(abstract) The Lunar and Planetary Institute,Houston,Texas.424-425.
22) Head,J.W. and Solomon,S.C.(1980) Lunar and Planetary Science XI,(abstract). The Lunar and Planetary Institute,Houston, Texas. 421-423.

A SIMPLE GEOMETRIC TEST OF THE NESTED CRATER MODEL OF RING FORMATION. J.L.Whitford-Stark, 501 Turner #5, Columbia, Missouri, 65201.

Proposed models for the formation of rings in basins fall into two basic categories. In the first the ring configuration is dependent upon the characteristics of the impactor and subsequent crustal modification (e.g.,1,2). In the second, the nested crater model, the ring configuration is more dependent on the target characteristics (3). A parameter often neglected in studies of basins is that of planetary curvature. For structures of multiple-ring basin size, the effects of planetary curvature play as large a role as in much smaller impacts into small diameter bodies (4). In effect, the larger the diameter of the basin, the greater is the amount of material required to be removed prior to the production of a cavity. In the present study a very simple geometric model (fig.1) has been employed to test the ability of the nested crater model to predict ring spacings. The ring diameters calculated in this analysis assumed (after 3) that the pre-slumping topographic rim of the basin represented the diameter of the transient cavity, that the depth/diameter ratio of the transient cavity was 1/10, and that the depth to subsurface layers were 20 and 55 km. It was furthermore assumed that the shape of the cavity was that of a spherical cap. To simplify calculation, the boundaries of the subsurface layers were made linear instead of curving. This has the effect of slightly underestimating the dimensions of the rings.

The results (Table 1) indicate that the post-excavation upper boundaries of these two subsurface layers would have dimensions comparable to those of basin rings. The least satisfactory results were obtained for Imbrium. To a certain extent this results from the variety of published values for the diameter of specific rings and the uncertainty in the size of the transient cavity. Difficulties are encountered with the nested crater model in that some basins of comparable size have rings of varying diameter (basins 38,39, and 40 of 5, all 410 km in diameter, have rings of diameter 135,205, and 220 km) and basins < 200 km in diameter would be incapable of penetrating the 20 km layer to produce the peak ring basins, based on the assumed depth/diameter relationship. Furthermore, applying the spherical cap geometry results in excavated volumes far in excess of those predicted by various methods; the calculated volume excavated from Orientale amounts to approximately 2×10^7 km^3.

The first of these difficulties can be overcome by assuming variable thicknesses of the subsurface layers both with time and location. Such thickness variations of the lunar elastic lithosphere have been proposed (6). The second difficulty can be over come if the depth/diameter relationship were not constant but gradually decreased with increasing basin size. The relationship depth = $0.196\ \text{diameter}^{1.010}$ (7) for small craters does not seem applicable for basins (8). Such a decrease in depth/diameter would be commensurate with the increasing volume of material needed to be ejected to produce a cavity as a result of planetary curvature effects. The volume difficulty is largely a

function of assuming the spherical cap geometry and can be obviated by employing different geometries (3).

In conclusion, the nested crater model appears to be capable of roughly approximating the dimensions of rings based on the present oversimplified analysis. If correct, the nested crater model implies that the central peak-peak ring-multi ring basin transitions are in part functions of subsurface layer thicknesses and that ring spacings can be employed to approximate the thicknesses of upper layers on planetary bodies. As noted by Boyce (9), however, the target characteristics may be but one of several variable influences on ring spacing. Subsequent modification of the transient cavity by slumping and rebound processes can account for part of the discrepency between the diameters calculated in the present analysis and those observed. A combination of several models employing target characteristics, impactor characteristics, and post-formational modification appears to be best capable of accounting for the morphology of multi-ring basins.

References:
1) Hartmann,W.K. and Wood,C.A.(1971) The Moon 3, 3-78.
2) Baldwin,R.B. (1972) Phys.Earth Planet Int. 6, 327-339.
3) Wilhelms,D.E. et al.(1977) in Impact and Explosion Cratering (eds.D.J.Roddy et al) Pergamon,(New York) 539-562.
4) Cintala,M.J. et al.(1978) Proc.Lunar Planet.Sci.Conf.9th. 3803-3830.
5) Schaber,G.G. et al.(1977)Phys.Earth Planet.Int.15, 189-201.
6) Solomon,S.C. and Head,J.W.(1980) Rev.Geophys.Space Phys. 18, 107-141.
7) Pike,R.J. (1980) U.S.Geol.Surv.Prof.Paper 1046-C, 77p.
8) Settle,M. and Head,J.W. (1979) J.Geophys.Res.84, 3081-3096.
9) Boyce,J.M.(1980)(abstract) NASA-TM-81776, 339-342.

BASIN	CRATER DIAMETER	RING DIAMETER	RING DIAMETER
Imbrium(1)	1060	700	-
Calculated	1060	840	489
Orientale	850	570	330
Calculated	850	651	303
Schrödinger	320	160	-
Calculated	320	117	-
Moscoviense	410	200	-
Calculated	410	208	-
Imbrium(2)	1250	700	-
Calculated	1250	1027	685

Table 1: Published(3) and calculated ring dimensions for lunar basins.

GEOMETRIC TEST OF NESTED CRATER MODEL

Whitford-Stark, J.L.

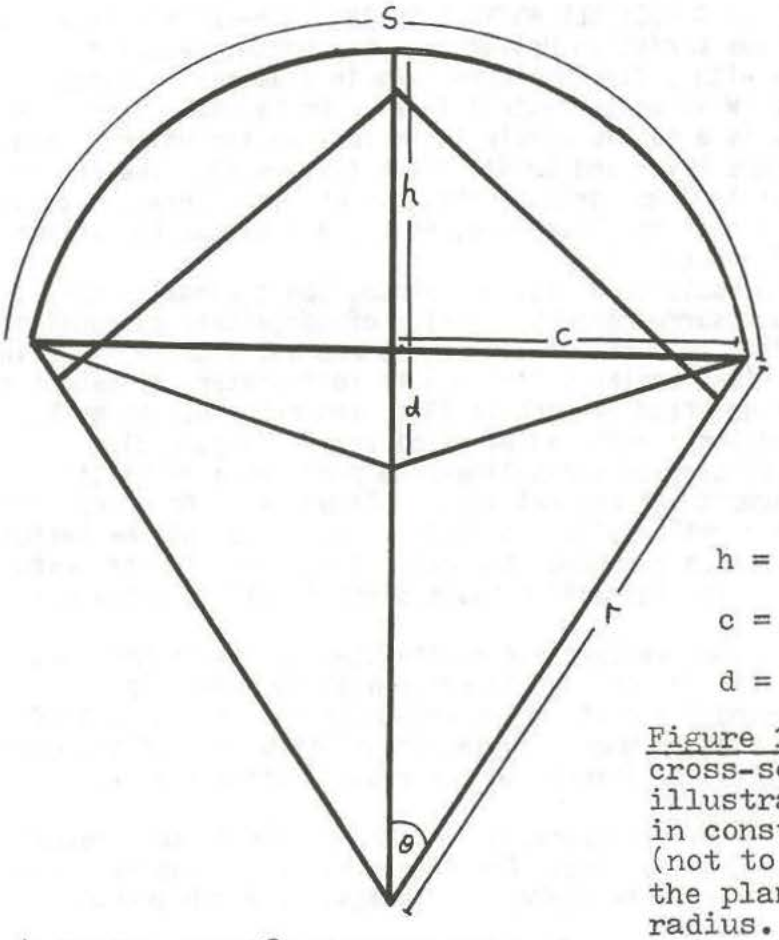

$$h = r - r \cos \theta$$

$$c = r \sin \theta$$

$$d = 1/10\ s - h$$

Figure 1a. Diagrammatic cross-section of planet illustrating parameters used in construction of Table 1. (not to scale). S represents the planet surface and r the radius.

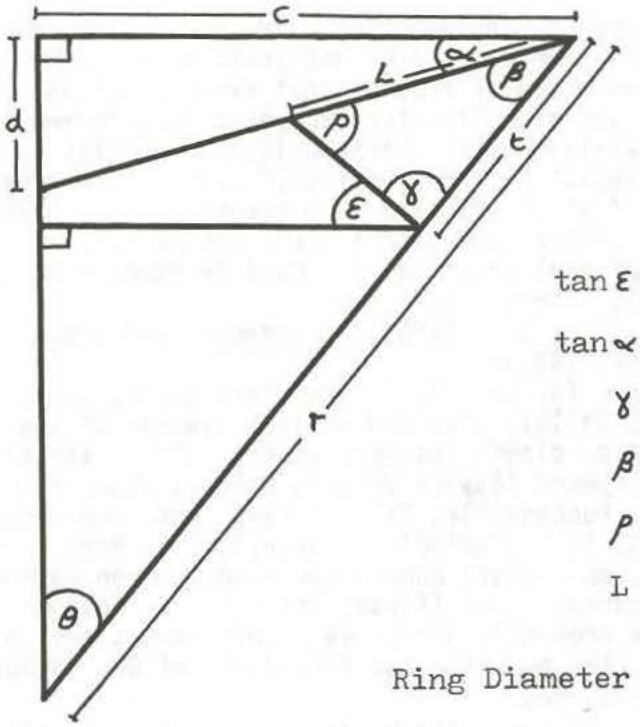

Figure 1b. Enlargement of part of figure 1a.t is the thickness of a subsurface layer, d + h is the excavation depth of the basin.

$$\tan \varepsilon = h/c$$

$$\tan \alpha = d/c$$

$$\gamma = 180 - (\varepsilon + (90 - \theta))$$

$$\beta = 90 - (\alpha + \theta)$$

$$\rho = 180 - (\beta + \gamma)$$

$$L = \frac{t \sin \gamma}{\sin \rho}$$

Ring Diameter $\simeq$ 2c - 2L

THE HICO STRUCTURE: A POSSIBLE ASTROBLEME IN NORTH-CENTRAL TEXAS, USA

Leanne Wiberg, Student (Texas Christian University, Ft. Worth, Texas) *

A possible astrobleme with a distinct core 3 km in diameter is centered near latitude 32° N and 98° W in north-central Texas. On Landsat images, the outer limit of the feature is a subtle circle 10 km in diameter which straddles a ridge separating the Bosque River and Duffau Creek (Figure 1). The center of the structure is approximately 3 km north of the town of Hico, Texas. Locally, Cretaceous sedimentary strata of the Glen Rose, Paluxy and Walnut Formations (Figure 2) dip less than 1° southeast.

The core of the Hico Structure, a distinct photographic anomaly, consists of an uplifted central block surrounded by a series of concentric discontinuous troughs and ridges emphasized by subtle tonal variations and arcuate tree lines. Within the central "block" (a circular inlier 0.8 km in diameter) limestone of the Glen Rose Formation is uplifted as much as 22 m and crops out in gently plunging synclines and anticlines with radial axial traces (Figure 3).

Differential erosion of sandstone and limestone produces a distinctly concentric drainage pattern around the central inlier (Figure 4). Downdrop of as much as 21 m along arcuate normal faults 1.5 km from the center of the feature indicates that a circular graben surrounds the central inlier. In the eastern section of the graben (A-A' in Figure 4) a fault block is tilted outward (Figure 5).

Significant erosion in southwestern and northeastern parts of the core has altered a once symmetrical and concentric structural configuration (Figure 6). The event causing the disturbance pre-dates the development of joints that controlled the establishment (during the Pleistocene) of the course of the Bosque River. On satellite images, joints cross-cutting the Hico Structure are unaffected.

Gravity and magnetic profiles traversing the core of the feature reveal no co-incident structure in the sub-surface. Correlated electric logs reveal an underlying sequence of undisturbed Pennsylvanian shales. The sub-surface limit of deformation is 200 m or less.

Several features diagnostic of impact, including shatter cones, high pressure mineral polymorphs and petrographic shock metamorphic features are absent. The feature may be in such an advanced state of erosion that evidence of an impact origin has been obliterated. The Hico Structure may have been formed under circumstances precluding the development of characteristics normally associated with impact. Either the impact of a projectile of volatile material or an impact into a Cretaceous tidal flat or both may have occurred. The high degree of plastic deformation in the central circular inlier, the relatively shallow disturbance, and the absence of explosive features must be accounted for in any theory on the origin of the Hico Structure.

REFERENCES: Miller, V.C. and Miller, C.F. (1961) Photogeology, McGraw-Hill Book Company, 248 pages

ACKNOWLEDGMENTS: Dr. C.R. Seeger (W. Ky Univ.) supervised the magnetic survey. Calvin Miller (Hunt Oil Co., Dallas) provided stereo-coverage of the feature and advised me concerning photogeologic interpretations. Other aerial photographs were loaned by Dr. O.T. Hayward (Baylor Univ.); Landsat image from Bob Borger (Mobil Field Research Lab, Duncanville, TX). I have conferred with Drs Rich Wetterauer (TCU), David Roddy (U.S. Geological Survey), Fred Horz, Dave Amsbury and Bevan French (NASA), and Robert Fudali (Smithsonian) on various aspects of the project. Dr. J.R. Underwood, Jr. (Kansas State Univ.) told me about the Hico Structure in 1976. He presently serves as my off-campus advisor for a geology thesis on the feature. The guidance and friendship of Dr. Carlos Aiken (UT Dallas) is especially appreciated.

* presently at Mobil Exploration and Producing Services, Inc.(Dallas, TX)

THE HICO STRUCTURE

L. Wiberg

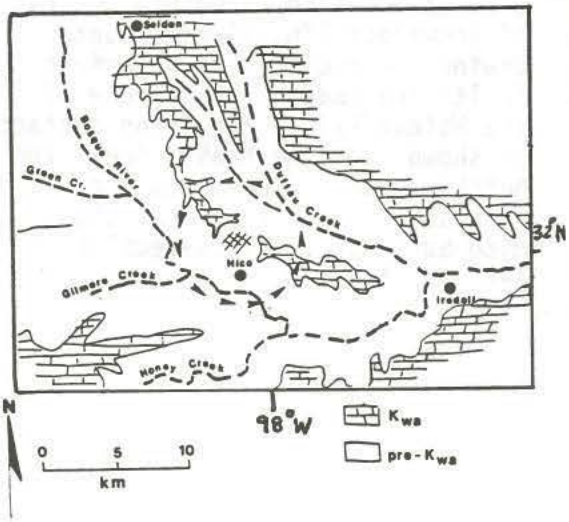

FIGURE 1: Geologic map showing the drainage courses of the Bosque River, its major tributaries and the topographic ridges between them. The outer limit of the Hico Structure is marked by arrowheads. The core of the Hico Structure is within the hatchured area. (After "Geologic Atlas of Texas" - Brownwood Sheet (1976), Abilene Sheet (1972), Waco Sheet (1970) and Dallas Sheet (1972); Bureau of Economic Geology, Austin, Texas)

FIGURE 2: Surface stratigraphic column of formations of the Lower Cretaceous Series in the vicinity of Hico, Texas

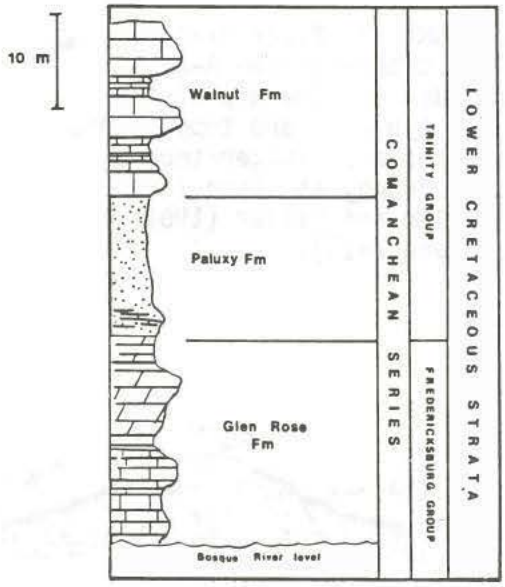

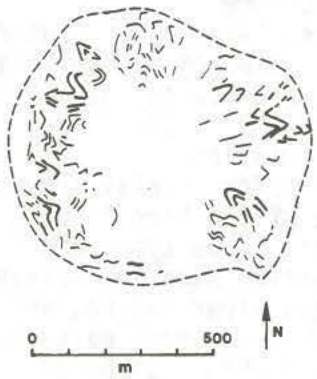

FIGURE 3: Generalized sketch of form lines of folds in the central circular inlier of the Hico Structure. Drawn directly from an overlay of an aerial photograph of the core of the Hico Structure. Heavier form lines mark outcrops clearly visible from the ground.

THE HICO STRUCTURE

L. Wiberg

FIGURE 4: Drainage map of the core of the Hico Structure. Zones of anomalous linear and arcuate drainage associated with surface faults are shaded. The trace of the Walnut/Paluxy Formation contact is shown with the heavy line. The hatchured area represents the central circular inlier of the Hico Structure. Cross-section A-A' is Figure 5.

FIGURE 5: Block diagram and cross-section A-A' on Figure 4. The dip of the fault blocks and topographic slopes are exaggerated. Topography as shown in Miller and Miller (1961, Figure 7-15).

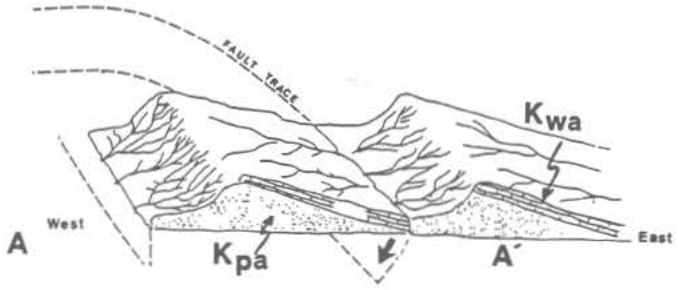

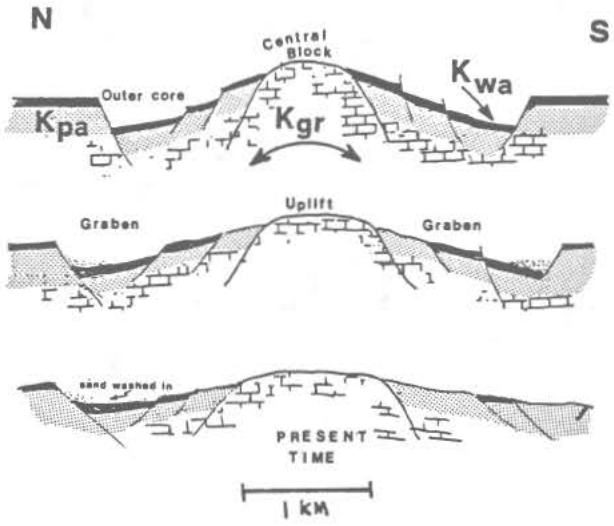

FIGURE 6: Differential degradation of the core of the Hico Structure
TOP: postulated configuration (near the time of its formation?) after overburden (if any) has eroded to the level of the Walnut Formation
MIDDLE: before Pleistocene time, the core of the Hico Structure was likely to be symmetric in its cross-section because drainage of the Bosque River had not yet been established to erode parts of its circular graben. Structural elements of the core are marked.
BOTTOM: the Hico Structure at present.

GEOLOGIC MAP OF LUNAR RINGED IMPACT BASINS Don E. Wilhelms, U. S. Geological Survey, Menlo Park, CA. 94025

Thirty-two basins ≥ 265 km across definitely exist on the Moon (table 1; full names on fig. 1) and 11 probably or possibly exist (table 2; initials only on fig. 1). Basin names are derived from superposed maria or from two superposed, unrelated craters [1]. Some new names are suggested [1-5; table 2] for previously unnamed or indefinitely named basins [6-11]. Ages reported on some geologic maps [1-5, 11] are superseded by ages from recent studies of superposition relations or crater densities [12; table 1].

Deposits and secondary craters have been identified around 18 basins (names in capitals, fig. 1). Identification criteria include radial textures and heavy obscuration of older craters near the basin and sparser, discontinuous gouging and pitting farther out. Young, large basins have very extensive visible deposits and secondaries. Similar deposits and secondaries undoubtedly surround the other 14 definite basins (names in lower case, fig. 1), but have been obscured by younger basins and craters. Only the two northern unpatterned patches on the far side (fig. 1B), which are very heavily cratered, are far enough from mapped rings to suggest absence of basin deposits.

Table 1 ranks the 32 definite basins in order of diameter where this is clear or of increasing total complexity of the ring systems where the most significant ring diameter is uncertain. My proposed diameters refer to what appears to be the highest encircling ring, the topographic basin rim. An apparent correspondence of basin size with total ring complexity bears on the subject of ring origin and will be discussed in the oral presentation.

TABLE 1

Basin	Diameter	Refs.	Age	Basin	Diameter	Refs.	Age
Milne	265	[10,1]	pN	Hertzsprung	570	[10,3]	N
Bailly	300	[6,5]	N?	Freundlich-Sharonov	600	[3]	pN
Schrödinger	320	[10,5]	I?	Humboldtianum	600(dbl.)	[6,4]	N
Schiller-Zucchius	325	"Near Schiller" [6,5]	pN	Mendel-Rydberg	630	"SE limb"[6,5]	N?
Planck	325	[10,5]	pN	Nubium	690	[9,11]	pN
Mendeleev	330	[1,3]	N	Fecunditatis	∿690	[9,11]	pN
Birkhoff	330	[10,4]	pN	Tranquillitatis	∿775(dbl?)	[9,11]	pN
Poincaré	340	[10,5]	pN	Humorum	820(560?)	[6,11]	N
Lorentz	360	[10]	pN	Smythii	840	[9,1]	pN
Coulomb-Sarton	400(?)	"Unnamed B" [10,4]	pN	Nectaris	860	[6,11]	N
Grimaldi	430	[6,10,11]	pN?	Australe	880	[9,1,5]	pN
Korolev	440	[10,3]	N	Serenitatis	∿880(dbl?)	[7,11]	N
Moscoviense	445	[10,3]	N	Orientale	930	[6,2]	I
Apollo	505	[10,3,5]	pN	Crisium	1060(635?)	[6,1,11]	N
Keeler-Heaviside	540(800?)	[3]	pN	Imbrium	∿1500	[6,7,11]	I
Ingenii	560(325?)	[3]	pN	South Pole-Aitken	∿2500	[3,5]	pN

FIGURE 1. Geologic map of ringed impact basins on the lunar near side (A) and far side (B). Heavy lines, raised ring or partial ring; inferred connections dotted. Deposits and secondary craters shown for basins named in capitals; contact dashed where approximate or buried. Equal-area projection.

GEOLOGIC MAP OF BASINS

Wilhelms, D. E.

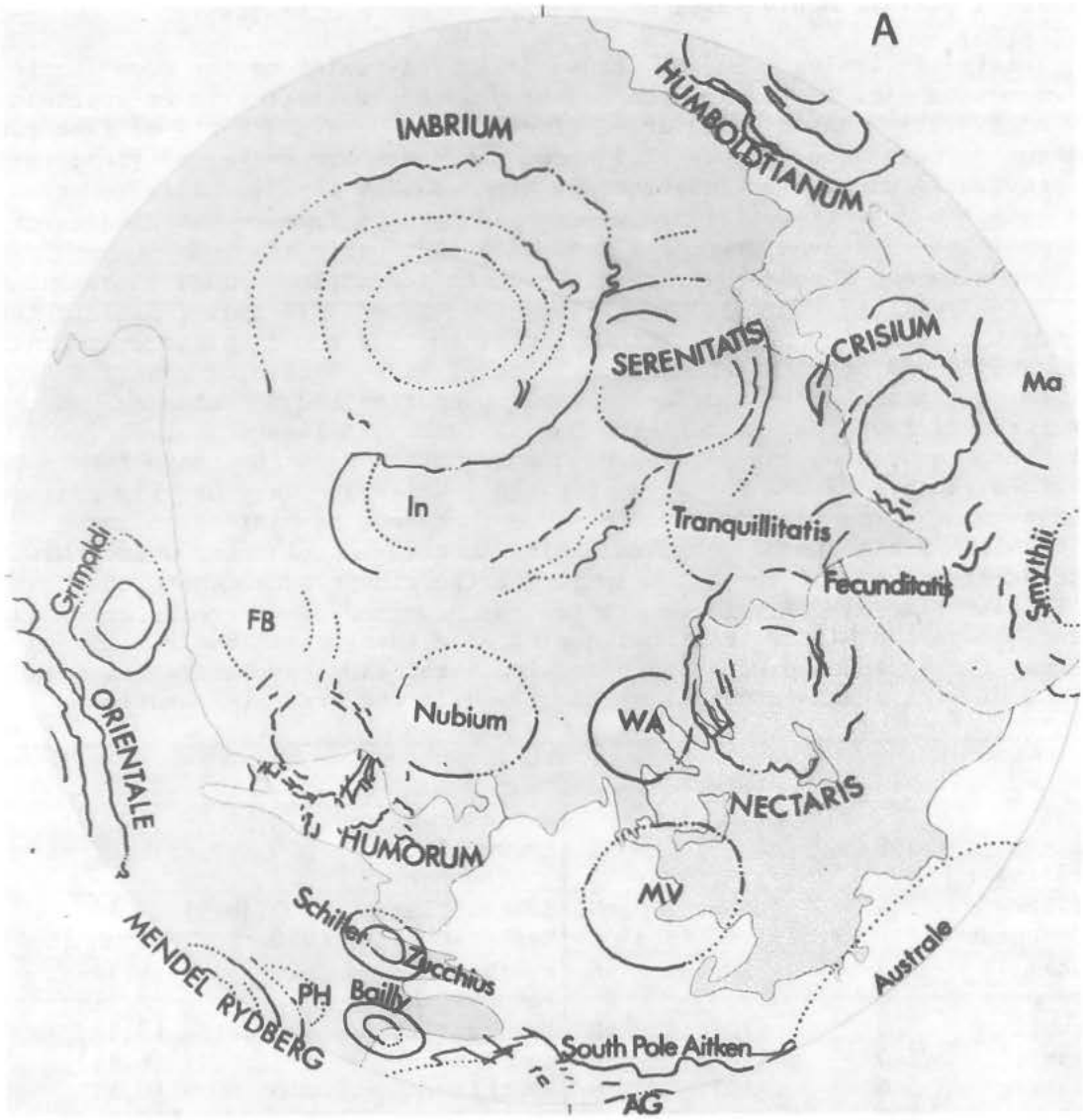

TABLE 2

Symbol (fig. 1)	Basin	Diameter	References
PH	Pingré-Hausen	~290	Pingré of [6]; [5]
SR	Sikorsky-Rittenhouse	310	"Unnamed A" of [10]; [8,5]
AG	Amundsen-Ganswindt	355	[8,5]
WA	Werner-Airy	~500	[7, p. 195]; named here
FB	Flamsteed-Billy	~570	[11]; named here
Ma	Marginis	580	[1]
AK	Al Khwarizmi-King	590	[1]
In	Insularum	~600	Basin south of Imbrium [11]; named here
LF	Lomonosov-Fleming	620	[1]
MV	Mutus-Vlacq	680	[5]
TS	Tsiolkovsky-Stark	~700	[8,1]

GEOLOGIC MAP OF BASINS

Wilhelms, D. E.

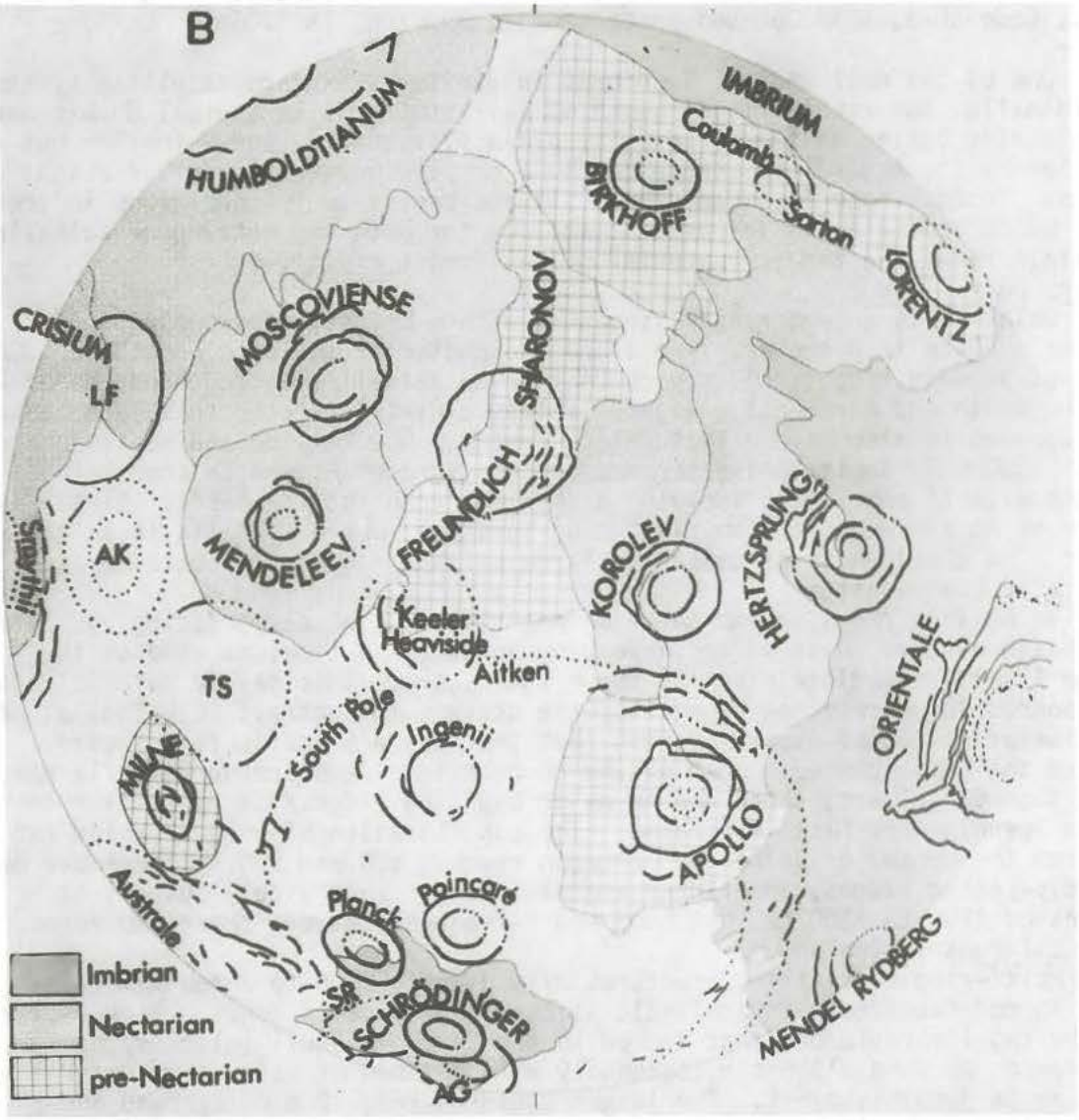

REFERENCES

[1] Wilhelms D.E. and El-Baz Farouk (1977) *U.S.G.S. Map 1-948*
[2] Scott D.H., McCauley J.F., and West M.N. (1977) *U.S.G.S. Map I-1034*
[3] Stuart-Alexander D.E. (1978) *U.S.G.S. Map I-1047*
[4] Lucchitta B.K. (1978) *U.S.G.S. Map I-1062*
[5] Wilhelms D.E., Howard K.A., and Wilshire H.G. (1978) *U.S.G.S. Map I-1162*
[6] Hartmann W.K. and Kuiper G.P. (1962) *Comm. Univ. Ariz. Lunar Planet. Lab.* 1,n.12
[7] Baldwin R.B. (1963) *The Face of the Moon* Chicago, 488 p.
[8] Baldwin R.B. (1969) *Astronomical Journal* 74, 570-571
[9] Stuart-Alexander D.E. and Howard K.A. (1970) *Icarus* 12, 440-456
[10] Hartmann W.K. and Wood C.A. (1971) *The Moon* 3, 3-78
[11] Wilhelms D.E. and McCauley J.F. (1971) *U.S.G.S. Map I-703*
[12] Wilhelms D.E. (1979) *Rept. Planet Geol. Prog. 1978-1979* NASA TM 80339, 135-137

ICE CAULDRONS AND BASINS IN ICELAND AND ON CALLISTO. Charles A. Wood, Code SN-6, NASA Johnson Space Center, Houston, TX 77058.

One of the most unusual landforms in Jupiter's bizzare satellite system is Valhalla, the ripple-ringed basin of Callisto. Unlike typical double and triple ring basins on the terrestrial planets, Valhalla (and a smaller but similar basin, Asgard) is surrounded by a complex wreath of tens of bright rings. In this note I compare these bizzare basins to ice cauldrons in Iceland which appear to be terrestrial analogs for both the pattern of Valhalla's multiple rings and the icy material of Callisto's crust[1].

Basins on Callisto.

Valhalla is a huge ringed structure with a bright, apparently ringfree center ∿850 km in diameter. The average diameter of the ring wreath is ∿3000 km, but arcuate ridges, clearly concentric to Valhalla, extend hundreds of km to the north and northeast. Asgard is less clearly depicted in Voyager images but appears to also have a featureless center ∿ 500 km wide and multiple rings of ∿ 1500 km diameter. The terminator cuts through Asgard in some Voyager I images without embayment, implying a shallow depth for the basin. Similarly, there is no appreciable limb flattening in images where Valhalla is at the limb. The shallowness of these two large basins probably reflects complete isostatic compensation.

Valhalla's rings appear to be bright ridges with scarps facing away from the basin center. Most ridges have grey zones 2 - 4 times as wide as the ridge itself, immediately behind the bright scarp. This may be material that has ponded in depressions bounded by the scarp. In contrast to Valhalla, near terminator images of Asgard suggest that that basin's scarps face inward, toward the basin center. Most of the concentric ridges around Valhalla span less than 60° of arc; there are no major bounding ridges/scarps similar to the lunar Apennines or Altai Mountains. The concentration of ridges varies radially from the center of Valhalla. Between roughly 600 and 900 km there are many closely-spaced ridges, and ridges are also common (but widely spaced) at ranges of 1200 to 1500 km, but they are infrequent between these two zones.

Ice Cauldrons in Iceland.

Multi-ring concentric structures with diameters up to a few kilometers have formed repeatedly in Icelandic glaciers in volcanic zones. Figures 1 and 2 show two ice cauldrons that formed in the Myrdalsjökull (glacier) by subsidence on 25 June, 1955 simultaneously with a flood of water from under the glacier (a jökulhlaup)[2,3]. The larger cauldron (Fig. 2 middleground and Fig. 1) was 1050 m in diameter and ∿ 80 m deep, and the smaller (Fig. 2 foreground) was 700 m wide and 15 m deep[2]. The depressed but unfractured central zones were surrounded by a wreath of concentric fractures. The fracture spacings increased radially away from the centers. The characteristics of these structures must be given in the past tense for both disappeared by 1960, presumably through viscous deformation and snow cover. The ice is about 250 m thick in the area of the glacier that the cauldrons formed[4].

Five additional ice cauldrons, ranging in diameter from 0.4 to 2 km, are shown on a map of the western half of the Vatnajökull icecap of Iceland[5], and Björnsson[6] suggests that the 6 km wide Grimsvötn depression is also an ice cauldron. The Vatnajökull ice cap is 400 to 600 m thick where these ice cauldrons formed[5]. A complex pattern of concentric and eccentric fractures defines another ice cauldron (2.8 km wide and 150 m deep; Fig. 3) ∿ 10 km northwest of Grimsvötn[6]. Photographs (Fig. 4) by R.J. Williams, Jr. (pers. comm.) of a smaller cauldron in the same area show that some of the ice blocks dip toward the cauldron center, and thus fracture plane scarps face away from the center. There does not appear to have been any extrusion of ice or water

ICE CAULDRONS

C.A. Wood

along the ice cauldron fractures, but a lake formed in the deeper Myrdalsjökull cauldron (Fig. 1) as the subsiding glacier surface intersected a free water table[3].

The intimate association in Iceland of ice cauldrons with glacial floods/jökulhlaups, and their occurrence in volcanic and geothermal areas has led to a general understanding of jökulhlaups, but little attention has been paid to the mechanics and structures of ice cauldron subsidence. Commonly, water accumulates in a dome shaped reservoir at the bottom of a glacier until the hydrostatic water pressure equals the ice overburden pressure and the water suddenly bursts from under the glacier[6]. The glacier sags into the void created by the outflow of water, forming an ice cauldron at the surface. The water in the reservoir accumulates through melting of glacier ice, slowly by constant geothermal heating or more rapidly by subglacial volcanic eruptions. The fractures that define the ice cauldrons result from brittle deformation of the ice due to the rapid subsidence.

Comparisons of Callistonian Basins and Icelandic Ice Cauldrons.

Although the mechanisms of formation were presumably quite different (impact cratering versus subsidence into void at depth), and their scales differ by 3 orders of magnitude, the general similarities of ring patterns and icy media suggest that similar styles of deformation may have affected both the ripple ring basins of Callisto and the terrestrial ice cauldrons. An alternative means of producing a depression on Callisto is suggested by thermal models which predict diapiric sinking of lithospheric material into the liquid water mantle[7]. This process may be very similar to the subsidence of ice cauldrons - but on a vastly larger scale - and would account for the morphological peculiarities of Valhalla, without recourse to impact events.

Acknowledgments. I thank Sigurdur Thorarinsson and Richie Williams for discussions and photographs of Icelandic ice cauldrons.

References. 1) G.J. Consolmagno and J.S. Lewis (1978) Icarus 34, 280. 2) S. Rist (1967) Jökull 17, 237. 3) H. Björnsson (1976) Jökull 26, 40. 4) same as 2. 5) H. Björnsson (1974) Jökull 24, 1. 6) H. Björnsson (1975) Jökull 25, 1. 7) E.M. Parmentier and J.W. Head (1979) Proc. Lunar Planet Sci. Conf. 10th 2403.

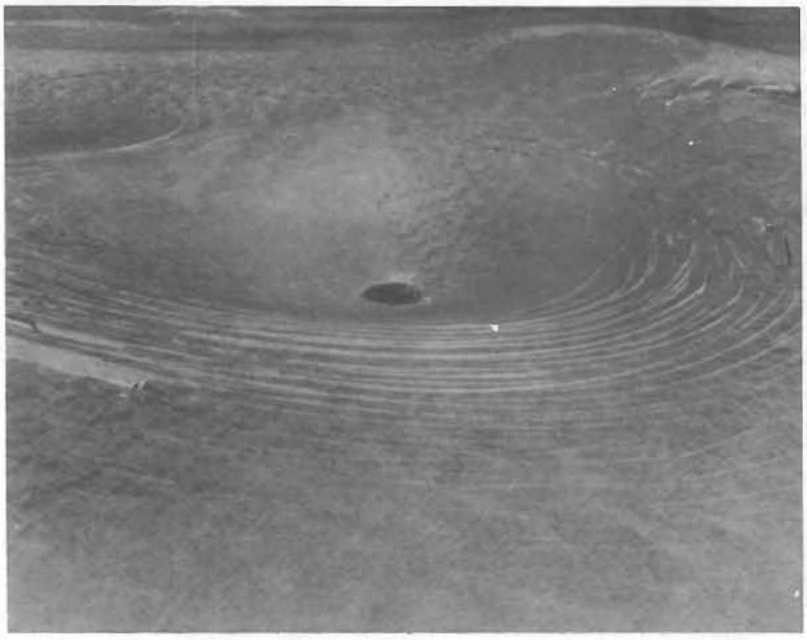

Fig. 1: Ice cauldron (dia. 1 km, depth 80m) formed on Myrdalsjökull (glacier) in Iceland on 25 June, 1955. Photo from Fig. 6 of reference 3.

ICE CAULDRONS

C. A. Wood

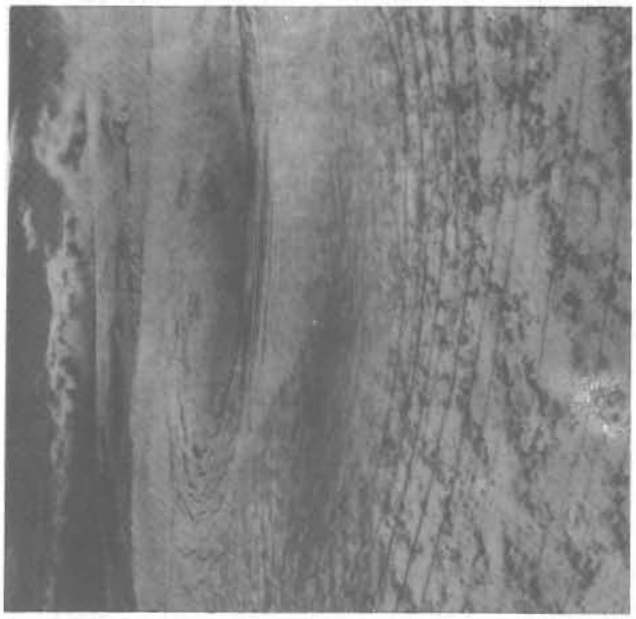

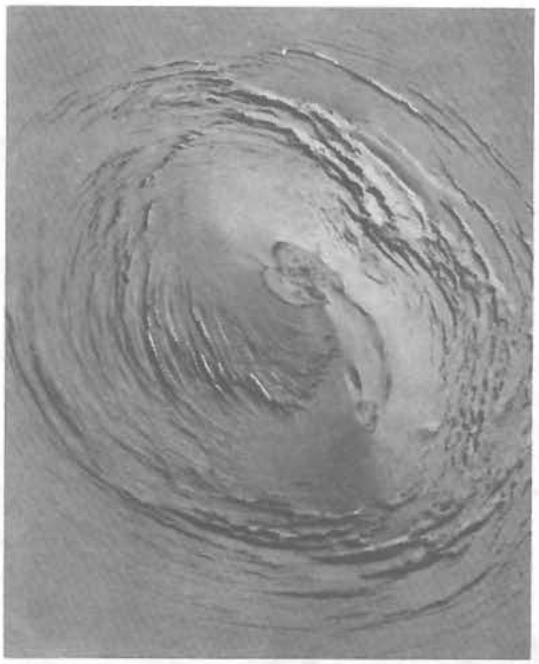

Fig. 2 (above): Ice cauldrons formed 25 June, 1955. Middle-ground: same feature as Fig. 1; foreground: 700 m wide, 15 m deep cauldron. Photo from Fig. 3 of reference 2.
Fig. 3 (left): Complex ice cauldron ∿ 10 km NW of Grimsvotn, Iceland on Vatnjökull. Photo from Plate 1 of ref. 6.
Fig. 4 (upper left): Close view of inward dipping blocks of ice in ice cauldron on Vatnajökull. Photo courtesy of R,J. Williams, Jr.

EVIDENCE FOR THE LUNAR BIG BACKSIDE BASIN. Charles A. Wood* and Ann W. Gifford, Air and Space Museum, Smithsonian Inst., Washington, DC 20560. *also at SN6 NASA Johnson Space Center Houston, TX 77058

Lunar basins have been investigated intensively and two of the largest well-defined basins - Imbrium (dia. ∿970 km) and Orientale (620 km) - have been critical indeveloping theories of basin origin and evolution. Remarkably, however, two older, more battered, but significantly larger basins - Gargantuan and the Big Backside Basin (BBB, also called South Polar-Aitken Basin[1]) - have yet to be systematically described. Gargantuan was postulated as a single 2400 km wide ring by Cadogan,[3] but Whitaker[4] has mapped it as a triple ring basin with diameters of roughly 1700, 2400, and 3200 km. As a stimulus to the study of such large ancient basins we present a preliminary map of the BBB, as well as a discussion of other available evidence for its existence. Much of the published data concerning BBB has already been compiled in regional mapping of the lunar farside[1,2].

Basin Dimensions and Center. The existence, diameter and location of the BBB were accurately predicted by Hartmann and Kuiper[5] in 1962, based on telescopic views of the large size and arcuate nature of the Leibnitz Mts. near the lunar south pole. These mountains (LM in Fig. 1), the highest on the Moon (7-9 km), led Hartmann and Kuiper to propose that the hidden basin was very large. The basin's most prominent mountain range (A in Fig. 1) was seen on Apollo 8 photographs[6], but was not related to any basin. Measurements of limb profiles of Zond 6 and 8 photographs revealed a striking topographic low (6 to 7 km deeper than the surrounding highlands) extending from 30°S to the south pole[7], and Apollo laser ranging confirmed the great depth of the hard-to-see basin[8]. Combining the available but scanty altimetric data, Bills and Ferrari[9] show the northern portion of the basin to be 2.5 km lower than the Moon's mean radius (MR), a much larger area is lower than the MR, and much of the area beyond the basin rim is 2 to 4 km higher than the MR (Fig. 1). No altimetric data exist for the central and southern parts of the BBB, but the restriction of the mare deposits to the northern portion of the basin may imply that the central and southern parts are shallow.

Based on isolated segments of a rim, Stuart-Alexander[1] proposed adiameter of about 2000 km with a basin center near 50°S, 180°W. Wilhelms et al[10] estimated a rim diameter of ∿2500 km (center 56°S, 180°W), with a speculative inner ring 1800-2000 km wide. Based on a visual best fit to 28 possible rim segments mapped from Apollo, Orbiter and Zond photography we estimate a basin diameter roughly 2600 km, with the center at 60°S, 180°W. This may not be the diameter of the basin's largest ring because the rim suggested by laser altimetry[8] is 300-600 km larger than the morphologically defined rim.

Basin Structure. Although the topographic low is the strongest expression of the BBB, numerous scarps and isolated massifs define a large skeletal[1] circle (Fig. 1). A heavily cratered 500 km long scarp centered at 17°S, 163°W helps define the northern rim of the basin (Zond 6 photos and Lunar Orbiter I-28), and the Leibnitz Mt. scarps (best seen in Hartmann and Kuiper's[5] Plates 12.70 and 12.71, and LO IV-166) anchor the rim on the earthward hemisphere near the south pole. Various ridges and scarps occur along the west rim, but the eastern rim is very poorly defined. Different from most of the features that define the basin rim are three massive but isolated mountains. The largest one (A in Fig. 1) is the 200 km long range originally noticed by Wilhelms et al[6]. The massif labeled B in Fig. 1 is ∿7.5 km high, according to profile measurements made on L.O.V-21M.

About one fourth of the linear features defining BBB lie significantly inside the best fit circle defining the main rim; if these scarps and mountains represent an inner ring it is very large, having a diameter of nearly 2200 km.

EVIDENCE FOR LUNAR BBB

Charles A. Wood and Ann W. Gifford

Lineament and Crater Counts. Counts of mapped craters >25 km in diameter illustrated that although the northern portion of BBB is obscure, its existence is clearly indicated by a lower than average crater frequency[10]. New counts of mapped craters >25 km for the entire southern hemisphere of the Moon confirm the deficiency of craters within BBB (18 craters/320,000 km^2) compared to other highland areas (25/320,000 km^2). This lack of craters is paralleled by a noticeable paucity of lineaments within the basin (Fig. 1 of Scott et al.[12]).

Volcanism. Hartmann and Kuiper[5] noted that the Leibnitz Mt. arc was a "major peripheral system to Mare Ingenii," and indeed, most of the lunar farside volcanism is concentrated within BBB[11]. This fact is apparent from Figure 1 which includes nearly all southern hemisphere examples of likely mare material as mapped by the USGS[1,2]. Scott et al.[11] noted that small volcanic features - cones, domes and rilles - were also concentrated within or near BBB.

Gravity and Magnetism. Although there are many difficulties in producing reliable gravity maps for the farside of the Moon[1], BBB is a region of negative free air anomalies, and includes the largest negative anomaly known on the Moon (centered at the Apollo basin)[12]. Thus, as expectable, the deep BBB is a region of mass deficiency. The largest magnetic field known on the Moon is also found within BBB, centered on the double crater Van de Graff, and a second large field anomaly occurs on the basin rim to the east[1].

Geochemistry. In an otherwise geochemically bland farside, most major anomalies appear to occur within BBB.[1] The highest concentrations of iron and radioactivity, as well as the lowest value for Ti, occur near Van de Graff crater in northern BBB[13]. These anomalies appear to be too large to simply be due to the small patches of mare in the area. A rare type of albedo anomaly - bright streaks and swirls on Mare Ingenii - occurs within BBB, but it is unknown whether the swirls are related to geochemical, magnetic, or some other effects.

Conclusion. The existence of BBB is clearly indicated by a deep and wide topographic low and a concentric alignment of isolated hills and scarps. The deficiency of large craters and tectonic lineaments within the basin demonstrates that although BBB is very ancient there has been insufficient cratering and lineament formation to restore typical highland morphology. BBB has clearly controlled the emplacement of most farside volcanism (Fig. 1), and each of the major anomalies of geochemistry, radioactivity and magnetism are centered within the basin. Formation of a 2600 km wide basin should have excavated deeply into the lunar mantle, but later impacts and volcanic events could have thoroughly mixed mantle and crustal material[14]. Finally, the diameters of BBB and Gargantuan are each $\sim$75% of the Moon's diameter, remarkably larger than the average crater-to-host ratio of $\sim$1/3 found for cratered objects with diameters ranging over 10 orders of magnitude[15]. The existence of BBB, Gargantuan and the Moon suggests that collisional fragmentation of moon size bodies is difficult.

References: 1. D.E. Stuart-Alexander (1978) USGS Map I-1047. 2. D.E. Wilhelms et al. (1979) USGS Map I-1162. 3. P.H. Cadogan (1974) Nature 250, 315. 4. E.A. Whitaker (1980) in "Lunar basin actually a meteor's footprint?" by C.E. Emery, Providence Journal 6/23/80, C-15. 5. W.K. Hartmann and G.P. Kuiper (1962) Comm. L.P.L. 1, 51. 6. D.E. Wilhelms et al. (1969) NASA SP-201, 16. 7. B.N. Rodionov et al. (1971, 1977) Cosmic Research 9, 410 and 14, 410. 8. W.R. Wollenhaupt et al. (1973) NASA SP-330, 33-41. 9. B.G. Bills and A.J. Ferrari (1975) Proc LSC 6, Frontispiece, pl. 2. 10. C.A. Wood and A.W. Gifford (1980) NASA TM 81776, 111. 11. D.H. Scott et al. (1977) Proc. LSC 8, 1119. 12. A.J. Ferrari (1977) JGR 82, 3065. 13. A.E. Metzger et al. (1973) Proc. LSC 4, Frontispiece, pl. 2, (1974) Proc. LSC 5, Frontispiece, pl. 2. 14. B.R. Hawke and J.W. Head (1977) Proc LPSC 8, 2750. 15. J.B. Hartung (1975) Lunar Sci. 6, 337.

EVIDENCE FOR LUNAR BBB

Charles A. Wood and Ann W. Gifford

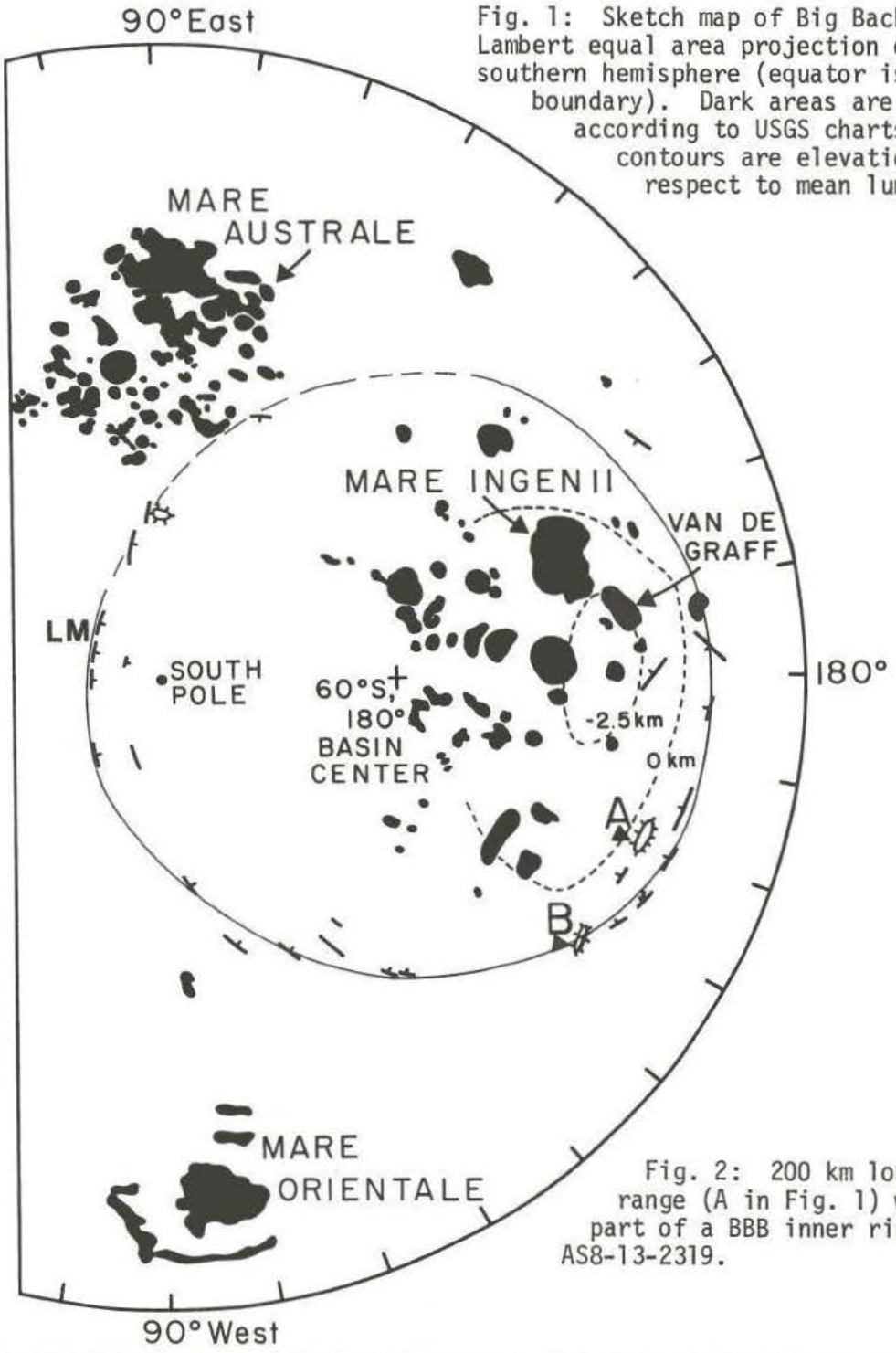

Fig. 1: Sketch map of Big Backside Basin. Lambert equal area projection of lunar southern hemisphere (equator is northern boundary). Dark areas are mare deposits according to USGS charts. Dashed contours are elevations with respect to mean lunar radius[9].

Fig. 2: 200 km long mountain range (A in Fig. 1) which may be part of a BBB inner ring. AS8-13-2319.

SAMPLE INDEX *

*Pagination refers to first page of the paper in which a sample number is mentioned.

SUBJECT INDEX *

*Pagination refers to the first page of the paper in which a subject is cited.

Subject Index

Subject Index

AUTHOR INDEX *

*Pagination refers to the first page of the paper in which an author is cited.

Author Index